

Impact of Radiative Exposures on the Mechanical Properties of Fire-Resistant Fabrics

A Thesis Submitted to the
College of Graduate and Postdoctoral Studies
In Partial Fulfilment of the Requirements for the
Degree of Master of Science
In the Department of Mechanical Engineering
University of Saskatchewan
Saskatoon

By

ANDREW NATHAN EPP

© Copyright Andrew Epp, May 2023. All rights reserved.

Unless otherwise noted, the copyright of the material in this thesis belongs to the author.

PERMISSION TO USE

In presenting this thesis in partial fulfillment of the requirements for a Postgraduate degree from the University of Saskatchewan, I agree that the Libraries of this University may make it freely available for inspection. I further agree that permission for copying of this thesis in any manner, in whole or in part, for scholarly purposes may be granted by the professor or professors who supervised my thesis/dissertation work or, in their absence, by the Head of the Department or the Dean of the College in which my thesis work was done. It is understood that any copying or publication or use of this thesis or parts thereof for financial gain shall not be allowed without my written permission. It is also understood that due recognition shall be given to me and to the University of Saskatchewan in any scholarly use which may be made of any material in my thesis/dissertation.

Requests for permission to copy or to make other uses of materials in this thesis/dissertation in whole or part should be addressed to:

Head of the Department of Mechanical Engineering
University of Saskatchewan
Saskatoon, Saskatchewan S7N 5A9
Canada

OR

Dean
College of Graduate and Postdoctoral Studies
University of Saskatchewan
Room 116 Thorvaldson Building, 110 Science Place
Saskatoon, Saskatchewan S7N 5C9
Canada

DISCLAIMER

Reference in this thesis to any specific commercial products, process, or service by trade name, trademark, manufacturer, or otherwise, does not constitute or imply its endorsement, recommendation, or favoring by the University of Saskatchewan. The views and opinions of the author expressed herein do not state or reflect those of the University of Saskatchewan, and shall not be used for advertising or product endorsement purposes.

Abstract

Firefighters' protective garments are designed to protect them from elevated temperature and heat flux environments. Typically, these garments are made of three layers: an outer shell, a moisture barrier, and a thermal liner. At present, new firefighters' garments must meet performance criteria specified in test standards, but these do not apply to in-use garments. As the performance of this clothing may degrade with use, quantitative methods for determining the useful life of these garments without destroying them is a need for the fire service. One area of such research has been the development of correlations between near infrared (NIR) spectral results and changes in fabric properties. Research at the University of Saskatchewan (U of S) has shown that NIR measurements can be correlated to deterioration in mechanical strength after thermal ageing.

This study examined the performance of two Kevlar®/PBI fabrics after exposures to heat fluxes ranging from 10 to 70 kW/m² for durations ranging from 15 to 1200 s. These exposures were conducted using a cone calorimeter and have been selected as representative of the wide range of conditions expected on the fireground. After examination using an NIR spectrometer, tensile testing was conducted on the specimens. The tensile strength values for thermally aged fabrics were then compared against criteria in standards for new clothing.

Three correlations between exposure and duration were developed based on multi-variable linear regressions, multi-variable nonlinear regressions, and single-variable nonlinear regressions. These correlations were constructed from this research and past research datasets. These correlations aim to predict the degradation these types of fabrics experience, and could be used in future degradation. It was found that the multi-variable nonlinear regression correlation was the most successful across different exposures, while the single-variable nonlinear regression was able to predict degradation more accurately to an average standard error of 4%.

Acknowledgements

I would like to start my thanks with Professor David Torvi for his continuous commitment to his graduate students, his work, and for his continual guidance and support throughout my program. His support and availability, sometimes at his own cost, has not been missed on me. I would also like to specially thank Professor Scott Noble for his help and expertise throughout this project. Dr. Jane Batcheller with the Department of Human Ecology at the University of Alberta, and their assistant Bronwyn Bates were of great help, particularly with the impact of the pandemic causing greater challenge in the tensile strength testing portion of this research. Dr. Piyali Dhar with the Department of Chemical Engineering at the University of Saskatchewan, who conducted the thermogravimetric analysis tests, is also acknowledged.

Examination of my advisory committee members is acknowledged. I wish to also extend my deep gratitude to my family and friends for their support and continued support as I strive to pursue my academic dreams. Your encouragements even through the various disappointments of life have been greatly appreciated.

Financial support from the Department of Mechanical Engineering, from the Natural Science and Engineering Research Council of Canada (NSERC), from the College of Graduate and Postdoctoral Studies at the University of Saskatchewan, and from the President's NSERC Fund at the University of Saskatchewan has been greatly appreciated.

Finally, and most importantly, I express my deepest thanks to my partner Mikayla. Without you, this journey would have been far more lonely.

Table of Contents

Permission To Use.....	i
Abstract.....	ii
Acknowledgements.....	iii
Table of Contents.....	iv
List of Figures.....	viii
List of Tables.....	xii
List of Symbols.....	xiv
Subscripts.....	xiv
List of Abbreviations.....	xv
1.0 INTRODUCTION.....	1
1.1 MATERIAL CHEMISTRY OF THE OUTER SHELL.....	3
1.1.1 Chemical Structure Of Kevlar®.....	3
1.1.2 Chemical Structure Of PBI.....	4
1.2 TEXTILE AGING.....	4
1.3 NON-DESTRUCTIVE TESTING.....	7
1.4 PROTECTIVE CLOTHING STANDARD TESTS.....	8
1.5 LITERATURE REVIEW.....	9
1.5.1 Aging Techniques.....	9
1.5.2 Non-Destructive Testing.....	13
1.5.3 Aging Models.....	14
1.6 SCOPE AND OBJECTIVES.....	16
1.7 CONTRIBUTIONS OF THIS RESEARCH TO THE LITERATURE.....	17
1.8 OUTLINE OF THESIS.....	17
2.0 METHODS AND MATERIALS.....	18

2.1 OUTER SHELL TEXTILE SPECIMEN CHARACTERISTICS	18
2.2 EXPERIMENTAL MATRIX	19
2.3 SPECIMEN PREPARATION AND CONDITIONING	22
2.3.1 Specimen Preparation	22
2.3.2 Specimen Conditioning.....	24
2.4 THERMAL AGING	27
2.5 NIR SPECTROSCOPY	31
2.6 TENSILE TESTING.....	33
2.7 THERMOGRAVIMETRIC ANALYSIS	35
3.0 EXPERIMENTAL RESULTS.....	37
3.1 COMPATIBILITY WITH PREVIOUS RESEARCH.....	37
3.2 TEMPERATURE MEASUREMENTS.....	37
3.2.1 Specimen Aging.....	38
3.2.2 Temperature Measurements.....	39
3.2.3 Ripstop Natural Test Comparisons With Previous Research	44
3.3 NIR SPECTROSCOPY	46
3.3.1 NIR Spectroscopy Results	46
3.4 TENSILE STRENGTH AND TEMPERATURE MEASUREMENTS.....	49
3.5 THE PARTIAL IGNITION AT 60 KW/M ²	57
3.6 THERMOGRAVIMETRIC ANALYSIS RESULTS.....	58
4.0 TENSILE STRENGTH CORRELATIONS.....	62
4.1 MULTI-VARIABLE LINEAR CORRELATION	63
4.1.1 Multi-Variable Linear Regression Correlation Graphical Representation	64
4.1.2 Multi-Variable Linear Correlation Accuracy And Limitations	67
4.2 MULTI-VARIABLE NONLINEAR REGRESSION CORRELATION	68

4.2.1 Multi-Variable Nonlinear Regression Graphical Representation	70
4.2.2 Multi-Variable Nonlinear Regression Accuracy And Limitations	74
4.3 SINGLE-VARIABLE NONLINEAR CORRELATION	75
4.3.1 Single-Variable Nonlinear Graphical Representation	76
4.3.2 Single-Variable Nonlinear Correlation Accuracy And Limitations	80
4.4 CORRELATION COMPARISON	81
4.4.1 Kombat Flex Correlation Comparison.....	82
4.4.2 Ripstop Natural Correlation Comparison	86
4.5 CORRELATION SUMMARY.....	90
5.0 CONCLUSIONS AND FUTURE WORK.....	91
5.1 CONCLUSIONS.....	91
5.1.1 Thermal Aging.....	91
5.1.2 Correlations and Tensile Strength Testing.....	91
5.2 FUTURE WORK.....	92
REFERENCES.....	94
APPENDICES.....	100
APPENDIX A. MASS MEASUREMENTS	100
APPENDIX B. NEAR INFRARED REFLECTANCE RESULTS WITH COMPARABLE EXPOSURE AND DURATIONS.....	103
APPENDIX C: TEMPERATURE MEASUREMENTS.....	108
APPENDIX D. LIST OF MULTI-VARIABLE LINEAR REGRESSION CORRELATION EQUATIONS	116
APPENDIX E. DEVELOPMENT OF MULTI-VARIABLE NONLINEAR REGRESSION CORRELATION.....	121
APPENDIX F. RIPSTOP BLACK AND PBI MAX ANALYSIS	126

APPENDIX G. DEVELOPMENT OF THE SINGLE-VARIABLE NONLINEAR
CORRELATION..... 135

List of Figures

Figure 1.1 Example of A Multilayer Ensemble For Fire Protective Garments (Rezazadeh 2014)	2
Figure 1.2 Chemical Structure Of Kevlar® (Torvi 1997)	4
Figure 1.3 Chemical Structure Of PBI (Torvi 1997)	4
Figure 1.4 Comparison Of The Two Levels Of Performance In Protective Garments Over Aging (Fulton 2017 from Slater 1986).	5
Figure 1.5 Classification Of Typical Firefighter Conditions. Test Window Indicates This Research’s Tests (Adapted From Veghte 1988).	7
Figure 2.1 Kombat Flex Test Matrix. Squares Represent Exposures Tests Were Conducted.....	20
Figure 2.2 Ripstop Natural Test Matrix. “F” Represents Exposures Tested By Fulton (2017), “O” Represents Exposures Tested By Ohalele (2020), And “E” Represents Exposures Tested In This Research.	20
Figure 2.3 Representation Of The Warp And Weft Of The Fabric Rolls (Adapted From Fulton 2017).	23
Figure 2.4 Fabric Exposure Window, With Representation Of The Tensile Test Strips (Fulton 2017).	24
Figure 2.5 The Conditioning Chamber Used For Preparing The Specimens For Thermal Exposure.....	25
Figure 2.6 The Inside Of The Conditioning Chamber.....	25
Figure 2.7 Loaded Convicon PGR15 Conditioning Chamber	26
Figure 2.8 The Cone Calorimeter (Left) And The Vertical Specimen Setup (Right).....	28
Figure 2.9 The Cone Calorimeter With The Specimen Holder	28
Figure 2.10 The Cone Calorimeter With A Specimen Of Kombat Flex, With Dimensions For The Exposed Side Of The Fabric.	29
Figure 2.11 Distribution Of 35 kW/m^2 At A Distance Of 25 mm Under The Conical Heating Circuit (Adapted From Rezazadeh 2014)	30
Figure 2.12 FLIR Photo Of Ripstop Natural With Thermocouple And Off Gassing.....	31
Figure 2.13 The Agilent Technologies Cary Series UV-VIS-NIR Spectrophotometer.....	33
Figure 2.14 Instron 5565 At The University Of Alberta (Fulton 2017)	34
Figure 2.15 TGA 8000 In The Department Of Chemical Engineering At The University Of Saskatchewan	36

Figure 3.1 Kombat Flex Specimen Aging For Different Heat Flux Exposures At 60 s	38
Figure 3.2 Ripstop Natural Specimen Aging For Different Heat Flux Exposures At 60 s.....	39
Figure 3.3 Temperature Measurement Comparison Between IR Thermometer And Thermocouples Measurements At 10 and 40 kW/m ² For Ripstop Natural.....	40
Figure 3.4 Temperature Measurements For Kombat Flex For First 60 s Of Exposure.....	41
Figure 3.5 A Temperature Measurements For Ripstop Natural For The First 60 s Of Exposure	42
Figure 3.6 Kombat Flex Temperature Rise Consistency At 20, 30, And 60 kW/m ²	44
Figure 3.7 Ripstop Natural Temperature Rise Comparison Against Previous Research (Ohalele 2020; Fulton 2017).....	45
Figure 3.8 Averaged Kombat Flex NIR Data For Unexposed Specimen, 20 kW/m ² Exposures, 40 kW/m ² Exposures, And Exposures Above 50 kW/m ²	47
Figure 3.9 Averaged Ripstop Natural NIR Data For Unexposed Specimen, 20 kW/m ² Exposures, And 40 kW/m ² Exposures.	48
Figure 3.10 Kombat Flex Temperature Measurements For 20 kW/m ² With Tensile Strength Data.	50
Figure 3.11 Ripstop Natural Temperature Measurements For 20 kW/m ² With Tensile Strength Data For Both This Research And Ohalele’s (2020) Research.	51
Figure 3.12 Kombat Flex Experimental Data For Exposures With Multiple Data Points. Error Bars Show Standard Deviation.	52
Figure 3.13 Ripstop Natural Experimental Data For Exposures With Multiple Data Points. Error Bars Show Standard Deviation.	53
Figure 3.14 Kombat Flex Front (Left) And Back (Right) Of Specimen KF.60.60.2 Exposed To 60 kW/m ² For 60 s, Highlighting The Partial Ignition Of The Specimen.	57
Figure 3.15 Kombat Flex NIR Measurement For A Specimen Exposed To 60 kW/m ² For 60 s, Measurements At Different Parts Of The Specimen.	58
Figure 3.16 Kombat Flex Thermogravimetric Analysis In Air	59
Figure 3.17 Typical Ripstop Natural Thermogravimetric Analysis In Air.....	60
Figure 4.1 Comparison Of Tensile Strength To Exposure And Duration Of Ripstop Black And PBI Max (Ohalele et al. 2022). Set 1 And 2 Represents Data From Fulton (2017) And Ohalele (2020) Respectively.....	62

Figure 4.2 Three-Dimensional Representation Of Kombat Flex Data With The Multi-Variable Linear Regression Correlation	65
Figure 4.3 Ability Of A Multi-Variable Linear Regression Correlation To Predict Tensile Strength For Ripstop Natural Fabrics After Exposures To Various Heat Fluxes (Ohalele 2020; Fulton 2017).	66
Figure 4.4 Ability Of A Multi-Variable Linear Regression Correlation To Predict Tensile Strength For Kombat Flex Fabrics After Exposures To Various Heat Fluxes	67
Figure 4.5 Ability Of A Split-Region Multi-Variable Nonlinear Regression Correlation To Predict Tensile Strength Of Kombat Flex Fabrics After Exposures To Various Heat Fluxes	71
Figure 4.6 Comparison Of Kombat Flex Heat Flux Experimental Data To The Multivariable Nonlinear Regression Correlation At 20 kW/m ²	72
Figure 4.7 Ability Of A Split-Region Multi-Variable Nonlinear Regression Correlation To Predict Tensile Strength Of Ripstop Natural Fabrics After Exposures To Various Heat Fluxes Using Multiple Datasets (Fulton 2017; Ohalele 2020)	73
Figure 4.8 Comparison Of Ripstop Natural Heat Flux Experimental Data To The Multivariable Nonlinear Regression Correlation At 20 kW/m ² (Fulton 2017; Ohalele 2020)	74
Figure 4.9 Ability Of A Single-Variable Nonlinear Correlation To Predict Tensile Strength Of Kombat Flex Fabrics After Exposures To Various Heat Fluxes	77
Figure 4.10 Ability Of A Single-Variable Nonlinear Correlation To Predict Tensile Strength Of Ripstop Natural Fabrics After Exposures To Various Heat Fluxes (Ohalele 2020) ..	78
Figure 4.11 Kombat Flex Single-Variable Nonlinear Method Compared Over Time For 10, 15, 20, 30, and 40 kW/m ²	79
Figure 4.12 Ripstop Natural Single-Variable Nonlinear Method Compared Over Time for 20 and 40 kW/m ²	80
Figure 4.13 Kombat Flex Correlation Comparison For Exposure 15 kW/m ² . Error Bars Represent Standard Deviation	83
Figure 4.14 Kombat Flex Correlation Comparison For Exposure 20 kW/m ² . Error Bars Represent Standard Deviation	84
Figure 4.15 Kombat Flex Correlation Comparison For Exposure 30 kW/m ² . Error Bars Represent Standard Deviation	85

Figure 4.16 Kombat Flex Correlation Comparison For Exposure 40 kW/m ² . Error Bars Represent Standard Deviation.....	86
Figure 4.17 Ripstop Natural Correlation Comparison Of Exposure 20 kW/m ² (Fulton 2017; Ohalele 2020).....	87
Figure 4.18 Ripstop Natural Correlation Comparison Of Exposure 30 kW/m ² (Fulton 2017; Ohalele 2020).....	88
Figure 4.19 Ripstop Natural Correlation Comparison Of Exposure 40 kW/m ² , Showing Epp's Correlations Only (Fulton 2017; Ohalele 2020)	89

List of Tables

Table 1.1 Select Examples Of Research On Effects Of Thermal Aging Of Fabrics	10
Table 2.1 Ripstop Natural And Kombat Flex Fabric Properties.....	19
Table 2.2 Kombat Flex Test Matrix As List.....	21
Table 2.3 Ripstop Natural Test Matrix As List, With Epp’s, Ohalele’s (2020), And Fulton’s (2017) Data	21
Table 2.4 Spectrophotometer Scanning Parameters	32
Table 3.1 Percent Difference Of Thermocouple Measurements Compared To IR Thermometer Measurements.....	41
Table 3.2 Temperature Increase At Different Heat Flux Exposures, With Comparisons Between Kombat Flex, Ripstop Natural, And Fulton’s Ripstop Natural (Fulton 2017).....	43
Table 3.3 Ripstop Natural Temperature Rise And Percent Difference Comparison Against Previous Research (Ohalele 2020; Fulton 2017).....	45
Table 3.4 Kombat Flex Tensile Strength Data.....	54
Table 3.5 Ripstop Natural Tensile Strength With Comparison Against Previous Research (Ohalele 2020; Fulton 2017).	55
Table 3.6 Ripstop Natural Tensile Strength Specific Point Comparisons (Ohalele 2020; Fulton 2017).....	56
Table 3.7 TGA Derivative Mass Peak Temperatures Compared To Experimental Thermal Aging Temperatures Which Produced Steady-State Temperatures Closest To TGA Derivative Mass Peaks For Both Kombat Flex and Ripstop Natural.....	61
Table 4.1 Multi-Variable Linear Regression Coefficients For Equation 4.1 For Kombat Flex And Ripstop Natural Using Heat Flux (Fulton 2017; Ohalele 2020)	64
Table 4.2 Average, Median, And Standard Deviation Of Standard Error For Multi-Variable Linear Regression Correlation Split By Duration For Kombat Flex.....	68
Table 4.3 Multivariable Nonlinear Regression Coefficients For Equation 4.3 With Standard Errors With Split Data Regions At 45 kW/m ² And 60 s Where Reaction Rate Changes	70
Table 4.4 Kombat Flex And Ripstop Natural Standard Error Statistics For Multi-Variable Nonlinear Regression With Comparative Splits For All Durations And For Durations Under 60 s / Exposures Under 45 kW/m ²	75

Table 4.5 Power Law Correlation Coefficients For Equation 4.4 For Kombat Flex, Ripstop Natural, PBI Max, And Ripstop Black Using The Five Exposures With Multiple Durations (Ohalele 2020).	76
Table 4.6 Average, Median, And Standard Deviation Of Standard Error For Kombat Flex And Ripstop Natural For Single-Variable Nonlinear Method (Ohalele 2020; Fulton 2017).	81
Table 4.7 Standard Error Comparison Across Correlations	82

List of Symbols

q''	Heat Flux
T	Temperature
TS	Tensile Strength
t	Time

Subscripts

abs	absolute
i	initial

List of Abbreviations

ASTM	American Society for Testing and Materials
DRA	Diffuse Reflectance Accessory
ePTFE	Expanded Polytetrafluoroethylene
FTIR	Fourier Transform Infrared Spectroscopy
KF	Kombat Flex
MgCl	Magnesium Chloride (MgCl)
NDT	Non-Destructive Test or Testing
NFPA	National Fire Protection Association
NIR	Near Infrared Spectrum of Light
PBI	Polybenzimidazole
PCR	Principal Component Regression
PLS	Partial Least Squares
PPE	Personal Protective Equipment
PU	Polyurethane Foam
RH	Relative Humidity
RPP	Radiative Protective Performance Test
RSB	Ripstop Black
RSN	Ripstop Natural
SEM	Scanning Electron Microscope
SIMCA	Soft Independent Modelling of Class Analogy
TGA	Thermogravimetric Analysis
TPP	Thermal Protective Performance Test
TTS	Time-Temperature Superposition
U of S	University of Saskatchewan
Vis-NIR	Visible-Near-Infrared

1.0 Introduction

Humankind have always had a cautious curiosity regarding fire. The ability to make and harness fire has often been thought of as the first achievement as a species, or perhaps one of the first revolutionary discoveries which spurred on new technology. The shift away from a hunter-gather society is often earmarked by the development of farming technology (Smith 1995). Perhaps another mark of this shift is the broadening use of fire beyond its use in cooking, such as the use of fire by indigenous communities to remove old growth as a mode of forest land management (Pellatt *et al.* 2015). Fire is extremely prevalent in society today, and with that prevalence a cautionary approach should be taken. In 2021, the United States had 135 on-duty firefighter deaths (Fahy and Petrillo 2022), with firefighter injuries estimated in 2020 at 64,875 (Campbell 2021). Fire injuries can have life-altering affects, and it is important that both scientists and engineers to do whatever possible to protect the lives of people.

The garments used by firefighters are specifically designed with properties such as heat resistance, shrinkage resistance, water resistance, and tear strength in mind (NFPA 1971, 2013). These garments are multilayered, often consisting of an outer shell, a moisture barrier, and a thermal liner. The outer shell is made up of flame resistant materials, which can be made of a blend of materials such as Nomex®, Kevlar®, and/or polybenzimidazole (PBI) in different proportions. The moisture barrier is made of materials such as expanded polytetrafluoroethylene (ePTFE) which is impervious to liquid water but allows water vapour to escape. The thermal liner primarily acts as fire resistant insulation, and can be made of materials similar to Nomex® batting. Figure 1.1 shows an example of what these materials look like.



Figure 1.1 Example of A Multilayer Ensemble For Fire Protective Garments (Rezazadeh 2014)

These garments are often designed specifically to meet standards set out by the National Fire Protection Association (NFPA), the American Society for Testing and Materials (ASTM), the International Organization for Standardization (ISO), and the Canadian General Standards Board (CGSB). These standards set out design criteria for new clothing, however, challenges are still present for deciding when these garments should be retired from the field. At present, garments are often retired based on visual inspection (see NFPA 1851, 2020). At the University of Saskatchewan, several graduate students have explored non-destructive testing (NDT) methods for evaluating firefighter turnout gear (considered to be pants and jacket for this research) to help identify end of service life in accordance with requirements for new clothing found in NFPA 1971 (2013).

Firefighters' protective clothing may be retired based on a recommended service life (McQuerry *et al.* 2015; NFPA 1851, 2020). Using NDT methods, the current state of firefighter gear could be evaluated, allowing for better retirement decisions to be made. In industry,

reliability engineering and predictive maintenance are used to maintain equipment based on the statistics of how often equipment breaks (Kiran 2017). This use of NDT would allow departments to employ reliability engineering methods to help manage their protective garments.

The following introduction will explain the background of this research, going into detail on: firefighters protective clothing, outer shell materials, how these textiles age and how they are commonly tested, a brief look at various types of non-destructive testing, a review of recent research in this area, and concluding with the scope and objectives of this specific research.

1.1 Material Chemistry Of The Outer Shell

The outer shell layer is made of fire-resistant materials. The yarns of these composites are often entirely spun, though sometimes that can be filaments. Some outer shells are made up of Kevlar®, PBI, Nomex®, or a blend of these (Alexander and Baxter 2016). This section briefly covers the material chemistry for the outer shell materials used in this research. Further background information on the other material layers of fire garments can be found in Rezazadeh (2014).

1.1.1 Chemical Structure Of Kevlar®

The commonly known material Kevlar® (also known as poly-paraphenylene terephthalamide) was invented by DuPont™ in 1971. Kevlar® is an aramid, or an aromatic polyamide, named so because at a molecular level it is made up of aromatic structures linked together by amides. A material is referred to as an aramid if at least 85% of its structure has amide linkages, attached directly to aromatic rings. (FTC 2009). Kevlar® is part of the para-aramid group due to the position of the amide within the phenylene group. Figure 1.2 shows the structure of Kevlar®.

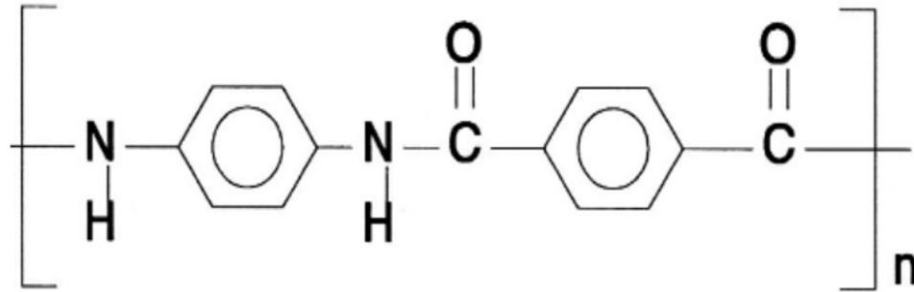


Figure 1.2 Chemical Structure Of Kevlar® (Torvi 1997)

1.1.2 Chemical Structure Of PBI

PBI, also known as polybenzimidazole, while being lesser known than Kevlar® is also of great importance in fire protective garments. This material was first synthesized in the late 1950s by Dr. Carl Marvel (NASA 2008). Similar to Kevlar®, PBI has excellent flame-resistant properties. Polybenzimidazoles are thermoplastic polymers with at least one aromatic unit (Mustarelli *et al.* 2009). This aromatic unit provides high mechanical and thermal stability to PBI, making it viable as an outer shell material. Figure 1.3 shows the chemical structure of PBI.

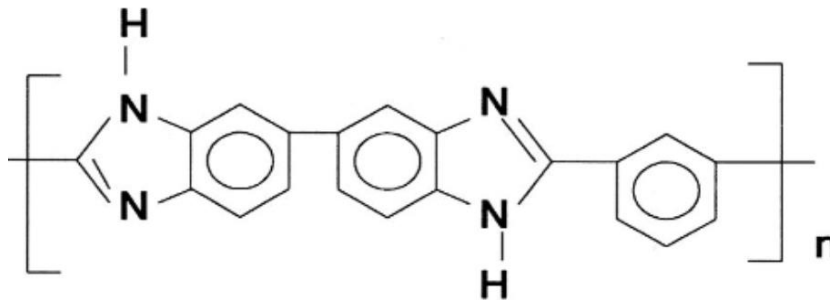


Figure 1.3 Chemical Structure Of PBI (Torvi 1997)

1.2 Textile Aging

Aging can be defined as the “accumulation of all changes in a system with the passage of time” (Timiras *et al.* 1995). For firefighters garments, factors that influence aging may include (but not be limited to):

- mechanical action (abrasion),
- environmental factors (UV radiation, weathering),

- cleaning and maintenance procedures, and
- thermal aging (Fulton *et al.* 2018).

Of preeminent interest for this research is thermal aging, though some of the other common aging types listed above have been explored by previous research conducted here at the University of Saskatchewan (see Fulton 2017; Besspflug *et al.* 2020).

As garments age, they become less effective at their intended function. This degradation is of primary concern for garments designed to protect firefighters. For high performance textiles, this degradation can occur with little or no visual indication – to the point that the garment no longer meets set standards for use (Slater 1986). This visual degradation performance curve is represented in Figure 1.4.

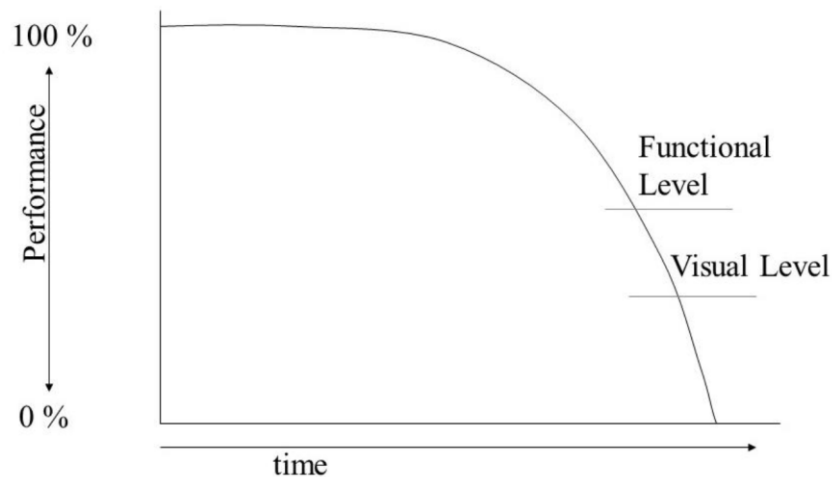


Figure 1.4 Comparison Of The Two Levels Of Performance In Protective Garments Over Aging (Fulton 2017 from Slater 1986).

Thermal aging that occurs in the field can be simulated in the lab using several different technologies (Fulton *et al.* 2018). Depending on the desired outcome and available resources, tests can be conducted at full-scale or bench-scale. Research is currently being conducted on improving the relationship between full-scale and bench-scale tests (e.g., Ugo-Okeke 2019). For bench-scale tests in textile research, two standard tests are the Radiant Protective Performance (RPP, ASTM F2700, 2020), and the Thermal Protective Performance (TPP, ASTM F1939, 2020).

The cone calorimeter (ASTM E1354, 2022) provides a number of advantages. First, it can consistently produce a wide range of heat fluxes with a uniform distribution of heat flux over the test specimens (Torvi *et al.* 2016). Through comparative tests at the University of Saskatchewan, the cone calorimeter, with a custom specimen holder, was compared against the Meker burner and quartz tubes for use as a heat source in small-scale fabric tests (Torvi *et al.* 2016). Cone calorimeter tests are another method to produce thermal exposures, and have a more consistent exposure window than laboratory burners and/or quartz tubes.

Conditions that firefighters face can range dramatically in severity, sometimes reaching temperatures over 1000°C (Veghte 1988). Figure 1.5 shows a classification of exposures proposed by Veghte which correlates exposure to temperature and heat flux into routine, ordinary, and emergency conditions. Included in this figure is the window of exposures examined in this research.

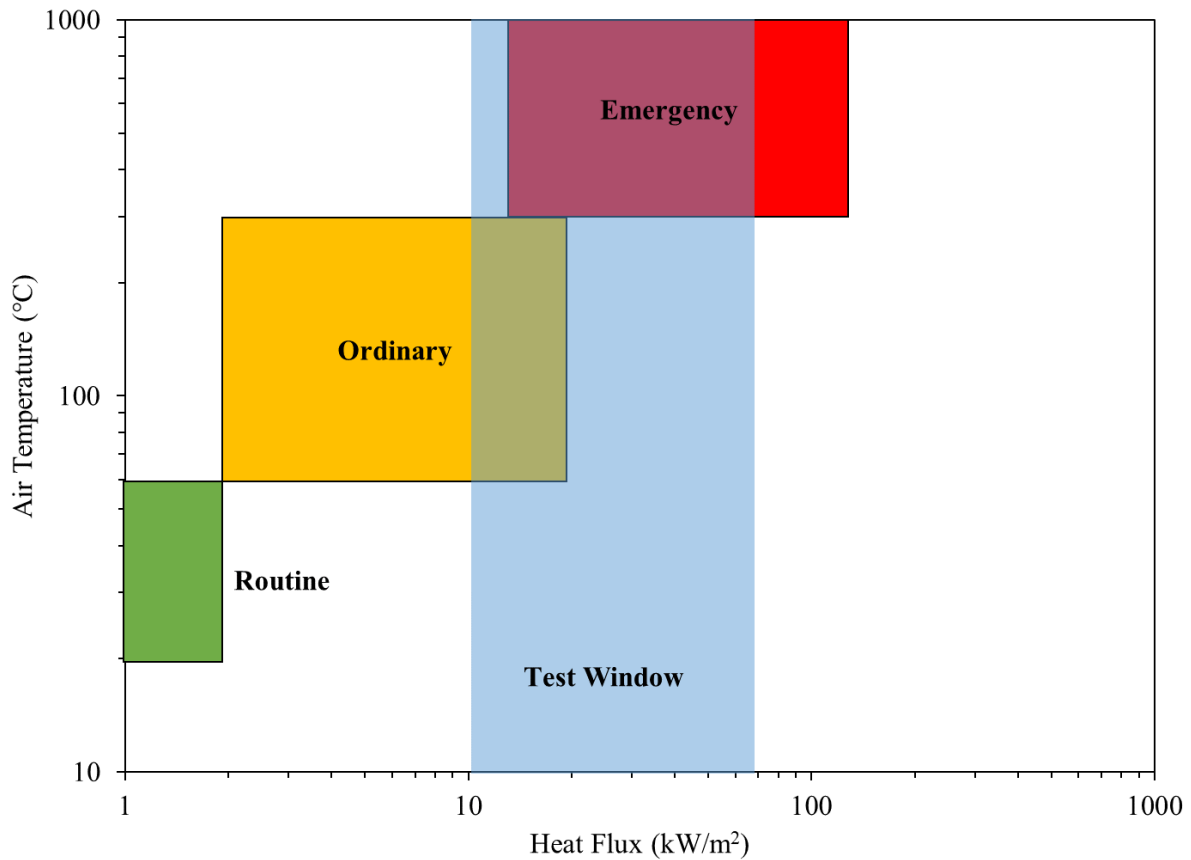


Figure 1.5 Classification Of Typical Firefighter Conditions. Test Window Indicates This Research's Tests (Adapted From Veghte 1988).

The intention of this research's aging component is to simulate typical heat flux situations under which materials readily age. To this end, exposures were selected with consideration to Veghte's classification of fire conditions.

1.3 Non-Destructive Testing

Destructive testing is often used to find a sample's material properties. Given the high cost of firefighters' protective clothing, even using small specimens of garments to carry out destructive tests to evaluate their properties can be very expensive. Therefore, finding a reliable way to measure material properties non-destructively would be beneficial.

There are several common approaches to non-destructive testing, typically through the use of imaging, light, and sound. At the University of Saskatchewan, research has been conducted in

the areas of colorimetry, Raman spectroscopy, and infrared spectroscopy (Thorpe 2004; Rezazadeh 2014). Infrared spectroscopy has been more extensively explored at the U of S (Thorpe 2004; Rezazadeh 2014; Fulton 2017; Ohalele 2020).

Near infrared light occupies the longer wavelength range of light beyond visible light. Visible light occupies at a wavelength range of approximately 400-700 nm, while the near infrared spectrum ranges is approximately 700-2500 nm. Typically, examining the NIR spectrum of a specimen is done by measuring the reflectance or transmittance at different wavelengths within the spectrum, with absorbance calculated from these results. In previous research at the University of Saskatchewan, all three of these measurement techniques have been correlated to tensile strength (Rezazadeh 2014; Fulton 2017; Ohalele 2020). As NIR spectroscopy was a minor factor in this research, only reflectance was measured in this study. This will be outlined further in Section 2.5.

In Fulton's (2017) and Ohalele's (2020) exploration of non-destructive tests, various NIR data analysis techniques were examined. The four correlation techniques they explored were:

- percent difference in absorbance,
- absorbance feature area,
- absorbance feature prominence, and
- normalized difference index.

Each of these approaches were found to have advantages and disadvantages, with promising results in the normalized difference index approach. This type of examination was not conducted in this research.

1.4 Protective Clothing Standard Tests

As previously mentioned, there are several standards that dictate the design of fire protective garments. These are set by governing bodies such as NFPA, ASTM, ISO, and CGSB. Within these standards bodies are several standards that affect this research. The most prominent of these standards will be mentioned in brief here.

For this research, NFPA 1971 (2013) is the most pertinent. This standard was established in 1973 as the "Standard on Protective Ensembles for Structural Fire Fighting and Proximity Fire

Fighting” (NFPA 1971, 2013). This standard outlines minimum design requirements for protective garments for various conditions and hazards such as thermal, physical, environmental, or bloodborne. The three key values of this standard are its outline of design requirements, performance requirements, and test methods for garments.

Another NFPA standard of importance to this research is NFPA 1851 (2020). This standard describes a standard operating procedure for firefighters to follow when inspecting and examining their ensemble. Since one of the aims of this research is to improve knowledge in understanding material degradation, this standard is an important reference for understanding how firefighters are currently addressing and managing in-use protective clothing.

1.5 Literature Review

This research is a continuation of a University of Saskatchewan project. As such, this literature review will supplement the previous work completed by Rezazedah (2014), Fulton (2017, and Ohalele (2020). A few works specifically related to this work will be highlighted that may have been covered by these researchers.

1.5.1 Aging Techniques

For any lab test, it is important to consider the real environment this clothing will be used in. Bessflug *et al.* (2020) explored soiled garments; varying the moisture conditions of the garments, abrading the garments, and exposing the garments to UV light to explore a simulated environment’s impact on the NIR spectroscopy. The soiling experiment utilized a charcoal rub which was added to the fabric in different levels. From this limited study, the researchers were able to differentiate between thermal aging and soiling. They recommend further exploration into this topic before definitive conclusions are drawn. Over the range considered, moisture content was found to have minimal impact on NIR spectroscopy. This relative humidity used was different from the tests conducted in this research. Abrasion testing did show a more significant impact on the tensile strength of the specimens. This testing, however, did not show up on reflectance NIR evaluation, which is expected as the thermal chemical change from thermal aging would make an impact on the NIR, while abrasion does not change the chemical structure. For the fabrics tested, UV had an impact on the tensile strength, but had less impact on NIR measurements. As was commonly mentioned in this article, further research is needed to confirm

these conditions for more fabrics to reach definitive conclusions. The work of Bessflug *et al.* (2020) is a great compliment to the present research in that it explores areas not covered here such as the impact of soiling and abrasion.

Outside of research at the University of Saskatchewan, there are several research groups exploring firefighter safety equipment ranging from full mannequin tests to material tests similar to those being conducted at the University of Saskatchewan. As this current research is a continuation of the general University of Saskatchewan project of thermally aged high-performance textiles, the following literature review will focus on research in recent years in thermal aging, non-destructive tests, and temperature modelling in the area of fire safety. Table 1.1 outlines selected examples of research on the effects of thermal aging and is a continuation of the literature reviews conducted by Rezazadeh (2014), Fulton (2017), and Ohalele (2020).

Table 1.1 Select Examples Of Research On Effects Of Thermal Aging Of Fabrics

Investigator(s)	Thermal ageing method	Duration	Parameters studied
Liu <i>et al.</i> (2021)	TPP tests at 30, 40, 50, and 60 kW/m ²	1-27 s	Developing thermal aging models based on on multi-linear regressions and artificial neural networks
Tian <i>et al.</i> (2020)	Heat Flux exposures at 30, 40, and 50 kW/m ² using a custom Meker burner apparatus.	17 s	Thermal shrinkage, mass loss, time to second degree burns based on air gaps
Dolez <i>et al.</i> (2019)	Convection oven 150-300°C	1-500 hr	Mechanical properties (tensile and tear strength), Thermogravimetric Analysis (TGA), and Fourier Transform Infrared (FTIR) spectroscopy

Table 1.1 Select Examples Of Research On Effects Of Thermal Aging (cont.)

Investigator(s)	Thermal ageing method	Duration	Parameters studied
Feng <i>et al.</i> (2019)	RPP tests at 20, 30, and 40 kW/m ²	30 s	Thermogravimetry, vertical burning tests, limiting oxygen index to compare thermal stability and flame retardancy. NIR spectroscopy between 800 and 2500 nm was also examined
Han <i>et al.</i> (2019)	TPP tests at 84 kW/m ²	4 s	Coating strength, ease of ice removal, and Scanning Electron Microscope(SEM) evaluation
Ormond and Gabler (2017)	Radiant heat flux of 0.2 cal/cm ² *s (8.4 kW/m ²)	10, 25, and 50 s	Trapezoidal Tear Strength, and FTIR spectroscopy
Collin <i>et al.</i> (2015)	In-service fire garments which received various exposures.	Various.	Visible-IR spectrum NDT using spectral absorptivity
Cui, Ma, and Lv (2015)	exposure from a quartz tube (6.5 and 9.7 kW/m ²)	5-30 min	Mechanical properties (tensile, tear strength and elongation at break), SEM evaluation, and FTIR-Raman spectroscopy

Table 1.1 Select Examples Of Research On Effects Of Thermal Aging (cont.)

Investigator(s)	Thermal ageing method	Duration	Parameters studied
Arrieta <i>et al.</i> (2010)	extended exposure, temperatures from 190-320°C	from hours for high temperatures and weeks for low temperatures	Mechanical properties (breaking strength, thermal life), and FTIR
Rossi <i>et al.</i> (2008)	two exposures to 40 kW/m ² (quartz tubes) or 80 kW/m ² (Meker burner)	17-33 s	Required time for, 12 or 24 °C temperature rise of a test sensor, and Mechanical properties (tensile, tear strength)

Fabric testing is often done as either a single layer or as an ensemble. When testing fabrics as an ensemble, consideration is given to the air gaps and how these contribute to the thermal protection of these high-performance fabrics. Tian *et al.* (2020) conducted an examination of high-performance textiles, examining tests of thermal shrinkage, mass loss, and time to second degree burns while varying air gaps between tests. They found that the inclusion of a 6.4 mm air gap improved thermal protective performance. However, they also found that these air gaps increased thermal shrinkage, discolouring, and mass loss. This presents an interesting balance any manufacturer of fire protective garments would have to consider in that increasing the air gap improves thermal protection but decreases the life of the garment overall. This present research does include ensemble testing, however, it is noted here that design does play a part in the impact thermal aging on garments.

An important consideration of fire protective garments is the impact of laundering on protective properties. Laundering is essential for this equipment as these garments are not exclusively used for thermal protection, but can see use in protection from biohazards, contaminants, and other related safety concerns. Horn *et al.* (2020) examined the change in the protective properties of firefighter garments that had been exposed to repeated simulated fireground exposures followed by 10, 20, 30, and 40 laundering cycles. For many of their tests, reduction of protection dropped more than one standard deviation when compared against a new garment. Yet, only outer shell tear strength dropped below the NFPA 1971 (2013) requirement after 40 cycles. No significant wear aside from this tear strength was noted between tests. They

speculate that increased damage resulted from the tumble cycles with the metal components of the garments. In a similar manner, Mayer *et al.* (2020) explored simulated aging and laundering cycles looking specifically at damaged caused by smoke particulates. They examined the chemical protective capabilities of personal protective equipment (PPE) using polycyclic aromatic hydrocarbons and compared different parts of the gear for their effectiveness. Their findings identified contamination in the neck region as higher than other regions, such as the chest with inconclusive results related to the laundering. Considering this research, it is recognized that thermal damage is not the exclusive type of aging that occurs on garments in service. Aging is cumulative, and even minor aspects of aging can have an impact on the safety of firefighters.

1.5.2 Non-Destructive Testing

The following is a brief look at recent works in NDT. For previous work in this area, please also see the literature reviews done by Rezazadeh (2014), Fulton (2017), Ohalele (2020), and Bessflug *et al.* (2020).

In an examination of the radiative properties of protective garments, Collin *et al.* (2015) explored the impact of high temperatures on in-service fire garments using the visible-IR spectrum with consideration to spectral absorptivity. These garments were acquired from fire and rescue services in France. Their findings showed that the mean absorptivities were close to 90%. With regard to this research, this shows an interesting alternative property of study using NIR spectroscopy that could be explored.

Outside of fire protection engineering, NIR spectroscopy has been applied in a number of different fields. One interesting study conducted by Huang and Yu (2019) examined a technique to identify cellulose, hemicellulose, and lignin content in flax fibres using NIR spectroscopy. At present, flax fibre composition is determined using the time consuming “wet chemical method” which uses chemicals that are harmful to the environment. With NIR spectroscopy, this composition can be determined in a matter of seconds. Using 215 spectra sets and FTIR spectrometry in conjunction with partial least squares (PLS) and principal component regression (PCR) analysis techniques, they were able to correlate results to the composition of these fibres accurately.

In a similar study to Huang and Yu (2019), Li *et al.* (2020) explored the identification of plant and chemically dyed cotton fabrics using NIR spectroscopy. At present, there is no effective technique for identifying between dyed textiles using this technique. Li *et al.* applied NIR spectroscopy in conjunction with soft independent modelling of class analogy (SIMCA), PLS, and PCR for the pattern recognition of 267 specimens, with a calibration set of 69 specimens. All three methods provided strong correlation and predictability for these fabrics. Overall, they found that through the use of this approach, one could quickly and non-destructively identify the types of dye used on cotton fabrics.

In a similar goal as this research, Feng *et al.* (2019) examined the effects of thermal degradation on the performance and radiative properties of Nomex IIIA fabrics. The researchers used thermogravimetry, vertical burning tests, and limit oxygen index methods to compare the thermal stability and flame retardancy of the two fabrics at their virgin and pyrolyzed states. These specimens were then examined using NIR spectroscopy in a wavelength range of 800 to 2500 nm. The results showed that the reflectance and transmittance of the fabrics were higher in their virgin state, but their radiant protective performance was lower in their charred state. This data could be used to estimate the continuing performance of firefighters' protective fabrics after thermal exposures during firefighting operations.

1.5.3 Aging Models

Arrieta (2011) examined the effects of aging on the properties of Kevlar-PBI blended fabrics. Arrieta examined the impact of hydrolytic, photochemical, and thermal aging through the use of non-destructive test methods such as XRD and Raman spectroscopy. All these approaches were blended with the potential use of aging models to predict the damage these fabrics experienced. Arrieta's aim was to model the effect of temperature, humidity, and UV light. Their testing was based on yarn strength (as opposed to this research's use of 35 mm wide fabric strips). Arrieta's specimens were aged at temperatures ranging from 190 to 320°C, with durations ranging from hours to days.

Within the XRD and Raman results, Arrieta found an interesting contradiction in results, with XRD indicating increased crystallinity with thermal aging, while Raman indicating reduced crystallinity. They posit that there are two different processes occurring simultaneously, one of an increase in the size of crystallites in the fibre axis, and an increase in gap separation in

lamellar crystallites, causing a non-measurable reduction of crystallinity. Differential thermal analysis indicated a reduction in glass transition temperature of PBI, which points to a decrease in molecular weight. Though these types of approaches were not used in this research, this type of study could be an interesting avenue to explore in the materials researched at the University of Saskatchewan.

In a similar research project as Arrieta (2011), Dolez *et al.* (2019) expanded upon the use of an Arrhenius aging model on Kevlar-PBI blended fabrics to apply a quantitative technique for comparing thermal aging and mechanical performance. This study took a similar thermal exposure approach to Arrieta in that they examined exposures between 150 and 300°C and for durations up to 500 hr. They compared the Arrhenius aging model to the three-parameter Hill equation, one of the common models used for fitting sigmoid curves. These parameters include temperature, time rate, the degradation midpoint time, and the ultimate tensile strength. In their comparison, they found good correlation between the Arrhenius model and the Hill equation. However, they posit that none of the seven fabrics they examined displayed ideal behaviour for prolonged fire protection. This idea comes from the hope that this comparative study would assist with the optimization of the composition of fabrics based on typical conditions gear experiences.

Fire material degradation modeling is a valued area of research outside of textile sciences. Structural fire engineering has particular interest in models as full-scale tests are expensive. Rippe and Latimer (2021) developed a post fire model for aluminum structures. Their study focused on aluminium alloys (AA6061) and low exposure material degradation. Their model focused on temperature-time modeling and utilized Arrhenius kinetic models. This model was developed using experimental tests at 50 and 60 kW/m² for 20 min exposures, water quenching and finally loads in 4-point bending. Their temperature-time findings were accurate within 25°C during transient response, and 10°C during steady state response as well as peak bending predictions accurate within 8% of the experimental values. Ultimately these studies indicate that it is possible to predict material degradation. In contrast to Arrieta's (2011) use of Arrhenius kinetic modelling, this approach used a much higher temperature exposure.

Kinetic parameters for solid state degradation (which is typically done using Arrhenius modeling) are typically estimated from thermogravimetric analysis (TGA) results of a material.

To assist with modelling new fabrics, Bruns and Leventon (2020) endeavoured to create an automatic method of pulling these material properties directly from TGA data. Through the use of a script applied on TGA data, they were able to calculate the kinetic parameters for a material. They verified this approach against the TGA data from the manufacturer for one and two reaction mechanisms using Nylon 6,6, PVC, and PU foam. This study has interesting implications on the research project present at the University of Saskatchewan as parameter data could be found for a new fabric rapidly. This would allow for a material to be tested using TGA, which then could calculate the kinetic parameters for a material which could then provide an Arrhenius model for thermal degradation.

Arrhenius kinetic degradation modelling is a well-established material aging prediction approach. Outside of Arrhenius kinetic modelling, there are a number of alternative ways to model thermal degradation. Liu *et al.* (2021) approached thermal aging modelling of Kevlar-PBI blended fabric ensembles using multi-linear regressions and artificial neural networks. Experiments for this study were conducted using a thermal protective performance tester (TPP) at exposures of 30, 40, 50, and 60 kW/m² at durations ranging from 1-27 s. Their approach is similar to this research for exposures, but differs in that they used ensembles of fabrics and much shorter durations. Between the use of neural networks and multi-linear regressions they found better correlation in neural network data when comparing thermal aging to tensile strength. Neural network predictions had an R² value of 0.88, and an RMSE of 96.91. Their predictive equations were first order comparisons similar to the correlations discussed in Section 4.1. As their model resides within the first half minute of tests with multiple time steps, there is better correlation as the initial tensile strength loss is being captured.

1.6 Scope And Objectives

As this is the fifth study in this project, some of the premises and aims of this research are reflections of what has come before. Overall, this research posits that there are correlations that can accurately portray the effect of heating on tensile strength and other material properties using temperature, heat flux, and duration. One of the main purposes of this research is to develop correlations, which was the primary driving factor behind the selected experiments. The objectives are to develop correlations of the effects of heating on tensile strength that account for both temperature and duration, and in doing so investigate the effects of multiple aging

mechanisms on tensile strength and other material properties. These correlations are a useful tool in identifying the end of life of these protective garments, but are limited in application to tested materials.

This study also expanded on this project's material library to include an additional fabric. This research also explored several techniques for finding curves and correlations for tensile strength, with the most successful presented here.

1.7 Contributions Of This Research To The Literature

As outlined in Section 1.4, there are several projects happening in relation to fabric aging models based on thermal exposures. Many of these models heavily rely on the Arrhenius Kinetic degradation model. Several of these studies are predominately focused at (relatively) low thermal exposures, with durations ranging up to days with extrapolation. This research occupies a higher range of exposures and lower durations for its correlation approach. Aside from these correlations, this research does some limited exploration into non-destructive tests using NIR spectroscopy. Because of the exposures and durations selected in the test matrix, this allowed for an examination of exposure and duration points that have similar NIR wavelength results. Finally, this research contributes to the growing number of studies on thermal exposures on high performance textiles. To this end, temperature data was logged and organized with relationship to the tensile strength.

1.8 Outline Of Thesis

This research begins with an examination of the methods used in the experiment (Chapter 2), including an exploration of the material characteristics, experimental matrix, specimen preparation, methods used for thermal aging, NIR spectroscopy, and tensile testing. Chapter 3 outlines the analysis of the collected data, with examination on the temperature measurements, the NIR spectroscopy, and the tensile strength. Chapter 4 presents the three correlations developed in this research, their graphical representation, their accuracy and limitations, and a comparison between these correlations. Chapter 5 concludes this work, outlining the main findings of this thesis as well as future goals that could be explored.

2.0 Methods And Materials

The following chapter will discuss the fabrics used in this research, how they were prepared, and the experimental techniques employed. The three components of the experimental method, which are thermal aging, NIR spectroscopy, and tensile strength testing, are outlined after the discussion of the materials.

2.1 Outer Shell Textile Specimen Characteristics

The two fabrics examined in this research are Kombat Flex (KF) and Ripstop Natural (RSN). These are two Kevlar-PBI blended fabrics with different specifications that are used for the outer shell material of firefighter garments, because of their flame and abrasion resistance, and other properties. The definitions of warp, weft, and selvedge can be found in Figure 2.3.¹ Ripstop Natural is a heavier fabric which has a ripstop pattern within the weave. This pattern is designed to help improve abrasion resistance. Kombat Flex does not have this ripstop pattern but does have a 2/1 twill weave pattern (a type of weave pattern which passes the warp thread twice over the weft thread) which promotes abrasion resistance. Both fabrics have roughly the same blend of Kevlar and PBI, however Kombat Flex has a filament thread within 1/3rd of the yarns. This yarn is a z twist weave (where the fibres have been twisted to form the shape of a “z” in the yarns) of Kevlar and the spun blend. Table 2.1 shows some relevant fabric properties for Kombat Flex and Ripstop Natural that were gathered for this research. Ripstop Natural properties were obtained using equipment at the University of Alberta Department of Human Ecology. Material density measurements were averaged over five specimens and made using 50 nm die-punch disks using a Denver M310 (Denver, CO) electronic scale in accordance with ASTM D3766 (2018) (Fulton 2017). Thickness was measured with an average of five specimens using a 1 kPa pressure-foot driven Custom Scientific Instrument CS-55-225 (CSI, Whippany, NJ, USA). Yarn structure and patterns were analyzed using a Seiwa Optical Correct Tokyo® No.628471 microscope (Fulton 2017). Properties for Kombat Flex were taken from the manufacturer’s datasheets (TenCate 2014).

¹ For further detail into the definition of these and other textile terms, please see Collier *et al.* (2009).

Table 2.1 Ripstop Natural And Kombat Flex Fabric Properties

	Ripstop Natural*	Kombat Flex**
Mass per Unit Area (g/m²)	272	235
Average Thickness (mm)	0.69	0.72
Fabric Count	17 warp x 14 weft	19 warp x 19 weft
Weave	Plain	2/1 Twill
Yarn Structure	zzS twist	z twist (both filament and spun)
Blend (Kevlar/PBI)	60% / 40%	70% PBI/Kevlar spun, 30% Kevlar filament

*(Ohalele 2020, Fulton 2017)

** (TenCate 2014)

Previous research at the University of Saskatchewan has used materials with a variety of blends of Nomex®, Kevlar®, and PBI. The more recent research (Ohalele 2020; Fulton 2017) has been focused on Kevlar®/PBI blended materials with Ripstop Natural, Ripstop Black, and PBI Max. Kombat Flex was examined in addition to Ripstop Natural as a new material for this research. Using specimens from Ripstop Natural allowed this research’s results to be compared more directly to previous research, as well to use previous data when developing correlations.

2.2 Experimental Matrix

With the previous research conducted at the University of Saskatchewan, particularly by Fulton (2017) and Ohalele (2020), there are several sets of data which show that material properties are affected by both high heat fluxes and the length of exposure to these heat fluxes. Since Kombat Flex is a new addition to this research, the testing matrix for this material was much more extensive. There was a limited supply of Ripstop Natural left in stock, so a more selective matrix was created for that material. A change from previous research at the University of Saskatchewan is an extension of exposure duration. Ohalele’s (2020) previous tests were done at 10, 20, 30, and 40 kW/m² for durations of 60, 90, 120, and 300 s. This research will look at exposures ranging up to 1200 s (20 min) and as low as 15 s in some cases. Figures 2.1 and 2.2 present the combined test matrix for Kombat Flex and Ripstop Natural across Epp, Fulton, and Ohalele’s research. Tables 2.2 and 2.3 present the test matrices as lists.

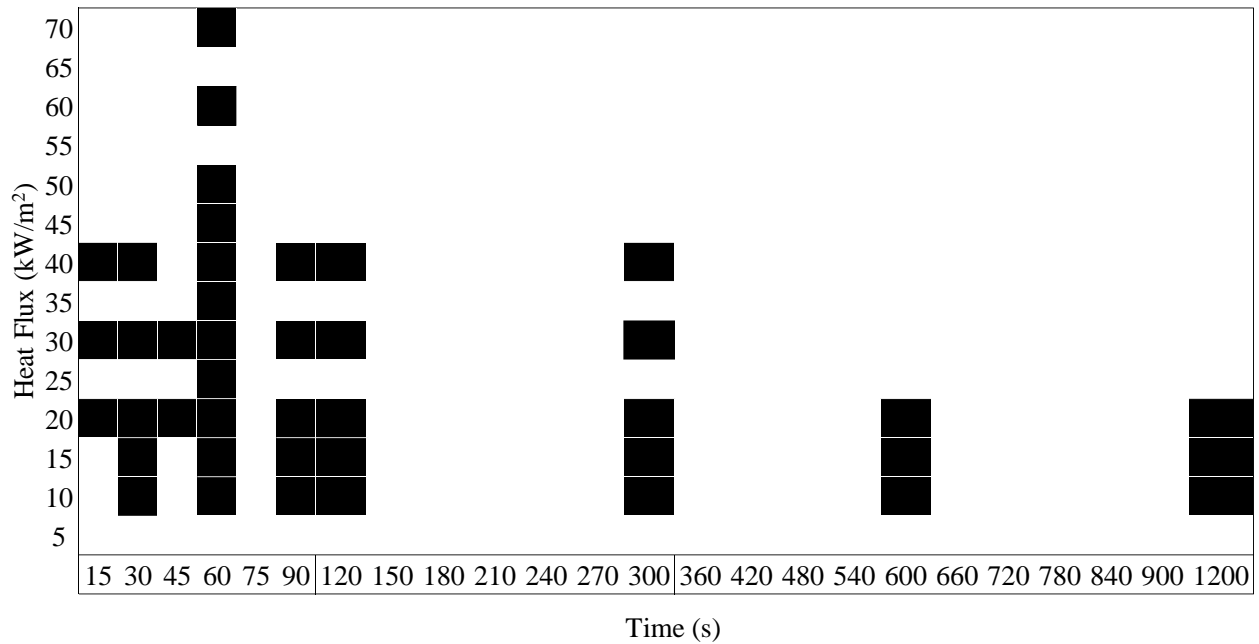


Figure 2.1 Kombat Flex Test Matrix. Squares Represent Exposures Tests Were Conducted

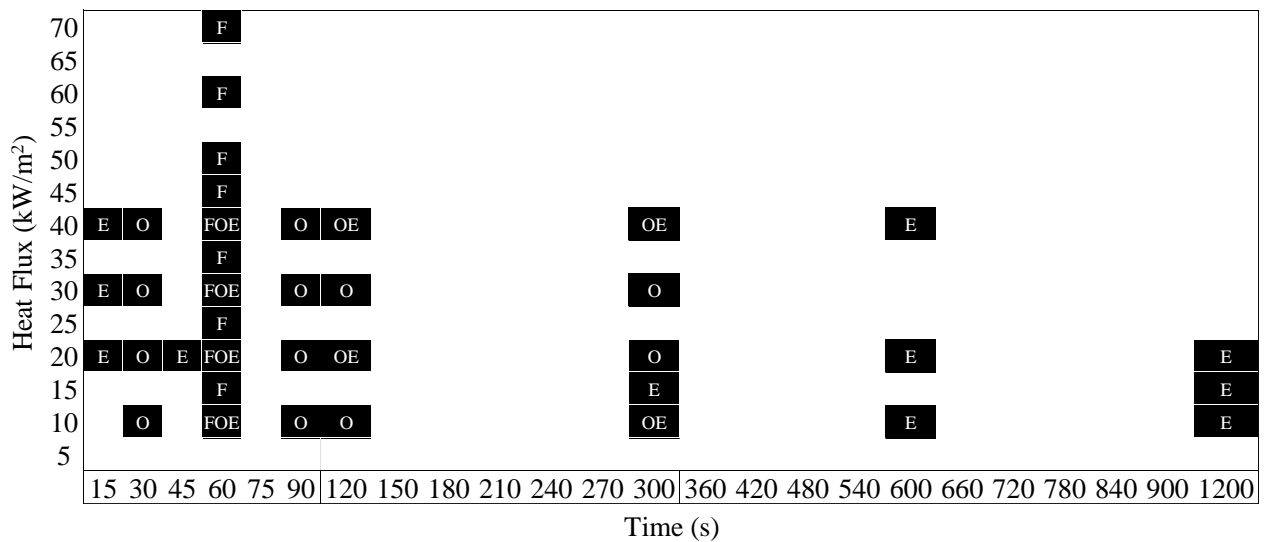


Figure 2.2 Ripstop Natural Test Matrix. “F” Represents Exposures Tested By Fulton (2017), “O” Represents Exposures Tested By Ohalele (2020), And “E” Represents Exposures Tested In This Research.

Table 2.2 Kombat Flex Test Matrix As List

Heat Flux (kW/m²)	Time (s)
10	30, 60, 90, 120, 300, 600, 1200
15	30, 60, 90, 120, 300, 600, 1200
20	15, 30, 45, 60, 90, 120, 300, 600, 1200
25	60
30	15, 30, 45, 60, 90, 120, 300
35	60
40	15, 30, 60, 90, 120, 300
45	60
50	60
60	60
70	60

Table 2.3 Ripstop Natural Test Matrix As List, With Epp's, Ohalele's (2020), And
Fulton's (2017) Data

Heat Flux (kW/m²)	Fulton Time (s)	Epp Time (s)	Ohalele Time (s)
10	60	60, 300, 600, 1200	30, 60, 90, 120, 300
15	60	300, 1200	-
20	60	15, 45, 60, 120, 600, 1200	30, 60, 90, 120, 300
25	60	-	-
30	60	15, 60	30, 60, 90, 120, 300
35	60	-	-
40	60	15, 60, 120, 300, 600	30, 60, 90, 120, 300
45	60	-	-
50	60	-	-
60	60	-	-
70	60	-	-

The purpose of the finer time steps at the shorter durations was to improve understanding of the thermal response of these fabrics right after exposure begins. Some of the short duration tests will be within the transient heating phase, which will become clear in the temperature traces presented in Chapter 3. This was done to help strengthen some of the correlations developed (see Chapter 4). Similarly, longer duration tests were conducted to improve correlations.

For each of these exposures, three tests were conducted with the exception of Kombat Flex at 60 kW/m² and 60 s, which was done nine times. Three tests were done to confirm consistency within each exposure. Likewise, for tensile strength testing, three tests were conducted per exposure. For both thermal aging and tensile testing this allowed for standard deviation to be calculated.

2.3 Specimen Preparation And Conditioning

Specimen preparation followed the same methods previously established in this research project (Fulton 2017; Ohalele 2020). This was done so that the experimental results from this research could be directly compared to previous research. The following outlines how specimens were prepared and conditioned.

2.3.1 Specimen Preparation

For both fabric samples, the material comes in fabric rolls, as represented in Figure 2.3. To ensure the specimen were randomly selected from the sample rolls, the rolls were unravelled, labelled, photographed, cut, and then shuffled. By labelling prior to cutting, a specimen could be referenced to its location on the roll, if needed.

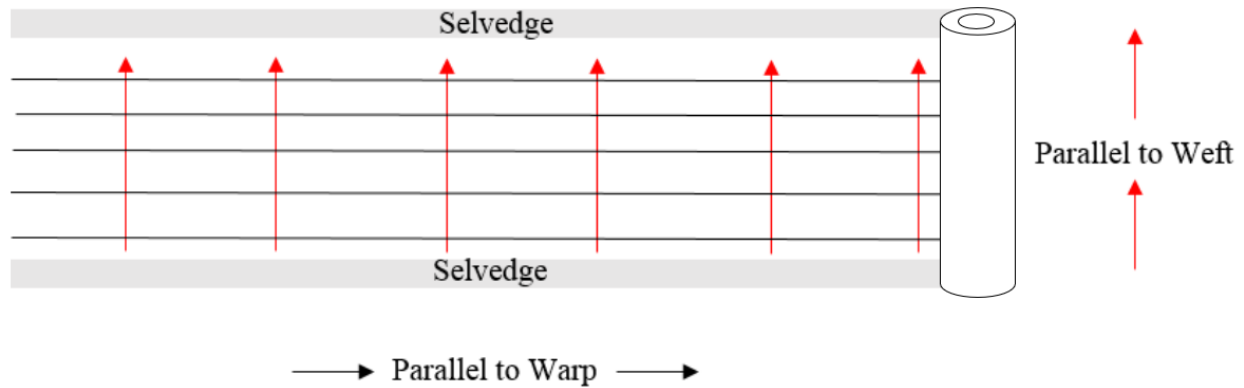


*Figure 2.3 Representation Of The Warp And Weft Of The Fabric Rolls
(Adapted From Fulton 2017).*

Samples were cut into 150 mm by 145 mm rectangles, with the longer edge in the warp direction. The warp direction was carefully noted as this would be the direction of tensile testing. Figure 2.4 represents the exposure window of these rectangular specimens. This figure also shows how these specimens were cut when they were tested for tensile strength. This exposure window is the area under which the cone calorimeter exposes the fabric to elevated temperatures. Figure 2.10 is a good representation of this exposure window.

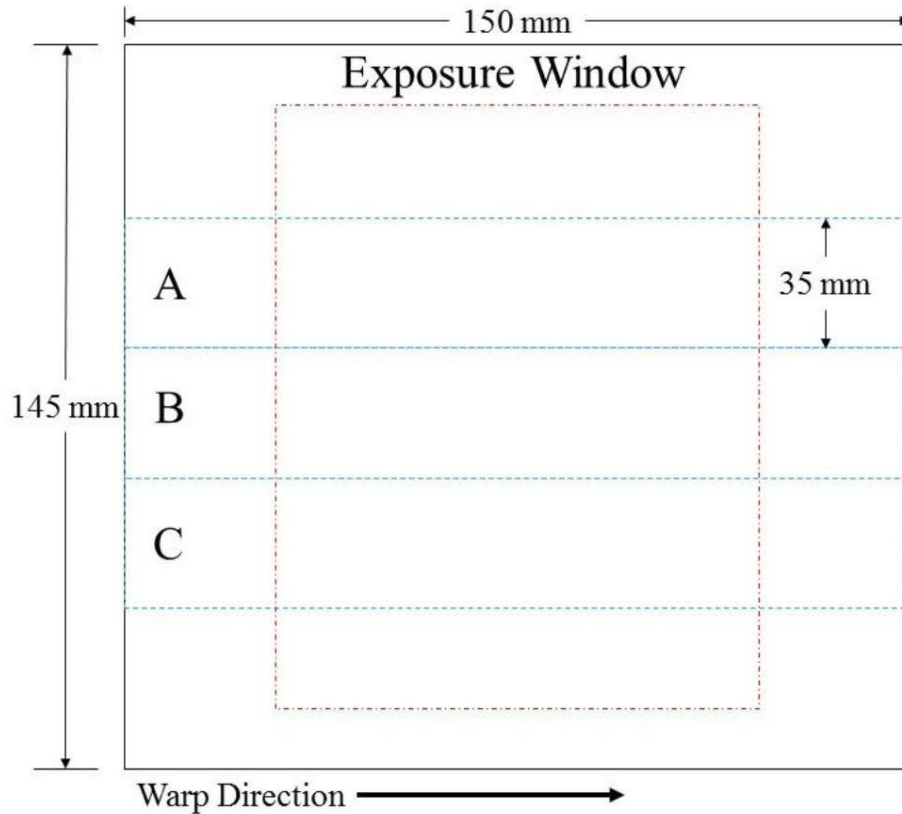


Figure 2.4 Fabric Exposure Window, With Representation Of The Tensile Test Strips (Fulton 2017).

2.3.2 Specimen Conditioning

The moisture content in a specimen can have a large impact on its thermal response. To control this, specimens were placed in a conditioning chamber controlled at $22 \pm 2^\circ\text{C}$ and $65 \pm 5\%$ relative humidity (RH) (ASTM D1776, 2020). Figures 2.5 and 2.6 show an example of the conditioning chamber used for this portion of the experiment. These conditioning chambers used a solution of Magnesium Chloride (MgCl) with a concentration of 0.6-0.8 g/L for this purpose. This solution was prepared as outlined in ASTM E104 (2020). All specimens were conditioned for a minimum of 24 hours before thermal testing.



Figure 2.5 The Conditioning Chamber Used For Preparing The Specimens For Thermal Exposure

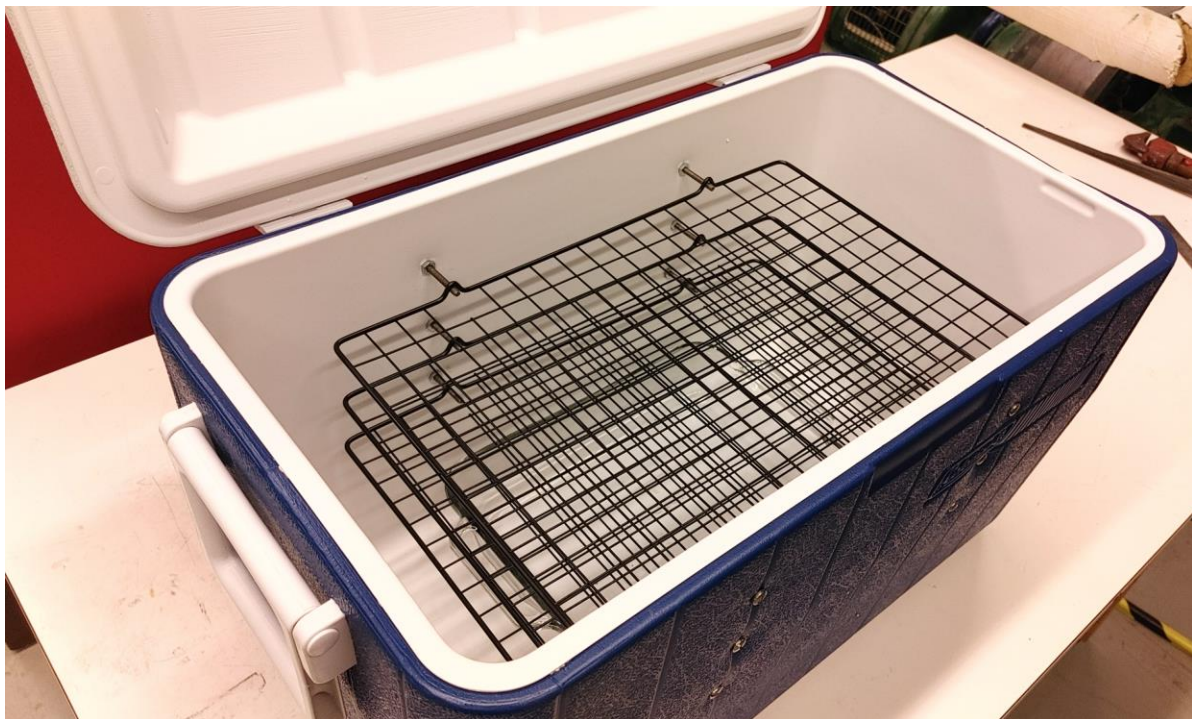


Figure 2.6 The Inside Of The Conditioning Chamber.

After thermal aging, specimens were reconditioned in a much larger conditioning chamber to the same standard (ASTM D1776, 2020). This chamber was selected due to its size, allowing for NIR testing to be conducted rapidly. This chamber is located at the College of Agriculture Controlled Environment Facility (Phytotron). This is slightly different from previous research wherein specimens were transported in plastic bags from the conditioning chamber in Figure 2.5 to the NIR Spectrophotometer for testing. All specimens were conditioned for a minimum of 24 hours before NIR testing. Transport between these conditioning chambers and the NIR Spectrophotometer was done by placing the specimen into the conditioning chamber in Figure 2.5 and moved to the laboratory with the NIR equipment to maintain the conditions up to the point of the NIR test.

At the University of Saskatchewan's Phytotron facility, the specific chamber used was a Conviron PGR15 (Conviron, Winnipeg, Manitoba) capable of relative humidity control of $\pm 3\%$ (additive only), and a temperature control of $\pm 0.5^\circ\text{C}$. This much larger conditioning chamber was selected to better streamline the NIR tests. This chamber is pictured in Figure 2.7



Figure 2.7 Loaded Conviron PGR15 Conditioning Chamber

2.4 Thermal Aging

For the purposes of this research, the cone calorimeter (Fire Testing Technologies, East Grinstead, West Sussex, UK) was selected for thermal exposures. The cone calorimeter is an instrument designed for small-scale material fire behaviour testing, described in ASTM E1354 (2022). The primary purpose of the cone calorimeter is to measure heat release rates using changes in the concentrations of oxygen, carbon dioxide, and carbon monoxide in combustion products (Dewaghe *et al.* 2011). The heating element is a conical heating circuit which is controlled by three thermocouples evenly distributed around the conical heating circuit. The cone is capable of producing heat fluxes up to 100 kW/m^2 at a distance of 25 mm. For this research, a water-cooled Schmidt-Boelter heat flux gauge (GTW-10-32-485A, Medtherm, Huntsville, USA) was used to set the heat flux for each of the tests. Prior to testing, a calibration of the cone was conducted to ensure accurate measurements were being taken. For data logging, the cone calorimeter uses an Agilent 34970 data acquisition system (Agilent Technologies Inc, Santa Clara, USA) paired with an HP 34970A Multiplexer (Hewlett-Packard Company, Palo Alto, USA). The cone has been equipped with an air-cooled shutter system that minimizes pre-heating of the specimens. Specimens are mounted in a fabric specimen holder that was fabricated for this research project (Torvi *et al.* 2016). Temperature data was captured using a Minolta Cyclops 300bAF infrared thermometer (Minolta, Dronfield, UK), using an emissivity of 0.9, logging at an interval of 0.1 s for each exposure. The Minolta infrared thermometer was positioned at a distance of 55 ± 5 cm from the back of the specimen, aimed at the centre (or just above if a thermocouple was used). Additionally, video footage of all exposures was captured using a Canon Vixia HF R500 video camera (Canon, Brampton, Ontario, Canada) for later reference. Figure 2.8 shows the cone calorimeter, the video camera, and the IR camera setup used in this experiment. Figure 2.9 shows the heating circuit and some of the key dimensions.

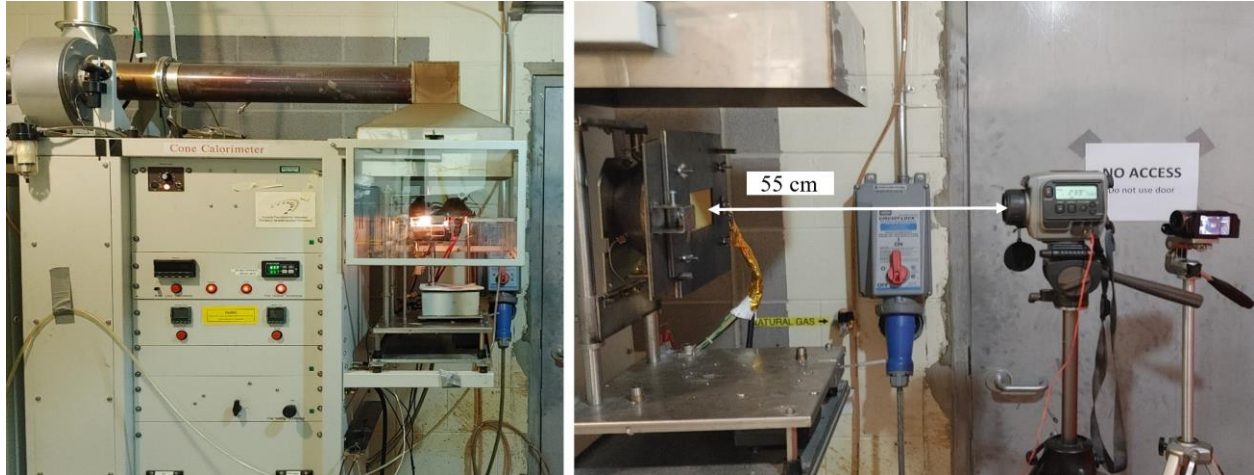


Figure 2.8 The Cone Calorimeter (Left) And The Vertical Specimen Setup (Right)

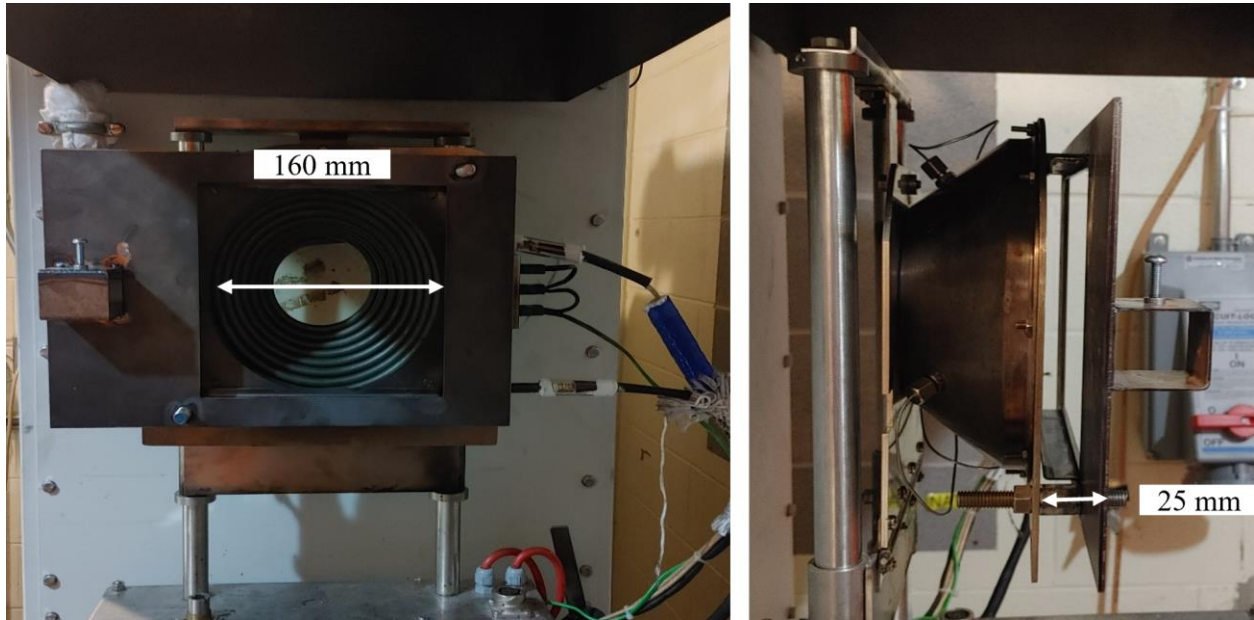


Figure 2.9 The Cone Calorimeter With The Specimen Holder

For this experiment, the cone calorimeter was set up in a vertical orientation. The specimen holder was adjusted to a consistent distance of 25 mm between the heating circuit and the specimen. Figure 2.10 shows the fabric specimen holder during an exposure with a specimen of Kombat Flex. In this figure, notice the darkening of the fabric from the heat as well as the off gassing from the fabric rising above the fabric. Dimensions in this figure are for the window on the exposed side of the specimen.

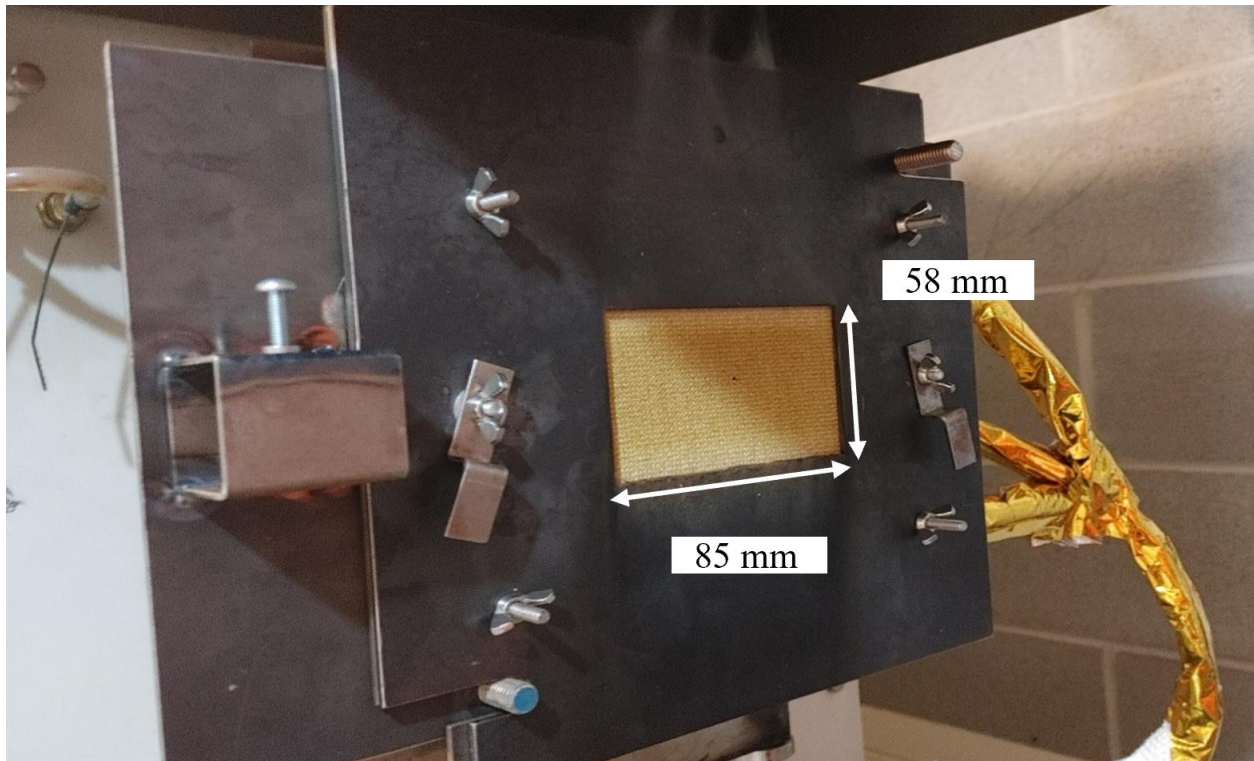


Figure 2.10 The Cone Calorimeter With A Specimen Of Kombat Flex, With Dimensions For The Exposed Side Of The Fabric.

There are several different types of thermal aging equipment that could have been used for this research. The cone calorimeter was selected, not only to be in line with previous research at the University of Saskatchewan, but also because of the cone calorimeter's consistent exposure across the fabric window. Previous research conducted on the cone calorimeter's heater showed that it is capable of a consistent heating range of $\pm 2 \text{ kW/m}^2$ across the specimen exposure window at an exposure of 35 kW/m^2 (Rezazadeh 2014). Figure 2.11 shows the exposure heating consistency across a larger area, where the exposure window for the specimens would reside within the centre area of this representation.

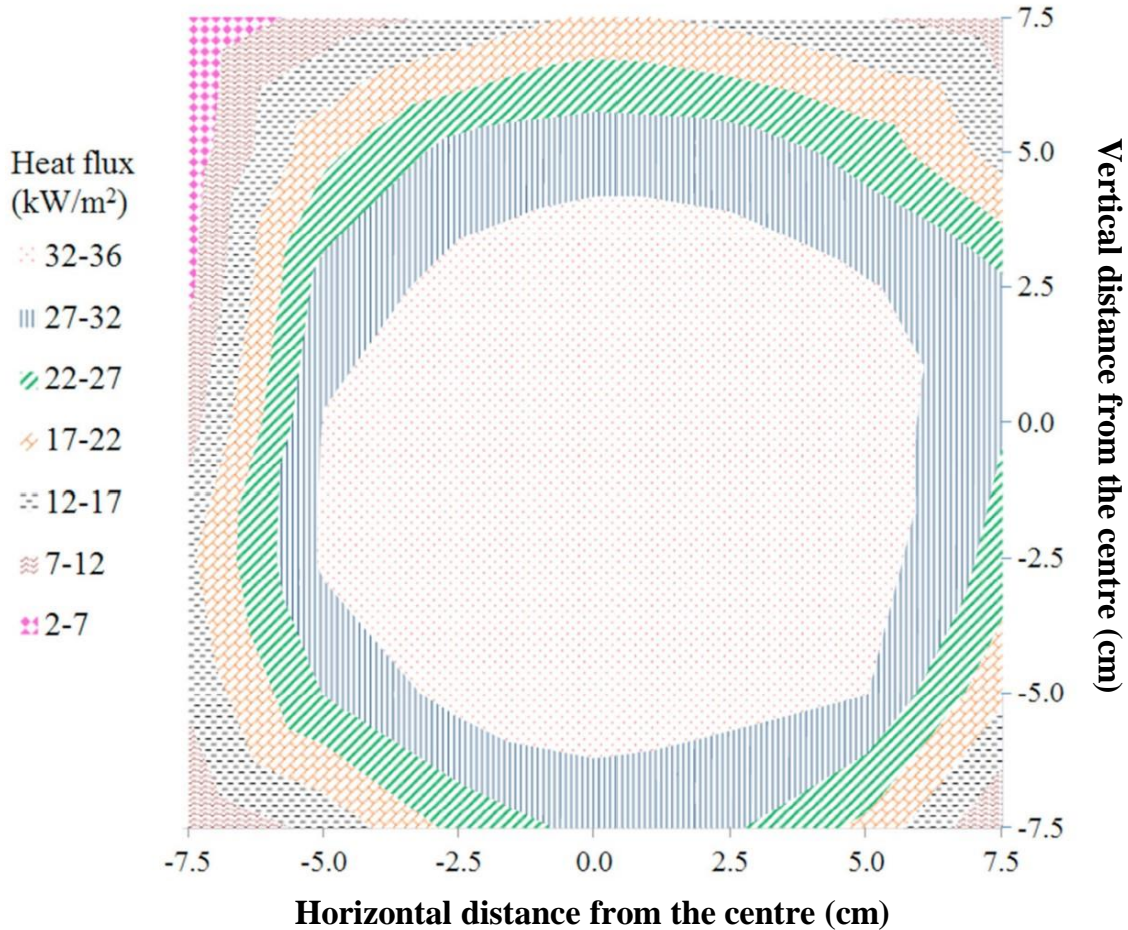


Figure 2.11 Distribution Of 35 kW/m² At A Distance Of 25 mm Under The Conical Heating Circuit (Adapted From Rezazadeh 2014)

During thermal exposures, mass loss and temperature data were gathered to characterise the specimens. Mass was measured prior to an exposure as well as right after a test. This was done using an Ohaus Adventurer™ Scale (Ohaus Corp, Pine Brook NJ, US). Mass measurement results can be found in Appendix A. Intermittently, IR photographs were taken to capture the thermal variance across the exposure window using a FLIR E60 (FLIR Systems, Inc, Wilsonville OR, US). Figure 2.12 shows an example of Ripstop Natural with a thermocouple attached close to the centre. Notice the defined ripstop pattern in the fabric, as well as the slight off gassing visible above the exposure window.



Figure 2.12 FLIR Photo Of Ripstop Natural With Thermocouple And Off Gassing

In an initial set of tests, temperature measurements were conducted using both the IR camera and thermocouples sewn to the front and back of the specimens. This was done to validate the IR temperatures used for the rest of the tests. The thermocouples used for this were 36-gauge AWG Type K thermocouples, and are visible in FLIR photo in Figure 2.12. They were sewn to the specimens using off-threads from the specimens themselves, and were spaced so they were not directly on top of each other.

Each of these temperature measurement techniques produce slightly different results that are tied to how the measurement is taken. For example, the IR thermometer would measure the average over a window, and due to the nature of the material, would represent the temperature of the fabric structure within the window, rather than just the back surface of the fabric (Torvi 1997). Further, the thermocouples are measuring at the point where the junction contacts the material. For the purposes of this research, these differences are adequately small to not be a concern.

2.5 NIR Spectroscopy

After thermal aging, all specimens were scanned with visible-near-infrared (Vis-NIR) spectrophotometer to measure the reflectance of the aged material. Previous research had

measured both reflectance and transmittance, with absorbance calculated (Fulton 2017; Ohalele 2020). Though NIR spectroscopy was not explored in detail in this research, tests were still conducted for completeness. It has been established through the work of Rezazadeh (2014) as well as confirmed by Fulton (2017) and Ohalele (2020) that there is a correlation between NIR spectral measurements and tensile strength. This data will be useful in the development of non-destructive techniques for measuring the tensile strength of fire protective garments.

To measure the NIR spectrum, an Agilent Technologies Cary Series UV-Vis-NIR Spectrophotometer (AgilentCary 5000, Palo Alto, California, USA) was used in reflectance mode using the diffuse reflectance accessory (DRA) over a wavelength range of 400 nm to 2500 nm (Figure 2.13). This range encompasses most of the near infrared range as well as visible light. Baseline zero calibrations were performed prior to testing, and were done using a SRS-75 spectralon reference (Labsphere, North Sutton, NH, USA). Table 2.4 shows the settings of the spectrophotometer parameters used in these tests. Figure 2.13 shows the spectrophotometer used in this research.

Table 2.4 Spectrophotometer Scanning Parameters

Scanning Parameter	Value
Slit height	Reduced
Beam mode	Double
Start wavelength range	2500.000 nm
Stop wavelength range	400.000 nm
Scan rate	600.000 nm/min
Data interval	1.000 nm
Source changeover	350.00 nm
Detector changeover	800.00 nm
Grating changeover	800.00 nm
Spectral bandwidth (SBW)	2.000 nm
Baseline	Zero/baseline correction
Spot size	12.5 mm Height x 7.5 mm Width
Mode	% Reflectance



Figure 2.13 The Agilent Technologies Cary Series UV-VIS-NIR Spectrophotometer

2.6 Tensile Testing

After NIR spectroscopy, specimens were selected and sent to the University of Alberta where tensile tests were conducted by Dr. Batcheller and their team using an Instron 5565 (Illinois Tool Works Inc., Norwood, MA, USA). Figure 2.14 shows the Instron 5565 used for this research. Tensile strength testing was conducted in accordance with NFPA 1971 (2013) which specifies the standard ASTM D5035-11 (2019).



Figure 2.14 Instron 5565 At The University Of Alberta (Fulton 2017)

Test specimens were cut into 35 mm by 150 mm strips, with the thermally aged area covering the centre of each strip. Prepared specimens were subject to a 60 mm/min constant rate of extension, which is different from the standard 300 mm/min outlined in ASTM D5035-11 (2019). This was done to gather more detailed information during failure (Fulton 2017). The jaws of the Instron grip area measures at 25 mm by 75 mm. Specimens were consistently mounted to make full contact with this area. As was the case in previous research, some of the fabric types would slip in the typical rubber faced jaws (Rezazadeh 2014; Fulton 2017; Ohalele 2020). Specimens of Kombat Flex fabric experienced this issue, while Ripstop Natural performed well using the rubber grips. In line with previous experiments with PBI Max, the jaws used for Kombat Flex were lined with 100-150 grit sandpaper to provide needed friction. A test

was considered complete when a 40% drop in an applied load was seen by a specimen (Ohalele 2020).

2.7 Thermogravimetric Analysis

An important aspect of this research is understanding the temperatures at which changes to the samples are expected to occur. To find these temperatures, thermogravimetric analysis (TGA) testing was conducted to observe how these materials degrade and to identify the points at which the reaction rate changes. These tests were conducted by Dr. Piyali Dhar and were carried out using a PerkinElmer TGA 8000 (PerkinElmer, Woodbridge, Ontario, Canada) in the Department of Chemical Engineering at the University of Saskatchewan. A TGA measures the change in mass as a function of temperature. It can be conducted in different atmospheric environments. The TGA tests conducted for this research were conducted in an air environment, with the temperature increased at a rate of 20°C/min to 900°C with a starting temperature of 50°C. These samples were not conditioned prior to testing. Figure 2.15 shows the TGA 8000 used in this research.

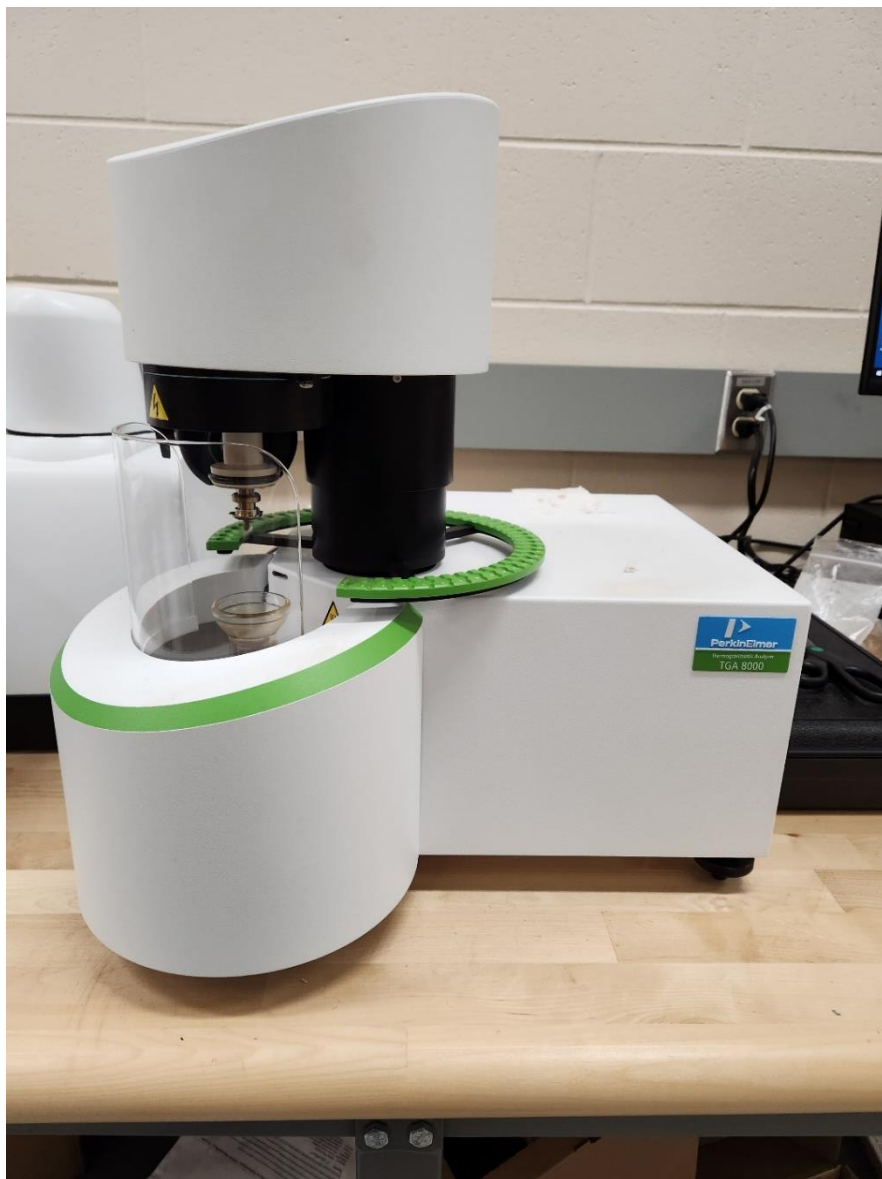


Figure 2.15 TGA 8000 In The Department Of Chemical Engineering At The University Of Saskatchewan

3.0 Experimental Results

The experiments in this research were conducted with the intention of establishing correlations to model degradation in material properties due to thermal aging. The exposures were selected to relate to previous research conducted at the University of Saskatchewan. This chapter presents results for temperature, NIR reflectance, and tensile strength. Correlations developed using these measurements and previous data will be presented in Chapter 4.

3.1 Compatibility With Previous Research

Because this research relies in part on previous data from the University of Saskatchewan, it is worth noting the differences in these experiments in handling specimens. Fulton (2017) laundered his Ripstop Natural fabrics before testing, while fabrics were not laundered before testing in Ohalele's (2020) experiments and in the present study. For Ohalele's (2020) tests, tensile strength testing of Ripstop Natural fabrics was done in the weft direction, which is different from this research and Fulton's (2017) research in which fabrics were tested in the warp direction. For Ripstop Natural, the weft direction has seven threads for every nine threads in the warp direction. This resulted in Ohalele's tensile strength measurements being lower than measurements made by Fulton (2017) and in this research. To overcome this difference, all tensile strength data has been represented by tensile strength retention for the purposes of developing correlations.

Prior to any cone calorimeter tests, a new heating element was installed and calibrated. This included the replacing of the thermocouples in the cone itself. This was also done prior to Ohalele's research (2020). Each researcher (Ohalele 2020; Fulton 2017; Rezazadeh 2014) calibrated the cone using the same Schmidt-Bolter heat flux gauge, and so specimens would have been subjected to similar exposures for a particular heat flux.

3.2 Temperature Measurements

The following is a look at specimen aging, the temperature data collected during these tests, and a comparison between this temperature data and previous data sets.

3.2.1 Specimen Aging

Figures 3.1 (Kombat Flex) and 3.2 (Ripstop Natural) show the visual change of the fabric for each heat flux (kW/m^2) at 60 s.

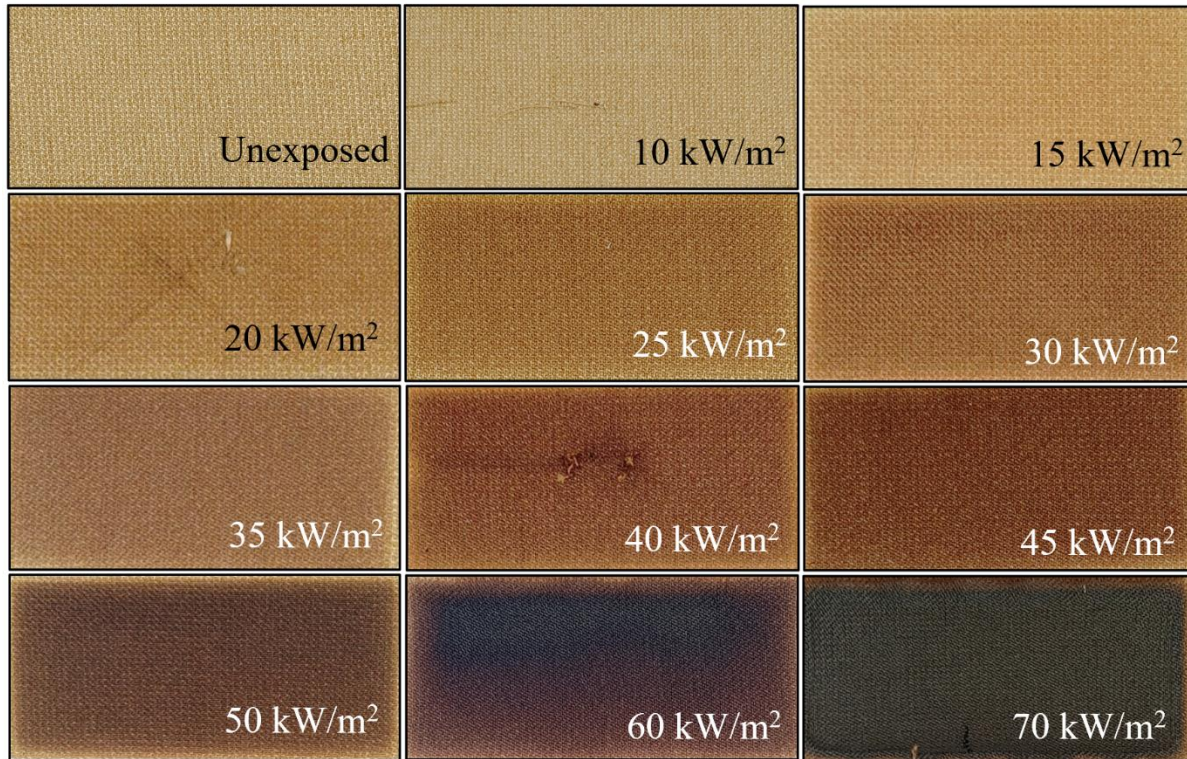


Figure 3.1 Kombat Flex Specimen Aging For Different Heat Flux Exposures At 60 s.

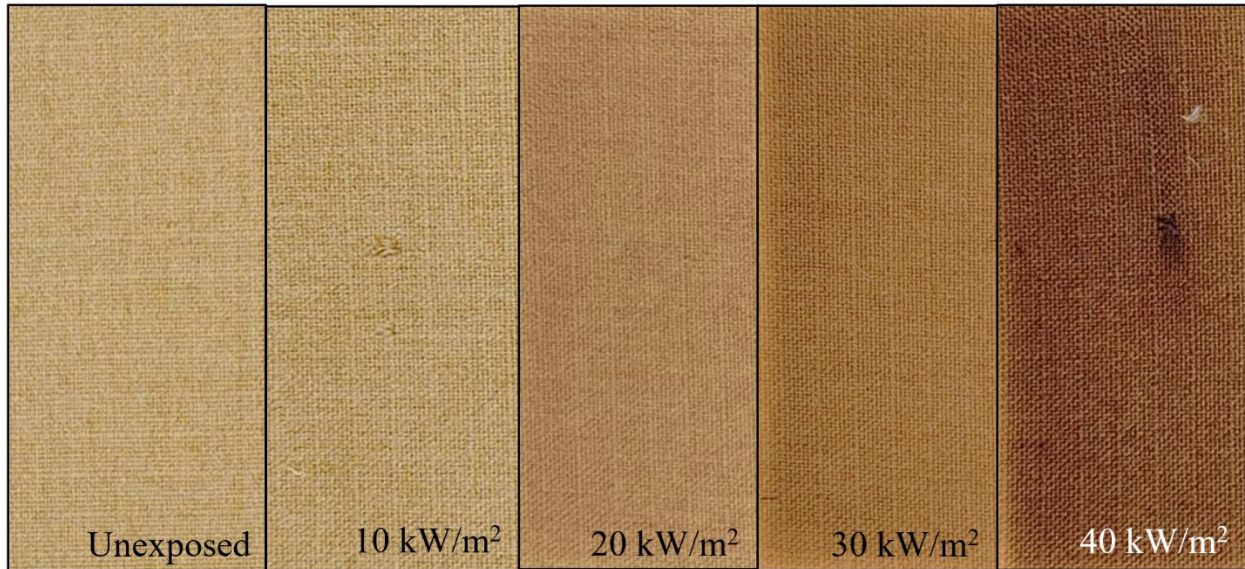


Figure 3.2 Ripstop Natural Specimen Aging For Different Heat Flux Exposures At 60 s

For both fabrics, an exposure to 10 kW/m² at 60 s had no impact on the visual appearance of the specimen. At 20 kW/m² however there is noticeable darkening. This darkening gradually continues until the specimen is blackened from ignition. The Kombat Flex specimen at 70 kW/m² is an example of a specimen that ignited prior to the end of the test. The 60 kW/m² exposure for Kombat Flex is an interesting situation where the specimen just began to ignite right at 60 s. A more thorough discussion of this can be found in Section 3.5, with a closer look at the NIR spectroscopic data for this exposure.

3.2.2 Temperature Measurements

To validate temperature tests, IR tests were first compared against thermocouples attached to the back of the fabric specimens. These thermocouples were sewn onto the fabric using threads pulled from the fabric itself. Figure 3.3 shows the consistency between the temperatures measured using the IR thermometer and thermocouples at exposures of 10 and 40 kW/m².

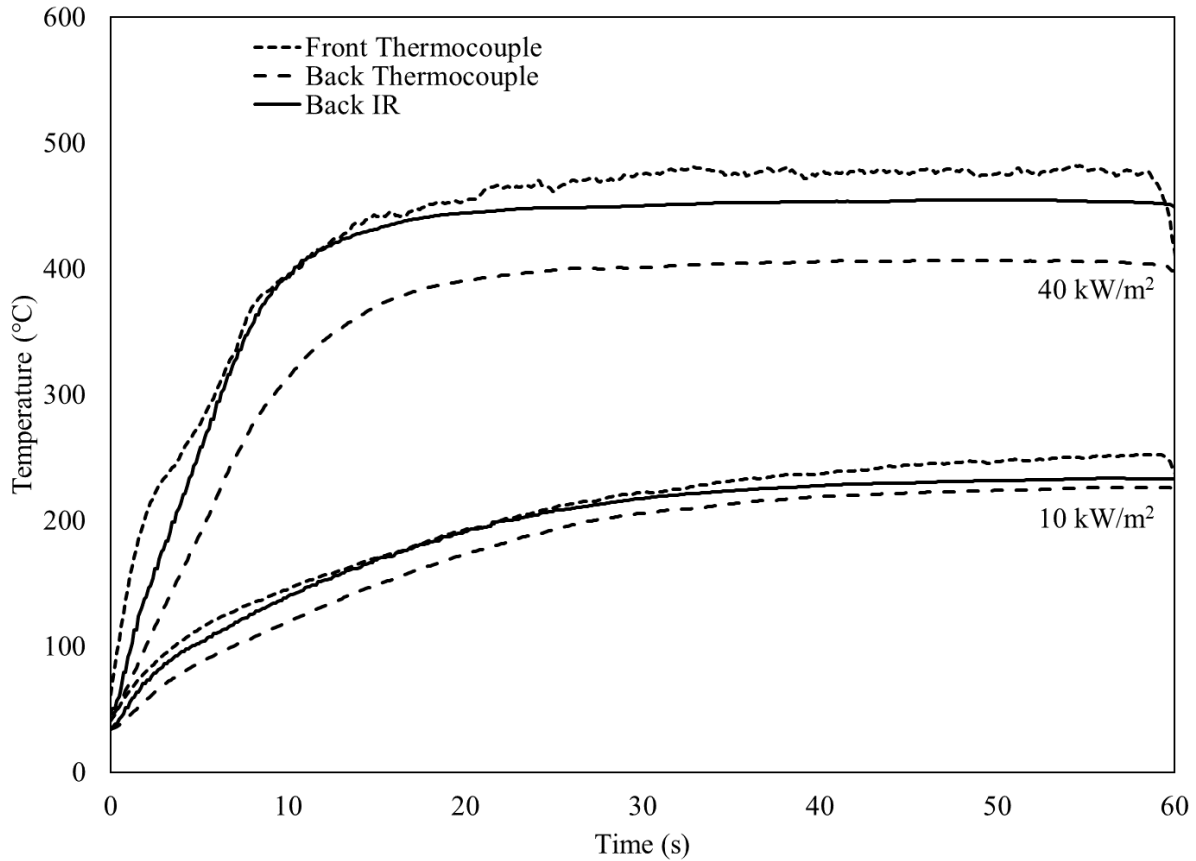


Figure 3.3 Temperature Measurement Comparison Between IR Thermometer And Thermocouples Measurements At 10 and 40 kW/m² For Ripstop Natural

Cone calorimeter tests were conducted using a range of heat fluxes from 10 to 70 kW/m². For these exposures, the IR temperature appears to follow the front thermocouple temperature closer than the back thermocouple. This is speculated to be due to the IR thermometer measuring within the fabric structure rather than just the back surface (Torvi 1997). Table 3.1 shows the percent differences between these temperature measurements. Figures 3.4 and 3.5 shows the temperature at different heat fluxes for 60 s exposures for Kombat Flex and Ripstop Natural.

Table 3.1 Percent Difference Of Thermocouple Measurements Compared To IR Thermometer Measurements

Percent Difference	10 kW/m ²		40 kW/m ²	
	Front-IR (%)	Back-IR (%)	Front-IR (%)	Back-IR (%)
Average	4.8	8.1	6.3	14.8
Median	4.3	5.6	4.8	11.4
Difference in Maximum Temperature	7.3	12.8	6.4	15.2

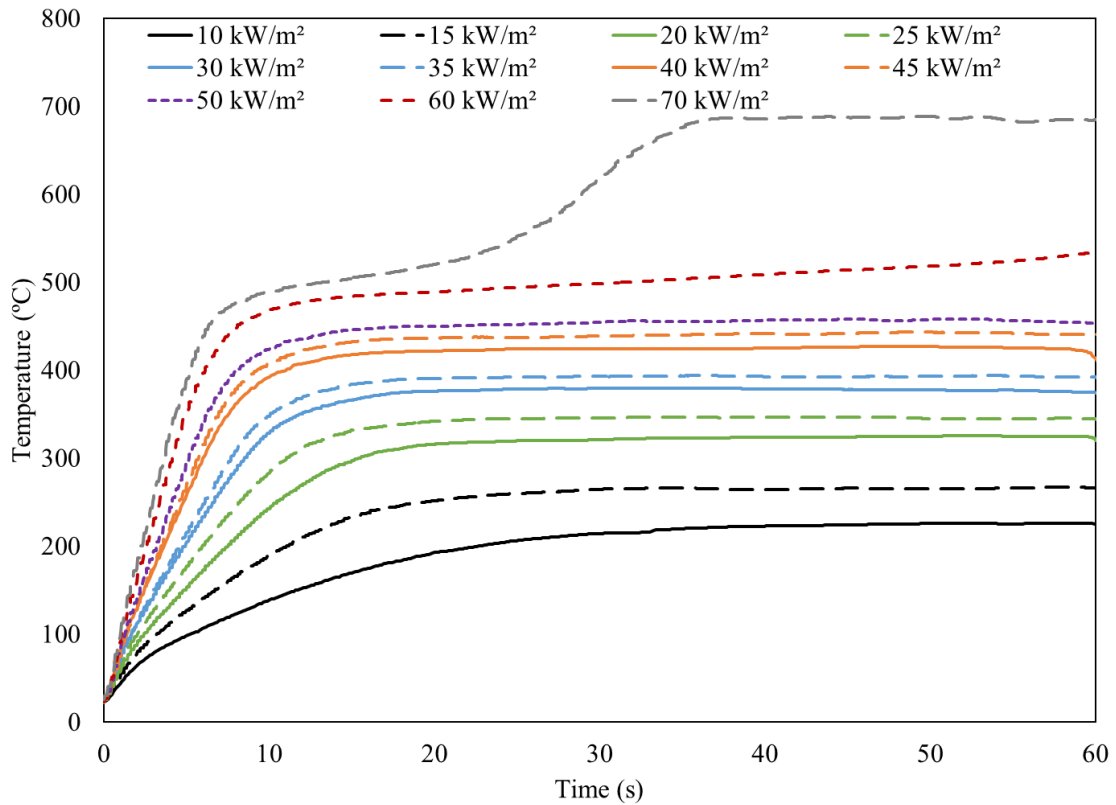


Figure 3.4 Temperature Measurements For Kombat Flex For First 60 s Of Exposure.

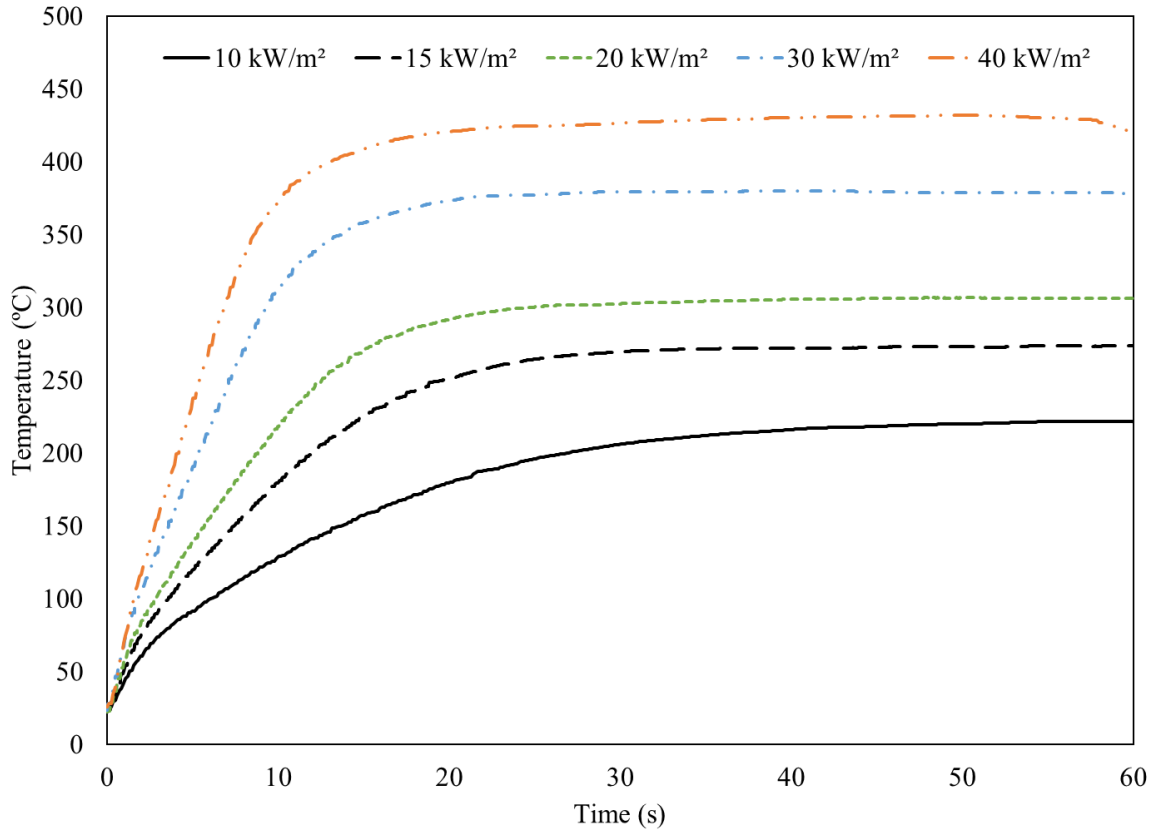


Figure 3.5 A Temperature Measurements For Ripstop Natural For The First 60 s Of Exposure

The time for specimens to reach steady state temperatures is typically within 10 to 20 s, depending on how intense the exposure is. This can be observed in Figures 3.4 and 3.5. The large jump in temperature at the 70 kW/m² exposure is due to the specimen igniting during the test. A small jump can also be seen in 60 kW/m² at the end of 60 s which is also due to ignition. Average temperature increase results can be seen in Table 3.2. These results were presented as increases to directly compare to previous research.

Table 3.2 Temperature Increase At Different Heat Flux Exposures, With Comparisons Between Kombat Flex, Ripstop Natural, And Fulton’s Ripstop Natural (Fulton 2017).

Fabric Type	Temperature Increase, ΔT ($^{\circ}\text{C}$)					
	Kombat Flex		Ripstop Natural (Epp)		Ripstop Natural (Fulton)	
Heat Flux (kW/m^2)	Avg	Std Dev	Avg	Std Dev	Avg	Std Dev
10	204	4.8	203	2.7	196	1.2
15	256	1.9	253	2.1	246	1.6
20	289	2.8	285	4.5	275	1.0
25	325	2.0	-	-	306	2.2
30	356	2.4	358	2.0	333	1.7
35	370	0.4	-	-	355	5.1
40	404	2.9	404	2.9	377	3.7
45	419	4.7	-	-	394	3.3
50	435	7.3	-	-	425	4.2
60	514	36.0	-	-	484	4.4
70	689	9.3	-	-	726	6.6

When Ripstop Natural results are compared to Fulton’s results, the average temperature rise of the current research is at most 7% higher than Fulton’s with increased exposure. In contrast, when comparing this research’s Kombat Flex and Ripstop Natural results, they remain close with very little difference. A further exploration of this can be found in Section 3.2.3. Kombat Flex temperature data at $60 \text{ kW}/\text{m}^2$ has a much higher standard deviation due to some specimens igniting in the last few seconds of the 60 s exposure, while others did not. This resulted in specimens that ignited having a much higher temperature reading which affected the standard deviation. This shows up in Figure 3.6 at the $60 \text{ kW}/\text{m}^2$ exposures whose temperature measurements shift at the end of the 60 s. 20 and $30 \text{ kW}/\text{m}^2$ exposures are also shown in this figure to highlight the consistency of these temperature tests.

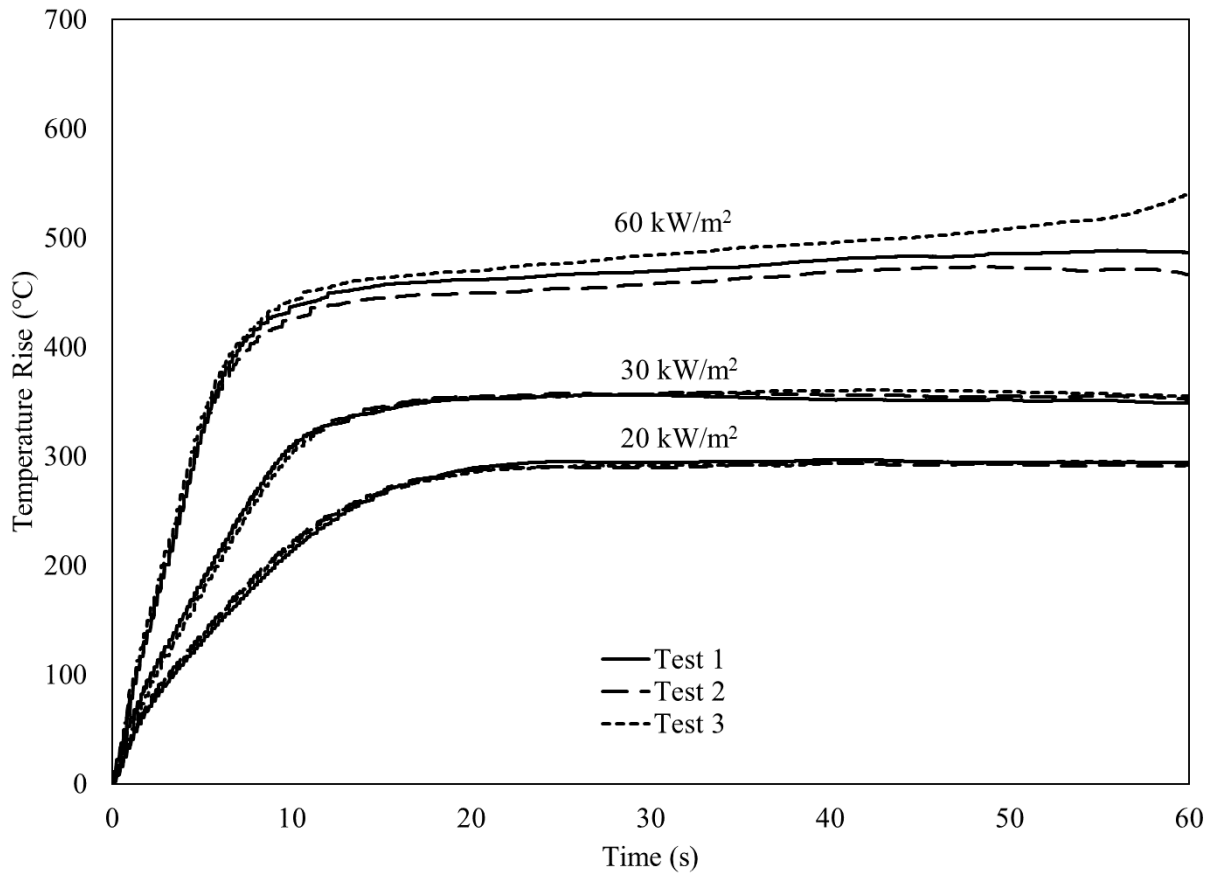


Figure 3.6 Kombat Flex Temperature Rise Consistency At 20, 30, And 60 kW/m²

3.2.3 Ripstop Natural Test Comparisons With Previous Research

With the previous research conducted at the University of Saskatchewan on Ripstop Natural, there are several tests that can be directly compared. Some of these previous datasets are used in developing the correlations outlined in Chapter 4. Figure 3.7 presents a comparison of the temperature rise over 60 s for 10, 20, 30, and 40 kW/m² for Ripstop Natural measured in this research and by Fulton (2017) and Ohalele (2020). Table 3.3 presents the maximum temperature increase for each test series as well as percent differences to this research. These results were presented as temperature rise for direct comparison with previous research.

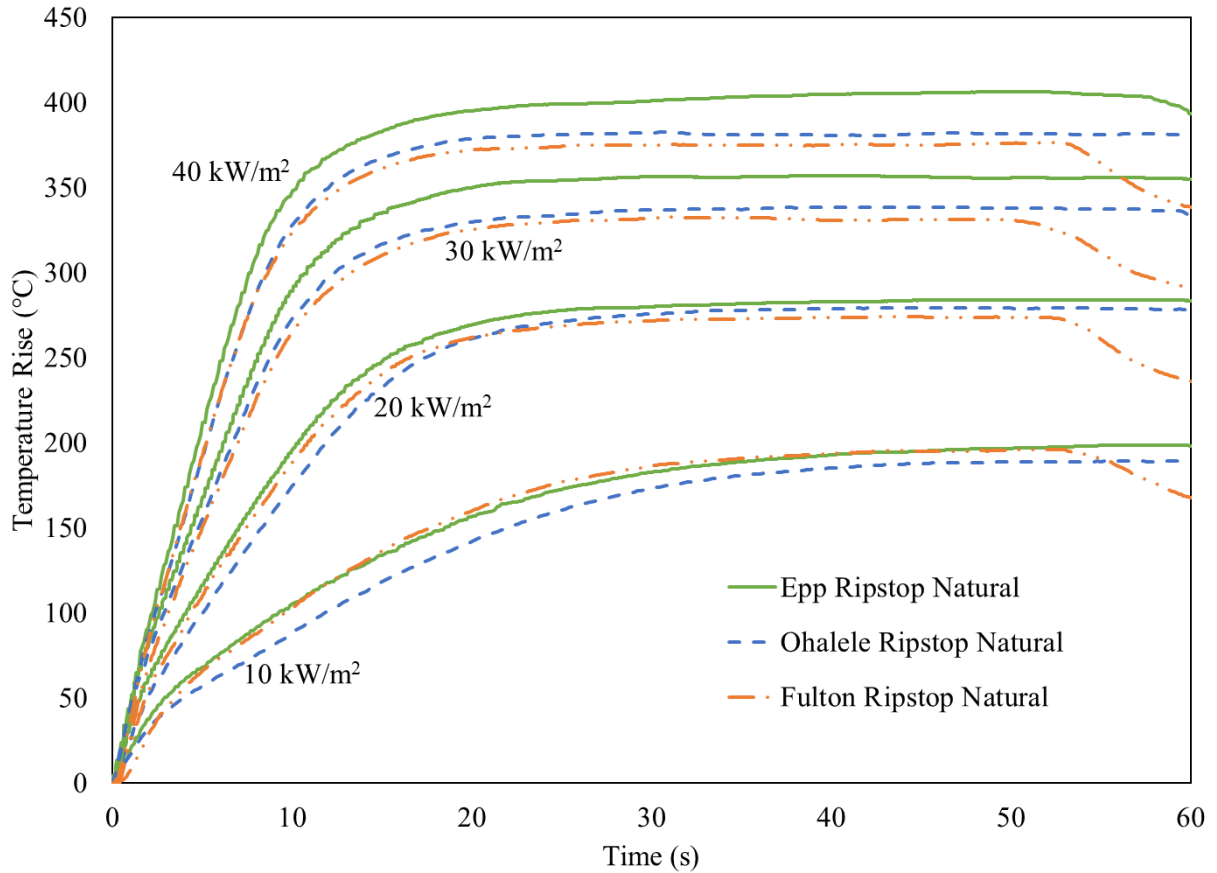


Figure 3.7 Ripstop Natural Temperature Rise Comparison Against Previous Research (Ohalele 2020; Fulton 2017).

Table 3.3 Ripstop Natural Temperature Rise And Percent Difference Comparison Against Previous Research (Ohalele 2020; Fulton 2017).

	10 kW/m ² Temperature Rise °C	20 kW/m ² Temperature Rise °C	30 kW/m ² Temperature Rise °C	40 kW/m ² Temperature Rise °C
Epp	199	284	357	406
Ohalele	189	279	339	382
Fulton	196	274	332	376
Percent Difference with Epp				
	%	%	%	%
Ohalele	4.9	1.6	5.3	6.1
Fulton	1.3	3.6	7.1	7.6

The temperature-time curves measured in this research were very similar to earlier measurements with maximum temperature increases being within 8% of each other. Temperature differences could be the result of differences in testing, such as differences in calibrating the heat flux gauge, or changes in the cone calorimeter with maintenance. Table 3.6 in a later section compares tensile strength for exposures at 10, 20, 30, 40 kW/m², and it was found that tensile strength values measured after thermal ageing in this research were slightly lower than in previous research, with the caveat that Ohalele's (2020) tensile strength was tested in a different fabric direction.

3.3 NIR Spectroscopy

Previously established by Moein Rezazadeh (2014) and confirmed by Fulton (2017) and Ohalele (2020), NIR spectroscopy can be correlated to tensile strength using analysis techniques such as the Normalized Difference Index (Rezazadeh 2014). NIR spectroscopy was not a main focus of this research. However, for completeness NIR spectroscopy tests were conducted. This data was gathered so that future research on NDT using these specimens could be conducted. Some limited exploration of these results is presented here. This research's NIR spectrum range was 400-2500 nm in reflectance. Previous NIR spectroscopy was conducted in incident wavelengths ranging from 400-2000 nm (Ohalele 2020; Fulton 2017), and 250-2500 nm (Rezazadeh 2014).

Materials, when exposed to an incident beam of light, in this case within the NIR wavelength, either absorb, reflect, or transmit light. As a result of thermal aging, there are both physical and chemical properties that are changing. This change is observable in the variation of the response from the incident light in the NIR spectrum. Of specific interest in reflectance spectroscopy is the comparison between the frequency of the incident light and the vibrational modes of known chemical bonds (Clark *et al.* 1984). For this research, diffuse reflectance was conducted on this dataset as it is an excellent technique for rough surfaces (Settle 1997).

3.3.1 NIR Spectroscopy Results

The major difference in this research's dataset compared to previous datasets is the inclusion of much longer durations of exposure. This has allowed for some longer duration exposures to lower heat fluxes to have similar losses in tensile strength to shorter exposures to higher heat

fluxes. For these interesting situations, see Appendix B which has a brief outline of what the NIR spectroscopy looks like for these points.

Figure 3.8 shows an example of how the scans change at different levels of exposure and duration for Kombat Flex. This figure has been reduced to show only a few of the durations for exposures 20, 40, 50, 60, and 70 kW/m². Figure 3.9 shows a similar set of results for Ripstop Natural for 20 and 40 kW/m².

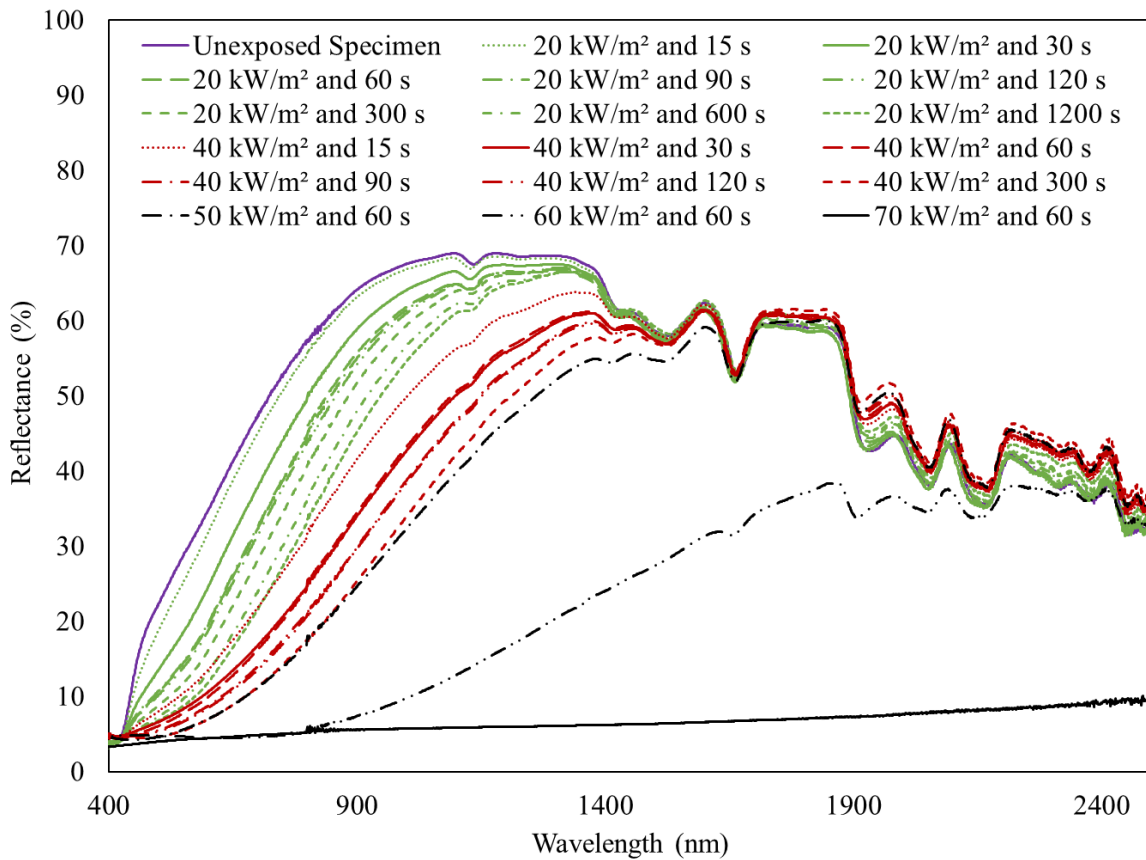


Figure 3.8 Averaged Kombat Flex NIR Data For Unexposed Specimen, 20 kW/m² Exposures, 40 kW/m² Exposures, And Exposures Above 50 kW/m²

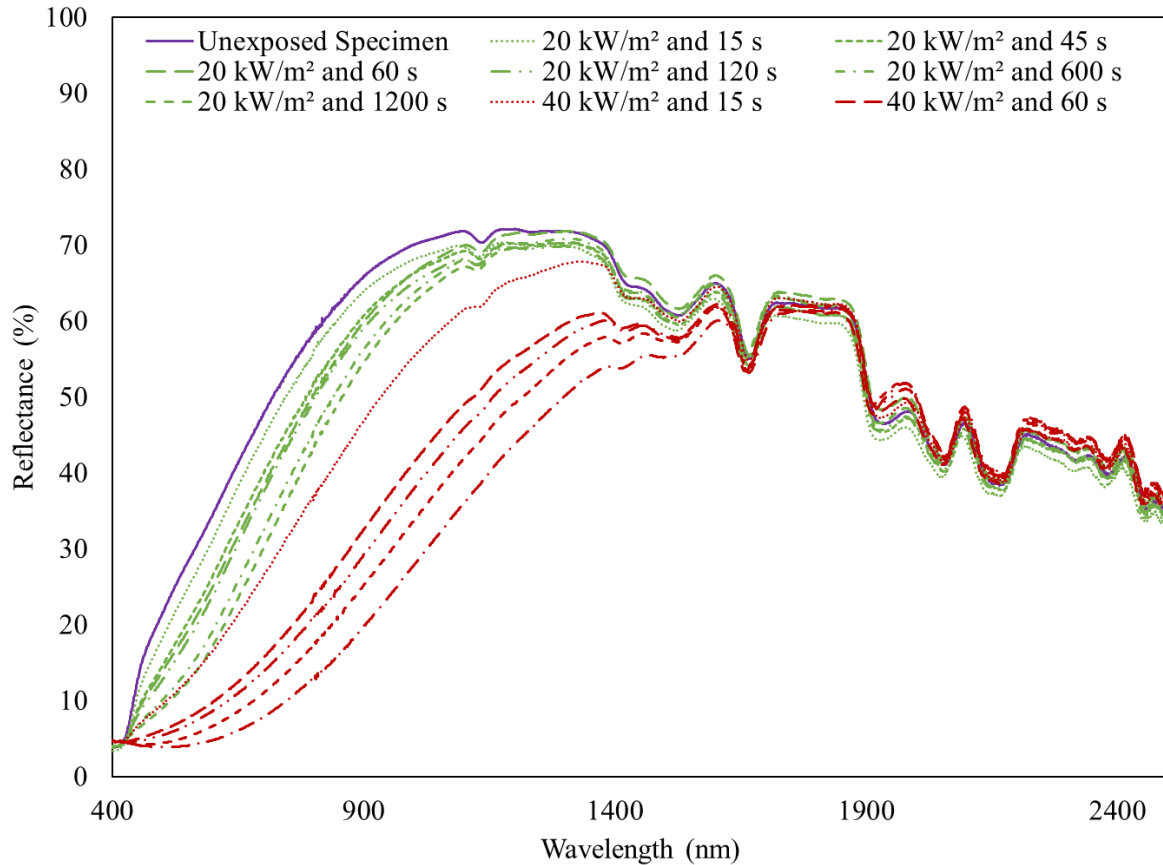


Figure 3.9 Averaged Ripstop Natural NIR Data For Unexposed Specimen, 20 kW/m² Exposures, And 40 kW/m² Exposures.

In Figure 3.9 thermal aging has the most change in NIR spectroscopy below 1400 nm. This is expected as within visual light (approximately 400 to 700 nm) the specimens in this research all become darker in colour as they are aged thermally. Of specific interest when examining these curves is how thermal aging affects the dips and curves above the visual band. Where does the exposure begin to flatten these curves, making them less defined? For a further look at how to analyze NIR spectroscopy and an explanation of the use of NDT to relate this information to tensile strength retention, see Ohalele’s (2020), and Fulton’s (2017) theses, as well as Rezazadeh’s (2014) dissertation.

For both fabrics, reflectance did not rise above 70%, which was the motivation for selecting a 75% calibration target. As the Kombat Flex specimens aged, this peak reflectance decreased to 65% at 20 kW/m², and to 60% at 40 kW/m². This is slightly different from Ripstop Natural

which at 20 kW/m² and 60 s was at a peak of 68% but had a much lower reflectance at 40 kW/m² at any of the durations, with the 60 s duration peaking at 60%.

3.4 Tensile Strength And Temperature Measurements

According to NFPA 1971 (2013), these protective fabrics are expected to have a minimum breaking strength of 623 N. This research concludes in the tensile strength testing of the specimens that have been aged and examined with NIR spectroscopy. Figures 3.10 and 3.11 show exposures at 20 kW/m² for both Kombat Flex and Ripstop Natural for the first five minutes. Both of these figures also present experimental tensile strength for both this research and Ohalele (2020) where applicable. For more temperature measurement results, see Appendix C. Figures 3.12 and 3.13 show a comparison between the heat flux exposures for which the largest number of exposure durations were tested. This research presents tensile strength as a ratio of the original strength in much of its comparisons ($\frac{TS}{TS_i}$) where TS is the tensile strength for the exposure of interest and TS_i is the initial tensile strength of the fabric before thermally ageing. This was done to draw better consistency between this and previous research.

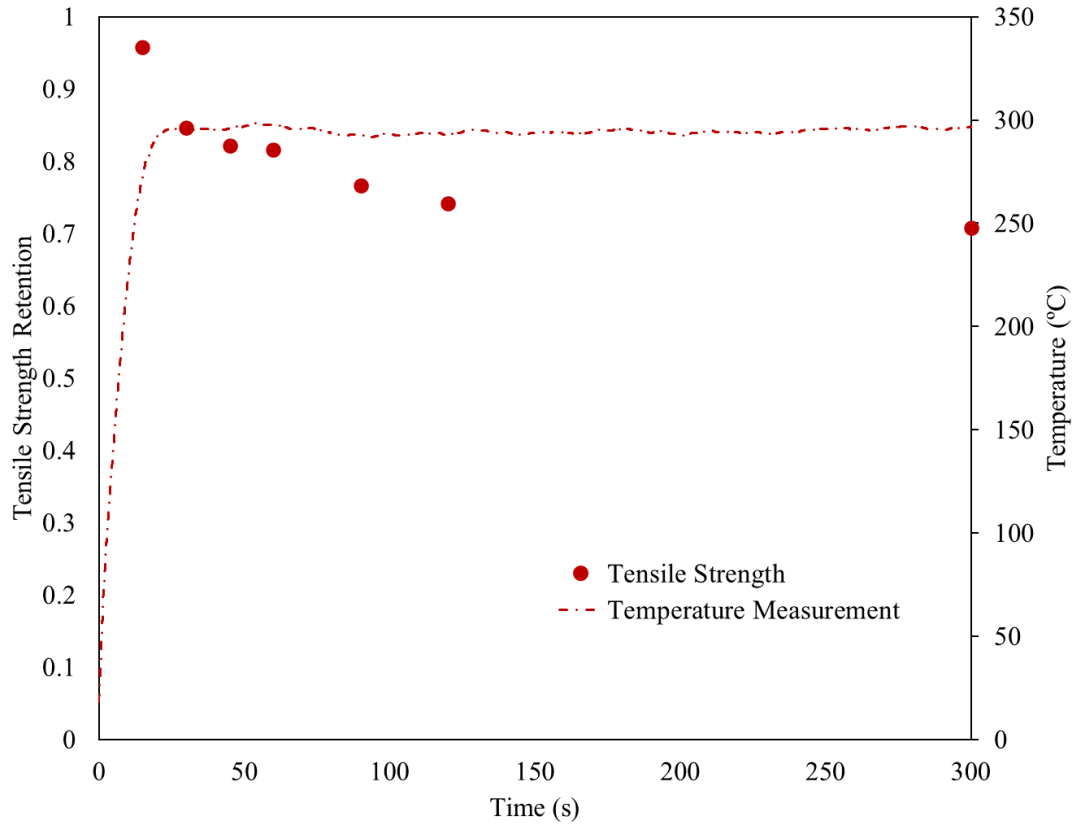


Figure 3.10 Kombat Flex Temperature Measurements For 20 kW/m² With Tensile Strength Data.

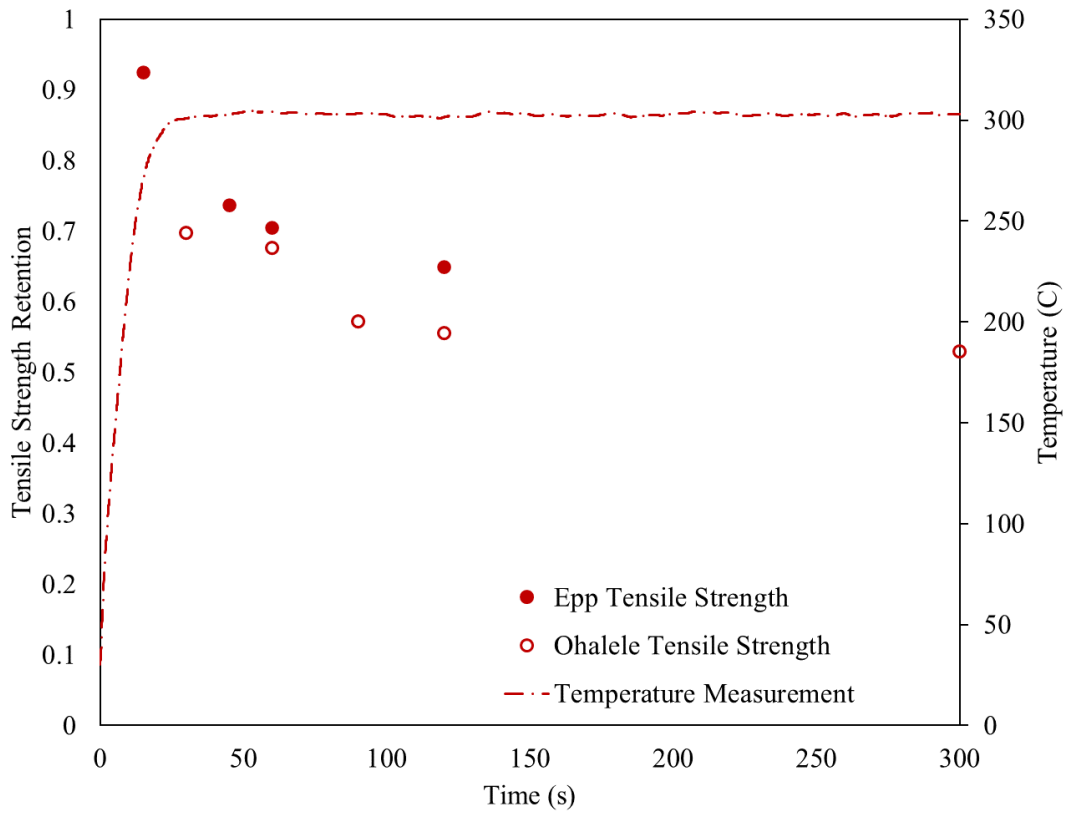


Figure 3.11 Ripstop Natural Temperature Measurements For 20 kW/m² With Tensile Strength Data For Both This Research And Ohalele's (2020) Research.

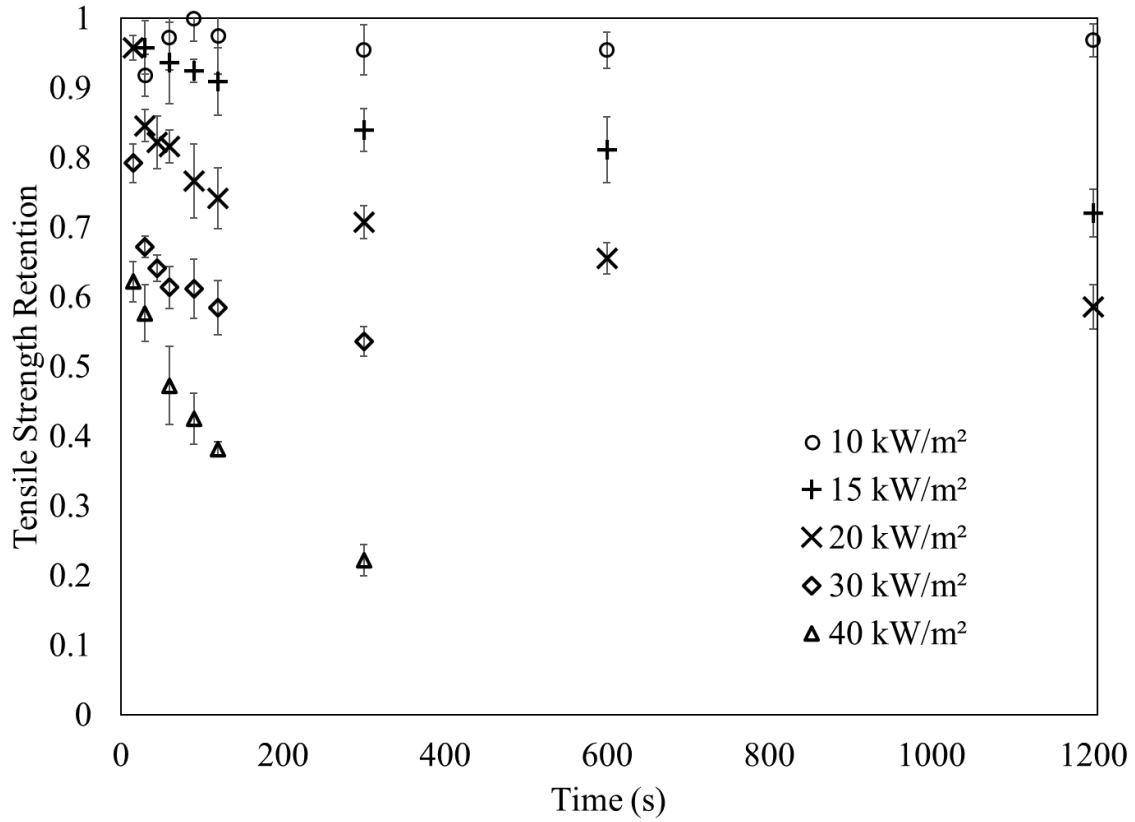


Figure 3.12 Kombat Flex Experimental Data For Exposures With Multiple Data Points. Error Bars Show Standard Deviation.

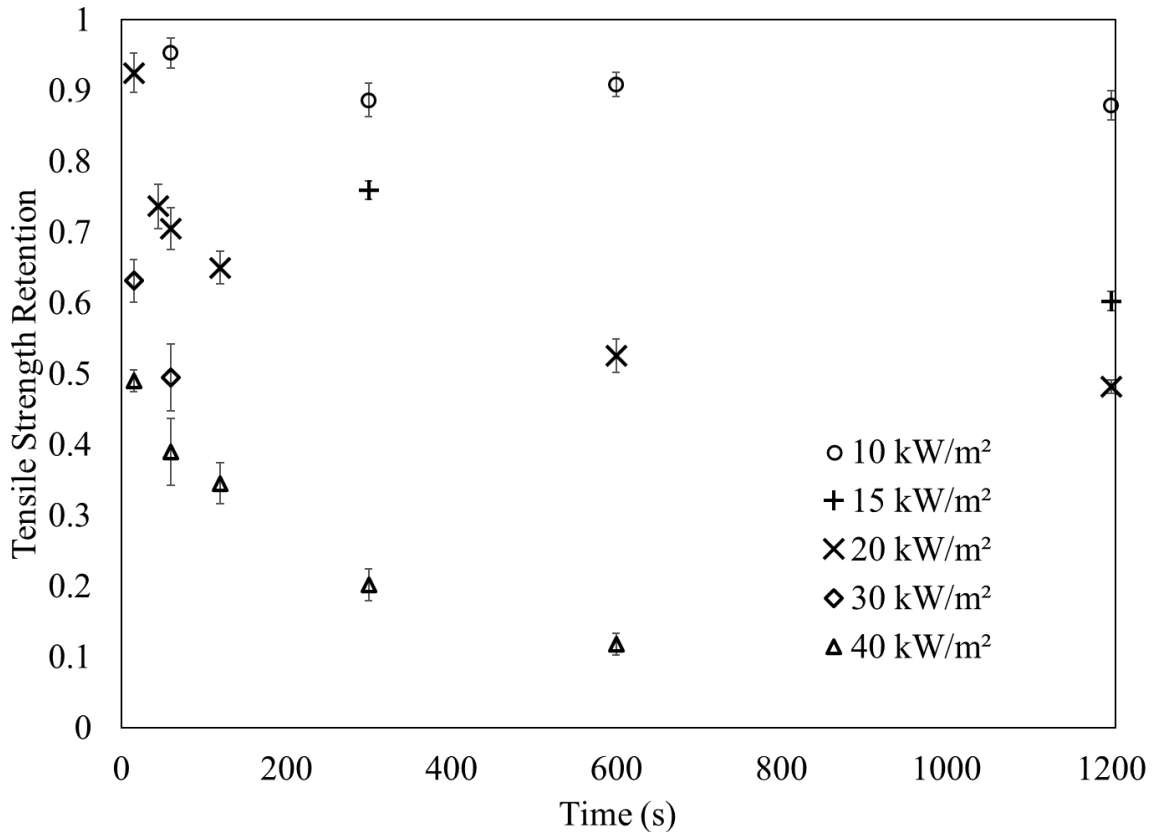


Figure 3.13 Ripstop Natural Experimental Data For Exposures With Multiple Data Points. Error Bars Show Standard Deviation.

For the 10 kW/m² data (Figures 3.12 and 3.13), tensile strength appears to improve partially before dropping. This is noted, but not explored as this research is focused on where tensile strength is reduced. For Kombat Flex at 20 kW/m² and 20 min (Figure 3.10), the tensile strength retention levels off roughly to around a tensile strength retention of 0.7 with minimal change from 5 or 10 min. This information is vital for the construction of correlations (Chapter 4). For both materials at exposures above 20 kW/m² most of the strength is lost in the first 30 seconds, with this becoming more severe the higher the exposure. For Kombat Flex, at 40 kW/m², tensile strength retention drops by 38% in the first 15 s. For a better idea of this interaction, see Tables 3.4, 3.5, and 3.6, which outline the tensile strength retention and standard deviation at all the exposures, as well as comparisons against Ohalele’s (2020) and Fulton’s (2017) results.

Table 3.4 Kombat Flex Tensile Strength Data

Heat Flux kW/m ²	Time s	Tensile Strength N	STD	TS/TS _i
0	0	969.4	18.7	1.00
10	30	890.1	29.4	0.92
10	60	943.3	45.7	0.97
10	90	985.2	31.1	1.02
10	120	945.2	52.8	0.98
10	300	925.4	35.0	0.95
10	600	925.3	25.2	0.95
10	1200	939.1	22.3	0.97
15	30	929.3	37.1	0.96
15	60	907.6	56.3	0.94
15	90	896.6	15.9	0.92
15	120	882.2	46.9	0.91
15	300	814.0	29.6	0.84
15	600	786.5	45.8	0.81
15	1200	699.1	33.1	0.72
20	15	929.0	16.9	0.96
20	30	820.5	22.6	0.85
20	45	797.1	36.2	0.82
20	60	791.6	23.2	0.82
20	90	743.5	51.8	0.77
20	120	719.4	42.4	0.74
20	300	686.3	22.6	0.71
20	600	635.4	21.7	0.66
20	1200	568.2	31.3	0.59
25	60	685.0	48.6	0.71
30	15	768.2	27.0	0.79
30	30	652.1	15.0	0.67
30	45	621.9	17.9	0.64
30	60	595.2	28.9	0.61
30	90	593.1	40.9	0.61
30	120	567.2	38.1	0.59
30	300	519.9	20.7	0.54
35	60	590.4	36.7	0.61
40	15	603.4	28.3	0.62
40	30	559.5	39.2	0.58
40	60	458.8	54.7	0.47
40	90	412.5	35.7	0.43
40	120	370.6	9.6	0.38
40	300	215.3	21.6	0.22
45	60	376.8	43.2	0.39
50	60	244.8	28.1	0.25
60	60	19.6	11.2	0.02
70	60	5.6	0.7	0.01

Table 3.5 Ripstop Natural Tensile Strength With Comparison Against Previous Research
(Ohalele 2020; Fulton 2017).

Heat Flux kW/m ²	Time s	Epp's RSN			Ohalele's RSN		Fulton's RSN	
		Tensile Strength N	STD	TS/TS _i	Tensile Strength N	TS/TS _i	Tensile Strength N	TS/TS _i
0	0	1139.5	11.0	1.00	788.0	1.00	1069.0	1.00
10	30	-	-	-	599.1	0.76	-	-
10	60	1086.6	24.0	0.95	698.4	0.89	1066.2	1.00
10	90	-	-	-	672.1	0.85	-	-
10	120	-	-	-	697.8	0.89	-	-
10	300	1010.9	27.4	0.89	633.0	0.80	-	-
10	600	1036.1	19.3	0.91	-	-	-	-
10	1200	1002.2	23.1	0.88	-	-	-	-
15	60	-	-	-	-	-	1030.3	0.96
15	300	865.5	14.7	0.76	-	-	-	-
15	1200	687.4	15.3	0.60	-	-	-	-
20	15	1054.4	31.8	0.93	-	-	-	-
20	30	-	-	-	549.9	0.70	-	-
20	45	839.6	35.2	0.74	-	-	-	-
20	60	803.7	34.0	0.71	533.3	0.68	796.7	0.75
20	90	-	-	-	450.7	0.57	-	-
20	120	740.8	26.5	0.65	438.1	0.56	-	-
20	300	-	-	-	417.8	0.53	-	-
20	600	598.9	27.2	0.53	-	-	-	-
20	1200	549.4	11.3	0.48	-	-	-	-
25	60	-	-	-	-	-	638.6	0.60
30	15	719.9	34.3	0.63	-	-	-	-
30	30	-	-	-	382.7	0.49	-	-
30	60	564.4	22.7	0.50	361.6	0.46	572.3	0.54
30	90	-	-	-	373.0	0.47	-	-
30	120	-	-	-	376.9	0.48	-	-
30	300	-	-	-	350.9	0.45	-	-
35	60	-	-	-	-	-	538.2	0.50
40	15	559.3	17.3	0.49	-	-	-	-
40	30	-	-	-	341.2	0.43	-	-
40	60	444.0	53.9	0.39	356.7	0.45	494.0	0.46
40	90	-	-	-	333.1	0.42	-	-
40	120	394.0	32.4	0.35	309.4	0.39	-	-
40	300	230.5	25.1	0.20	248.4	0.32	-	-
40	600	135.0	17.6	0.12	-	-	-	-
45	60	-	-	-	-	-	391.7	0.37
50	60	-	-	-	-	-	244.8	0.23
60	60	-	-	-	-	-	20.1	0.02
70	60	-	-	-	-	-	1.4	0.00

Finally, when handling each specimen set between researchers, calculating tensile strength retention was based on unexposed specimen tensile strength within each dataset. This mitigated much of the differences in approach between the three researchers specimen sets. As previously mentioned, Ohalele (2020) chose to test in the weft direction instead of the warp, and so direct comparisons across all three datasets was done looking at tensile strength retention. Looking across all tests, the majority of damage occurs within the first 60 s with exposures above 20 kW/m². For Kombat Flex, at 40 kW/m² this point of initial property drop off occurs before the first test (15 s) where 40% of the tensile strength retention is lost. This rapid drop is also observed in Ripstop Natural, where at 30 kW/m² and a duration of 15 s has a loss just below 40%. Both of these 15 s tests occurred during the transient phase of the exposure.

623 N is one tensile strength criterion specified in standards for new fire protective garments are designed to, and it is worth identifying at what exposure this tensile strength is reached in these tests (NFPA 1971, 2013). This tensile strength correlates to a tensile strength retention of 0.64 and 0.54 for Kombat Flex and Ripstop Natural respectively. For Kombat Flex, this strength is passed at 20 kW/m² test and a duration of 20 min, For Ripstop Natural, this strength is passed at 20 kW/m² and before 10 min.

Table 3.6 outlines the four tests that were conducted in all three datasets. For this research, the highest percent difference occurs with Fulton’s tests at 40 kW/m² at 16% while the lowest occurs with Ohalele’s tests at 20 kW/m² at 4%.

Table 3.6 Ripstop Natural Tensile Strength Specific Point Comparisons (Ohalele 2020; Fulton 2017).

Heat Flux kW/m ²	Time s	Epp's RSN			Ohalele's RSN		Fulton's RSN	
		Tensile Strength N	STD	TS/TS _i	Tensile Strength N	TS/TS _i	Tensile Strength N	TS/TS _i
0	0	1139.5	11.0	1.00	788.0	1.00	1069.0	1.00
10	60	1086.6	24.0	0.95	698.4	0.89	1066.2	1.00
20	60	803.7	34.0	0.71	533.3	0.68	796.7	0.75
30	60	564.4	22.7	0.50	361.6	0.46	572.3	0.54
40	60	444.0	53.9	0.39	356.7	0.45	494.0	0.46

3.5 The Partial Ignition At 60 kW/m²

Thermal exposures conducted at 60 kW/m² and 60 s presented an interesting situation where the specimens would just begin to ignite at the end of the test, resulting in an exposure window that has a portion that is darker than the rest. The following is a specific look at the results for the tests conducted at 60 kW/m². Figure 3.14 shows the 60 kW/m² Kombat Flex specimen after exposure.

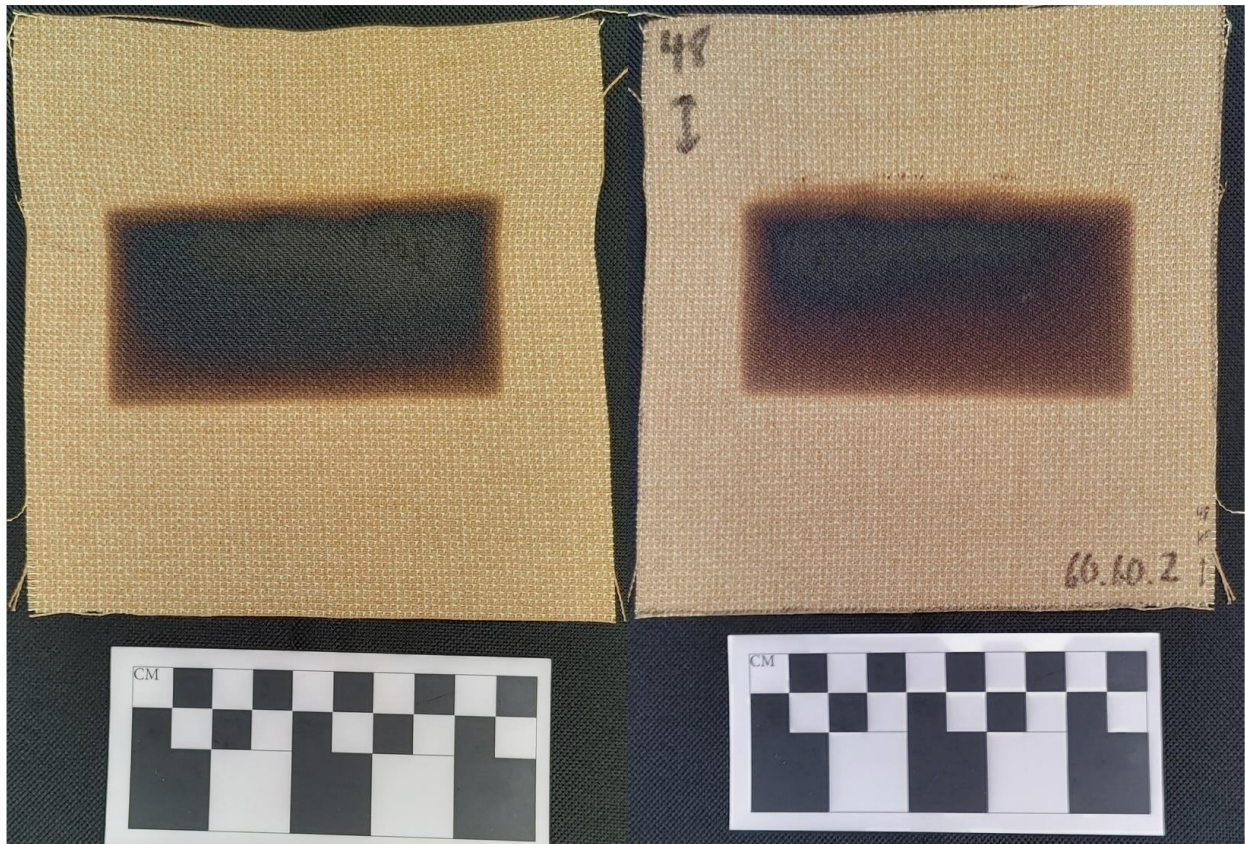


Figure 3.14 Kombat Flex Front (Left) And Back (Right) Of Specimen KF.60.60.2 Exposed To 60 kW/m² For 60 s, Highlighting The Partial Ignition Of The Specimen.

There is a portion of the window that has been inconsistently burned which occurred when the specimen ignited. This is an interesting problem as this will have an impact on the NIR test results. To explore this issue, nine specimens were selected for this exposure instead of the usual three. During NIR testing, each of these specific specimens were tested three times: at the centre of the specimen as well as on each side of the exposure window. Specimen KF.60.60.2 was

scanned four times along its length, the results of which can be seen in Figure 3.15. The average of these NIR scans is a good representation of this non-uniform burn pattern.

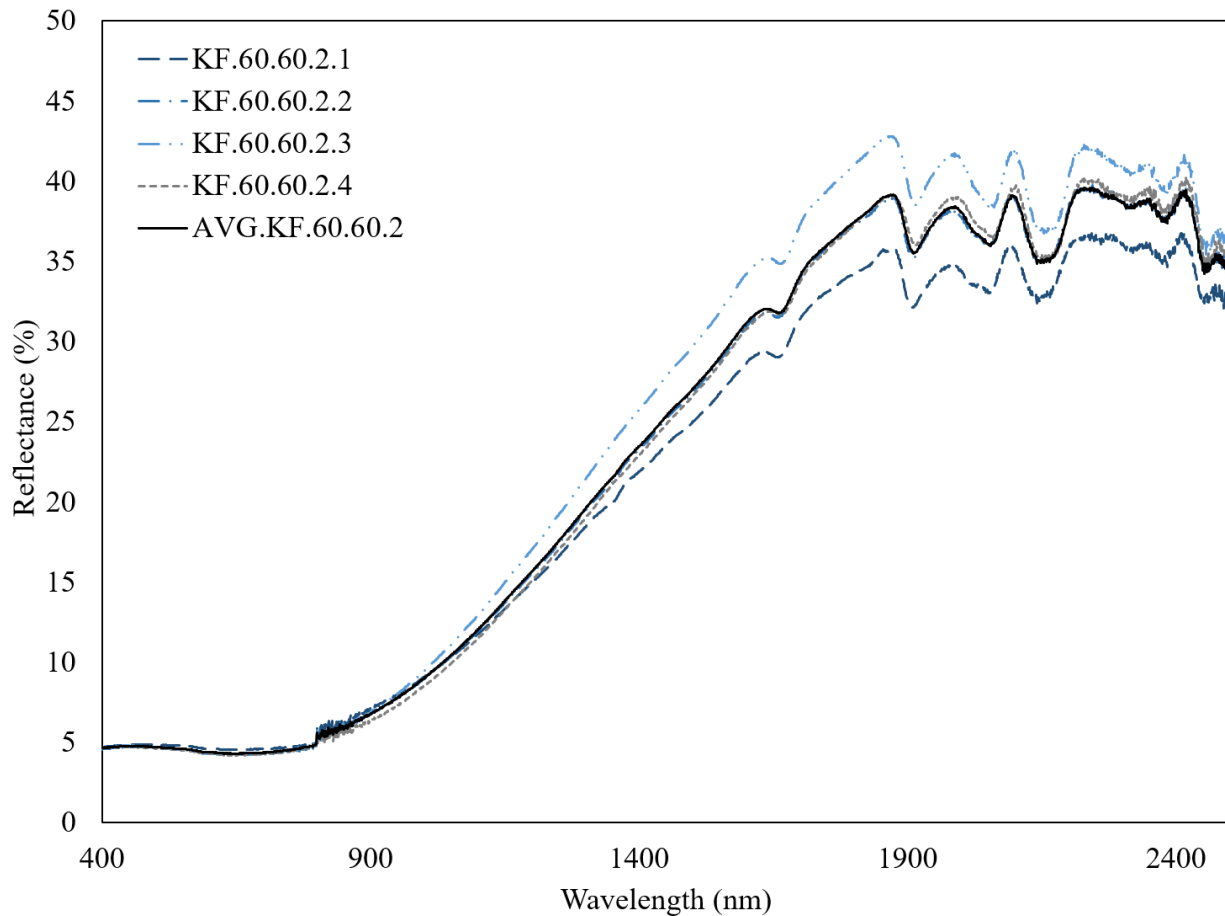


Figure 3.15 Kombat Flex NIR Measurement For A Specimen Exposed To 60 kW/m² For 60 s, Measurements At Different Parts Of The Specimen.

A firefighter's garment undergoes an uneven exposure over its lifetime. This averaging approach would be valid for localized variance, but when observing the damage overall, the worst burn locations should be examined first as those would be the places where the garment would be expected to fail first.

3.6 Thermogravimetric Analysis Results

Thermogravimetric analysis was conducted on Kombat Flex and Ripstop Natural specimens. Figures 3.16 and 3.17 show the average of three TGA tests for Kombat Flex and a typical TGA test for Ripstop Natural respectively. A typical test for Ripstop Natural is presented here because

there appeared to be errors and inconsistent behaviour in the data for the other tests. Previous TGA tests conducted on Kombat Flex and Ripstop Natural can be found in Fulton's thesis (2017).

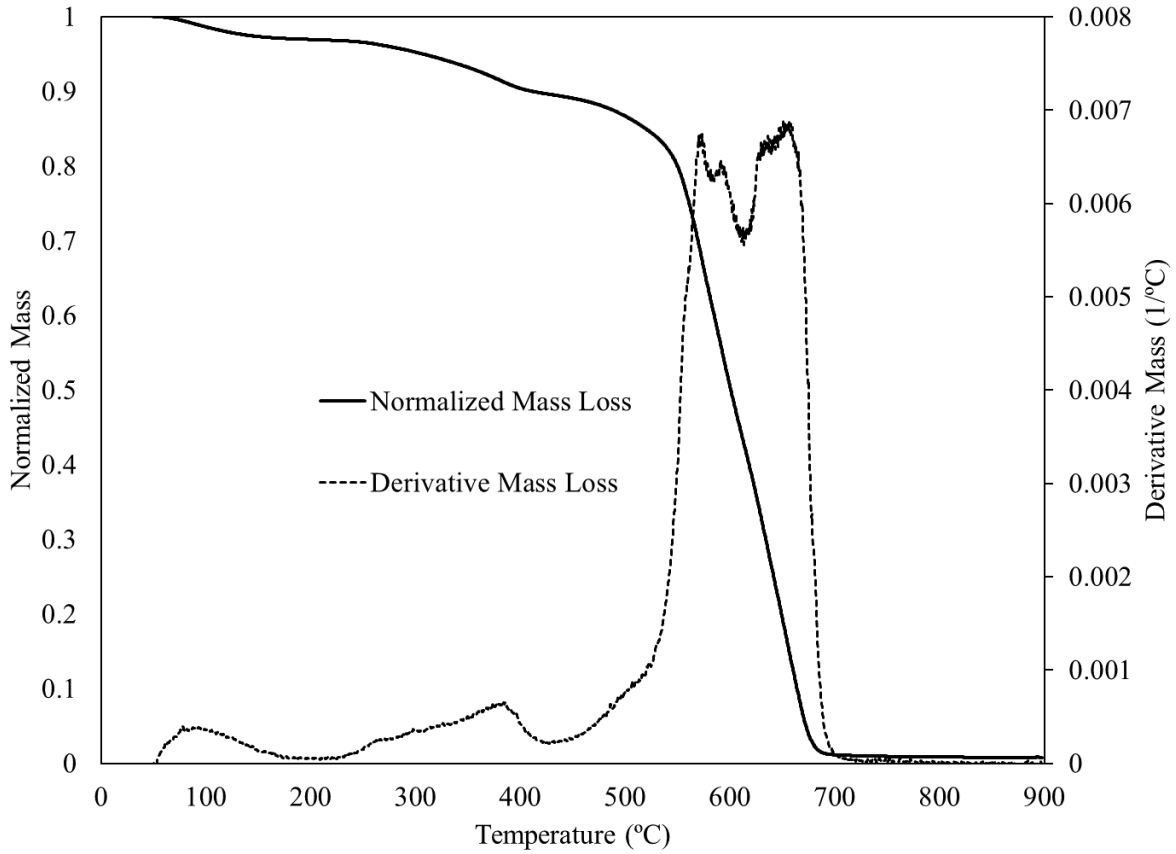


Figure 3.16 Kombat Flex Thermogravimetric Analysis In Air

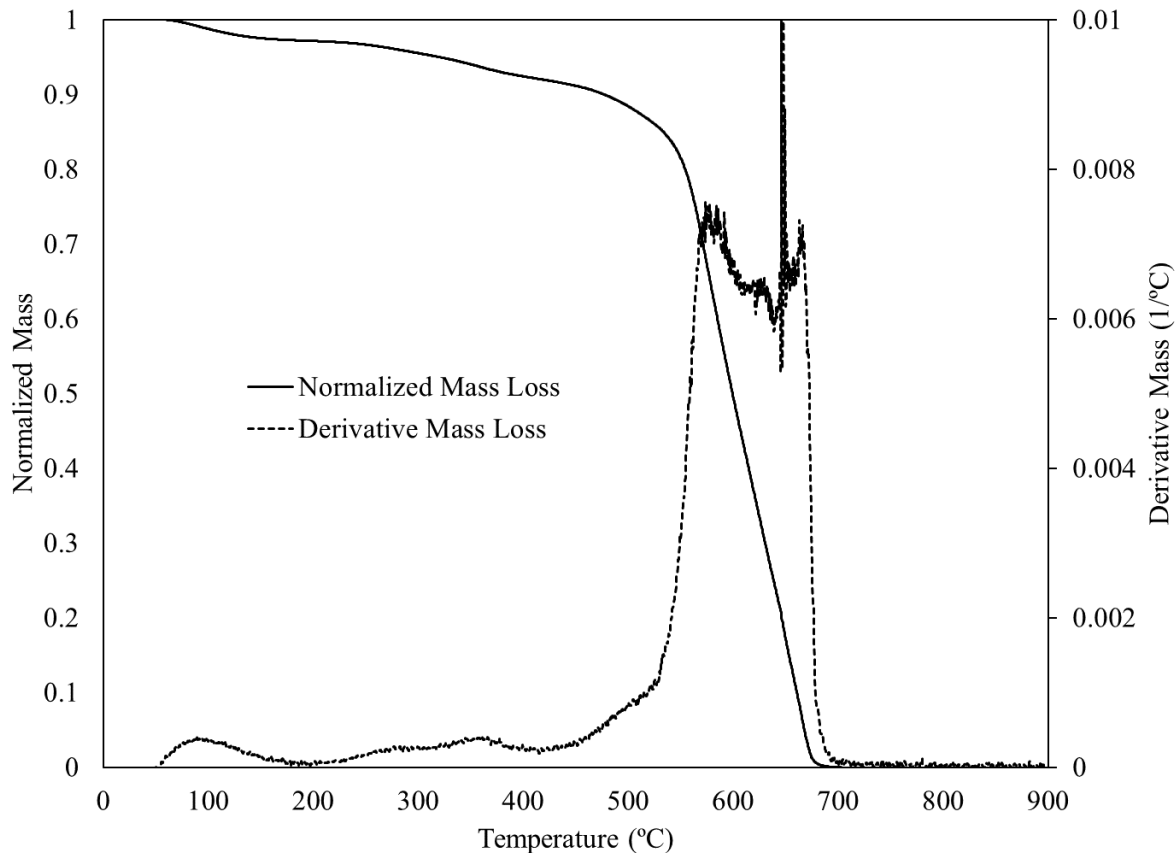


Figure 3.17 Typical Ripstop Natural Thermogravimetric Analysis In Air

In these figures, the derivative mass change is indicative of a change in the rate of reaction. It was expected that these materials would have similar TGA curves as the material composition is similar. These materials have small derivative mass peaks that occur at the temperatures specified in Table 3.7. This table also shows the heat fluxes that produced similar steady state temperatures in the cone calorimeter to the temperatures at which these mass peaks occurred.

Table 3.7 TGA Derivative Mass Peak Temperatures Compared To Experimental Thermal Aging Temperatures Which Produced Steady-State Temperatures Closest To TGA Derivative Mass Peaks For Both Kombat Flex and Ripstop Natural

TGA Temperature Peaks (°C)	Comparative Heat Flux (kW/m²)	Avg Temperature (°C)
60-70	-	-
260-270	15	256
365-380	35	370
485-495	60	514
555-565	-	-

Referring to Table 3.7, the first peak that occurs before 100°C is the mass loss that occurs from moisture coming out of the fabric, and is not indicative of any reactions for these materials. The final peak occurring at the end of the TGA test does not directly correlate with any of the steady-state temperatures measured in the thermal ageing tests in this research. As was established in sections 3.2 and 3.5, the specimens experienced ignition somewhere between 60 and 70 kW/m². This sudden drop in mass appears to correlate with an ignition of the fabric.

The remaining three peak temperatures do have comparable heat fluxes that were tested in this research. When observing Figures 3.12 and 3.13 in section 3.4, data points at 10 kW/m² indicate a very small impact on tensile strength, while a loss in tensile strength does occur at 15 and 20 kW/m². This indicates the effects of these reactions on the properties of the material. Furthermore, when examining the experimental data at 40 kW/m², there is a much more rapid tensile strength loss. This correlates with the TGA temperature peak noted in Table 3.7 near a temperature of 370°C. These observations cannot be made at 60 kW/m² without testing at a larger number of exposure durations, and could be an area of future research in this project.

4.0 Tensile Strength Correlations

One of the goals of this research was to develop correlations which are able to predict tensile strength. These correlations would be limited in their applicability within fabrics that were tested, but have the potential to be used as a tool to help identify service life of high performance fabrics. This was inspired by Ohalele (2020) who identified that tensile strength retention was dependent on both heat flux and exposure duration (Figure 4.1).

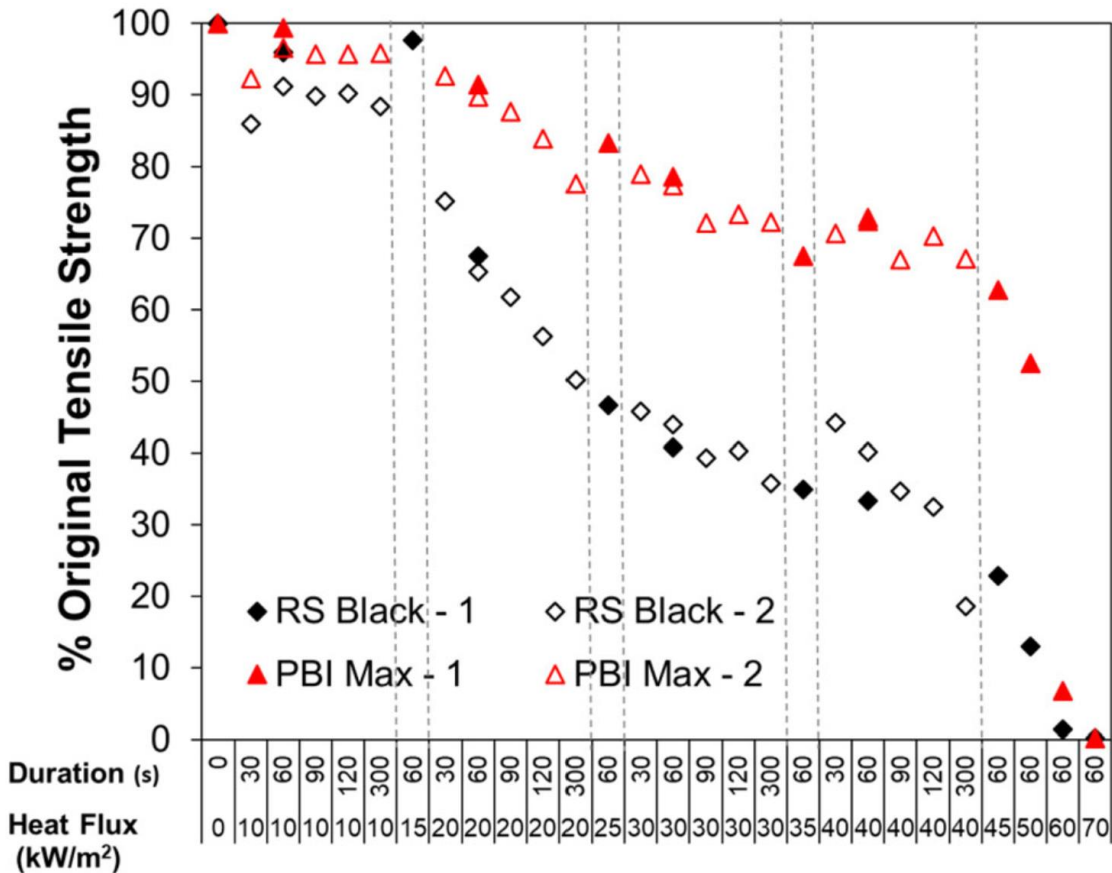


Figure 4.1 Comparison Of Tensile Strength To Exposure And Duration Of Ripstop Black And PBI Max (Ohalele et al. 2022). Set 1 And 2 Represents Data From Fulton (2017) And Ohalele (2020) Respectively.

Three approaches were taken to develop correlations: a multi-variable linear regression, a multi-variable nonlinear regression, and a single-variable nonlinear regression. When looking at this chapter, any relationship drawn between tensile strength, heat flux, and time can also be established between tensile strength, fabric temperature, and time.

4.1 Multi-Variable Linear Correlation

To begin, three-dimensional representations of these parameters were explored. This was done to establish a good visual understanding of how these materials degrade. For the purposes of creating a three-dimensional representation of this data, MathWorks® MATLAB (Natick, MA, USA) was used with the objective of observing the data in three-dimensions to help in identifying any natural or obvious correlations.

For a linear regression in three dimensions, the result is a simple plane equation. Equation 4.1 shows the general form of this equation, with the coefficients listed in Table 4.1. The coefficients listed in Table 4.1 were constructed using this research's data for Kombat Flex, and in two different sets for Ripstop Natural; one set with this research's data only and one set with all three researchers' datasets together (Fulton 2017; Ohalele 2020). This set of data is using heat flux and tensile strength retention. For the development of the multi-variable linear regression using temperature, and tables of coefficients for temperature, see Appendix D.

$$\frac{TS}{TS_i} = aq'' + bt + c \quad (4.1)$$

where,

$\frac{TS}{TS_i}$ is the tensile strength retention,

q'' is heat flux exposure (kW/m²),

t is the exposure duration (s), and

a , b and c are coefficients that can be found in the generalized Table 4.1.

Table 4.1 Multi-Variable Linear Regression Coefficients For Equation 4.1 For Kombat Flex And Ripstop Natural Using Heat Flux (Fulton 2017; Ohalele 2020)

Kombat Flex		Units	Coefficient Values
<i>a</i>	Heat Flux	m ² /kW	-1.80E-02
<i>b</i>	Exposure Time	1/s	-1.70E-04
<i>c</i>	Intercept	-	1.19E+00

Ripstop Natural	Epp Data Only		Coefficient Values
		Units	
<i>a</i>	Heat Flux	m ² /kW	-2.15E-02
<i>b</i>	Exposure Time	1/s	-2.16E-04
<i>c</i>	Intercept	-	1.20E+00

Ripstop Natural	Fulton, Ohalele, Epp Together		Coefficient Values
		Units	
<i>a</i>	Heat Flux	m ² /kW	-1.67E-02
<i>b</i>	Exposure Time	1/s	-1.72E-04
<i>c</i>	Intercept	-	1.06E+00

One problem that is present in this multi-variable linear regression is that it draws a straight line through any curves or inflections in the data as it attempts to correlate the data linearly. This makes a crucial error in that it does not capture any detail in the initial rapid tensile strength loss that occurs in this sort of thermal reaction.

4.1.1 Multi-Variable Linear Regression Correlation Graphical Representation

Figure 4.2 shows the three-dimensional representation of the effects of exposure and duration. More examples of this three-dimensional representation can be found in Appendix D. The plane presented in this figure is a linear regression based on the points present in this correlation. Each of the points are the experimental exposures conducted in this research. These points have been connected with lines to help highlight how the tensile strength changes when the severity of exposure or duration is increased.

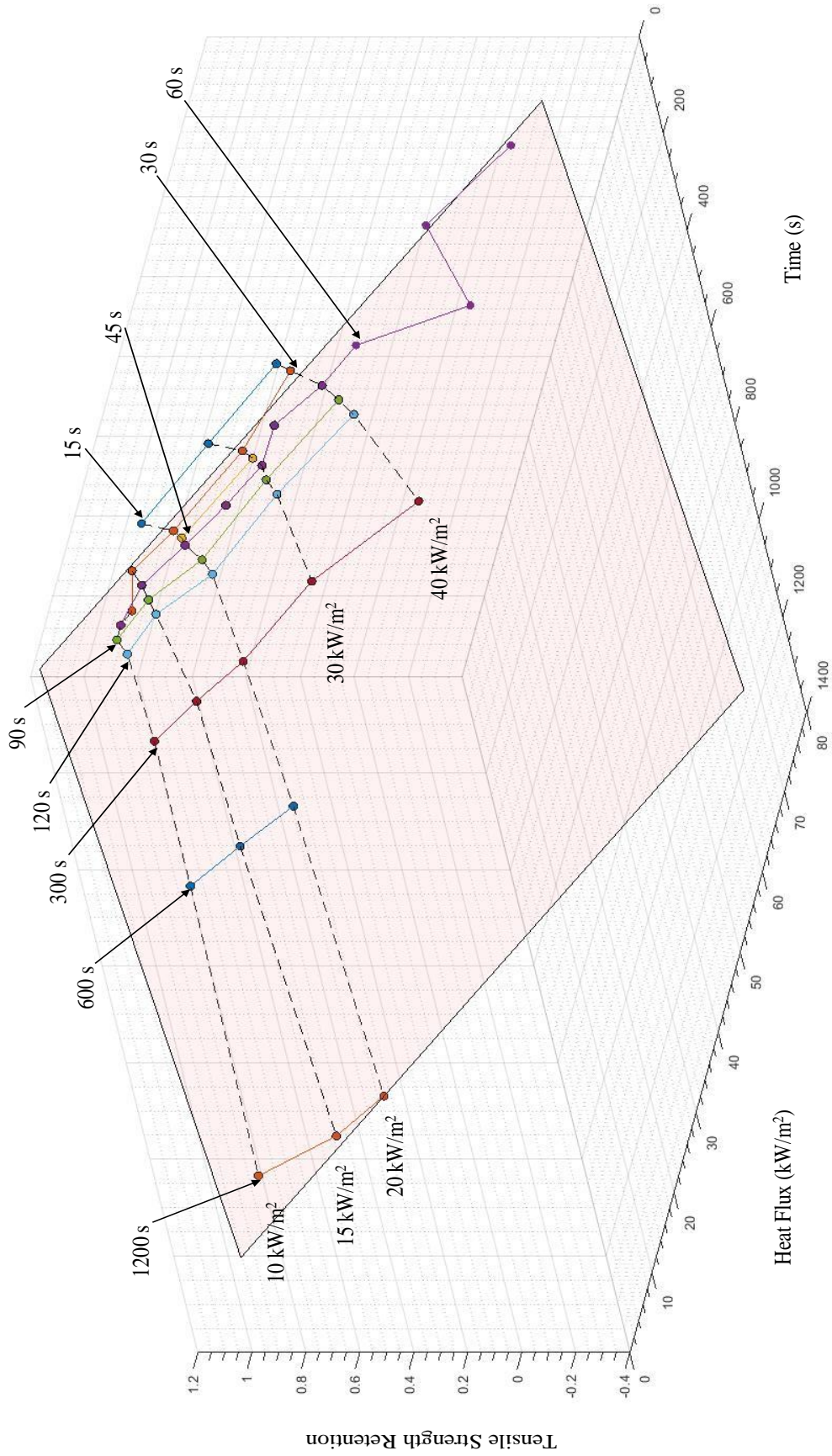


Figure 4.2 Three-Dimensional Representation Of Kombat Flex Data With The Multi-Variable Linear Regression Correlation

At short durations, there is a rapid decline in tensile strength. In Figure 4.2 at exposures of 15, 20, 30, and 40 kW/m², this rapid decline forms a curve during short durations, which then levels off into a more gradual tensile strength loss. Comparing the q'' and t axis of this graph, increasing heat flux has a higher impact on tensile strength loss than increasing duration. This is consistent with what was noted in Figure 4.1.

Naturally, this approach is not particularly effective in predicting tensile strength. This is visible in Figures 4.3 and 4.4 where there are inconsistencies between the prediction and experimental results when they are directly compared. Between these two figures, the correlation using Kombat Flex data better predicts the experimental data compared to Ripstop Natural. This data is presented using heat flux, correlations can also be developed using temperature data, which produce similar results.

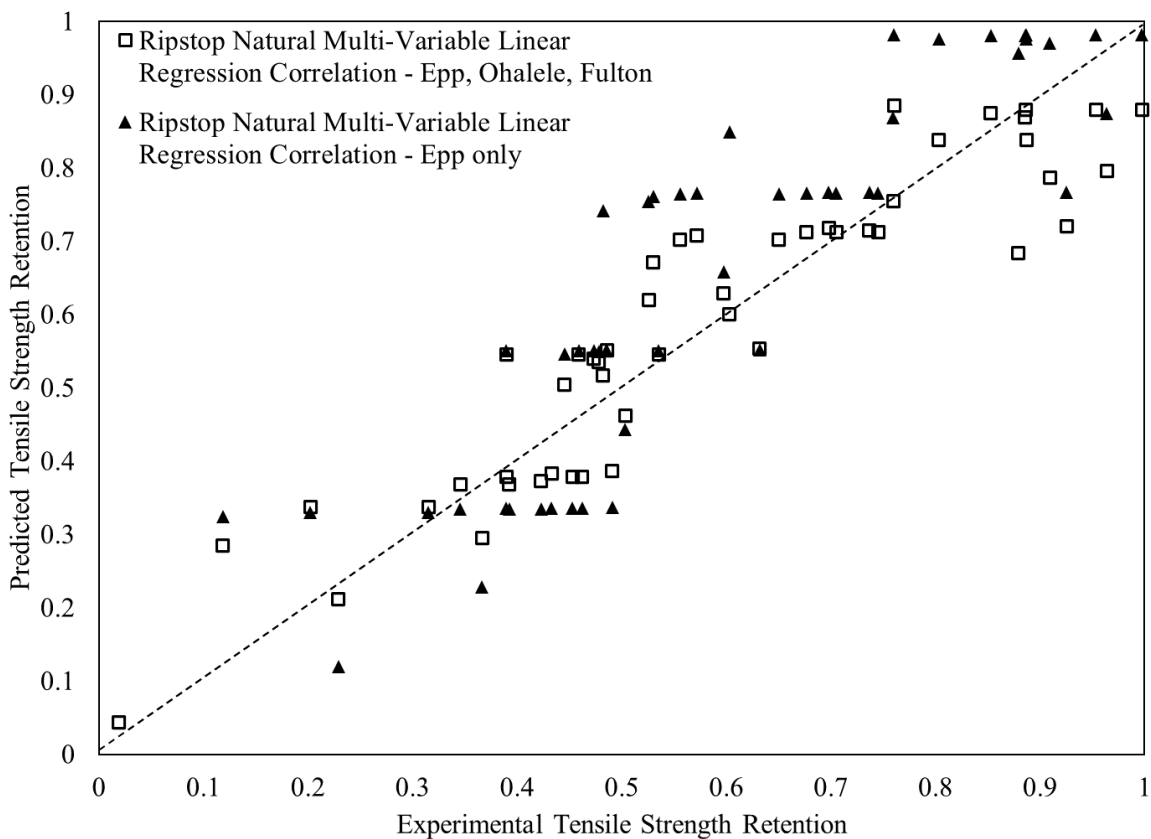


Figure 4.3 Ability Of A Multi-Variable Linear Regression Correlation To Predict Tensile Strength For Ripstop Natural Fabrics After Exposures To Various Heat Fluxes (Ohalele 2020; Fulton 2017).

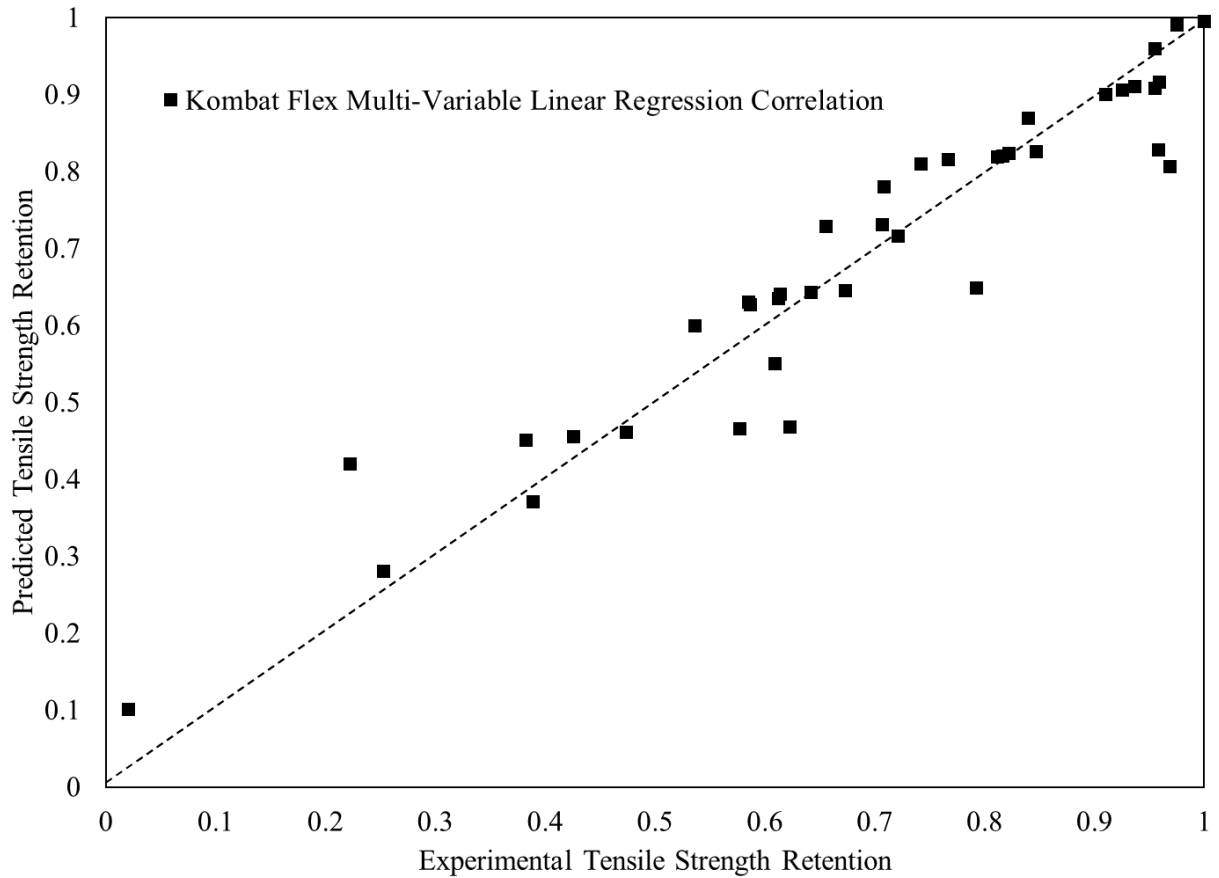


Figure 4.4 Ability Of A Multi-Variable Linear Regression Correlation To Predict Tensile Strength For Kombat Flex Fabrics After Exposures To Various Heat Fluxes

4.1.2 Multi-Variable Linear Correlation Accuracy And Limitations

The intention of the multi-variable linear regression correlation was to visualize how the tensile strength is affected by the change of the exposure and the duration. What has become clear is that the multi-variable linear regression correlation is not a useful correlation for predicting tensile strength. This is particularly noticeable in its inability to capture the rapid drop off of tensile strength at the start of any experiments. To fully capture this, Table 4.2 has been put together, which outlines the average, median, and standard deviation for Kombat Flex’s standard error in comparison between experimental and predicted points. This data has been split into exposures under 60 s, and exposures over 60 s to better capture the early tensile strength loss. Overall, the multi-variable linear regression correlation is less accurate than the other correlations in its ability to predict tensile strength retention.

Table 4.2 Average, Median, And Standard Deviation Of Standard Error For Multi-Variable Linear Regression Correlation Split By Duration For Kombat Flex

	Exposures Under 60 seconds	Exposures Over 60 seconds
Average (%)	16.4	7.9
Median (%)	4.7	6.0
Standard Deviation	27.4	10.3

4.2 Multi-Variable Nonlinear Regression Correlation

While the linear regression in three-dimensions resulted in an equation of a plane, this multi-variable nonlinear regression approach was used to consider an alternative correlation between exposure and duration. The following is a look at multi-variable nonlinear regressions that approach the problem when the independent variables are products with powers.

This method of correlation begins with the idea that a power law relationship between the independent variables could establish a reasonable estimation of the tensile strength, which is consistent with typical reaction models in solid thermal decomposition (Vyazovkin and Wight 1999). Equation 4.2 shows the relationship used here with respect to heat flux (Arrieta 2011; Dolez *et al.* 2019). The coefficients a , b , and c , correlate to the values present in Tables 4.3. For the development with respect for temperature, see Appendix E.

$$\frac{TS}{TS_i} = aq''^b t^c \quad (4.2)$$

where,

q'' is the heat flux exposure (kW/m²), and

t is time (s), and

a , b , and c are coefficients that can be found in the generalized Table 4.3.

Theoretically, a correlation should go through a tensile strength retention of 1 at a time of 0. As will be seen later, the exponent on time in equation 4.2 is negative and therefore the value would go to infinity when time is 0. Therefore, while constructing these equations it was recognised that they would not give a value of 1 at time equal to 0. As the intention was to develop a correlation to predict tensile strength retention for a range of exposure durations, this was not considered to be a major concern.

In an initial approach, all data was used in the multivariable nonlinear regression. When this correlation's estimates were compared against the experimental results, it was not effective at estimating the tensile strength over the entire range, specifically at the higher and lower ends. This is likely due to the different changes occurring over the range of exposures considered in this research. To mitigate this, the data was split into regions of exposure. Physically, this follows the idea that there are multiple effects on the reaction rate of the material. When considering the TGA curves for these fabrics (Figures 3.16 and 3.17 from Chapter 3) there are two important peaks in reaction rate near 265°C and another jump near 490°C (the peak of the jump in derivative mass, Table 3.7). The first temperature peak correlates with the thermal aging exposures near 15 kW/m² while the second important reaction rate begins to change near 425°C and peaks near 490°C. 425°C correlates to a thermal exposure of 45 kW/m², while the peak temperature correlates to an exposures of 60 kW/m².

Physically, the first change in reaction rate (near 15 kW/m²) indicates when thermal degradation in the specimens begin to rapidly take affect. Because of this, data before 15 kW/m² has been excluded from these correlations. Data at 45 kW/m² and above has been slotted into a second region which correlates to a higher reaction rate. What will become evident when examining this second region is that it is a weaker correlation than the main body, which is expected as it is has much fewer datapoints to support it. Additional testing would help to improve this correlation.

For this technique, three coefficients are determined by multi-variable nonlinear regression based on the collected data. This approach was conducted using a linear regression, which was done by linearizing the equation 4.2 into equation 4.3.

$$\ln\left(\frac{TS}{TS_i}\right) = \ln(a) + b \ln(q'') + c \ln(t) \quad (4.3)$$

For each linear regression that follows, calculations were done using Microsoft Excel. Kombat Flex data (Table 4.3) has been expressed as before and after 45 kW/m² and 60 s. Ripstop Natural has been split into correlations based on which data set was used as well as an overall set with Epp's, Ohalele's, and Fulton's datasets together. For further detail into how these coefficients were determined, testing the validity of this correlation with randomly selected exposures, and development for temperature, see Appendix E. This correlation was also applied to previously

tested materials at the University of Saskatchewan, namely Ripstop Black and PBI Max. For this work, see Appendix F. The coefficients of Table 4.3 are for equation 4.3.

Table 4.3 Multivariable Nonlinear Regression Coefficients For Equation 4.3 With Standard Errors With Split Data Regions At 45 kW/m² And 60 s Where Reaction Rate Changes

Kombat Flex				
	before 45.60	Standard Error	After 45.60	Standard Error
a	15.864	-	3.40E+16	-
b	-0.802	0.1	-10.188	1.6
c	-0.136	0.02	0	0
RSN.Fulton.Ohalele.Epp				
	before 45.60	Standard Error	After 45.60	Standard Error
a	28.276	-	1.75E+21	-
b	-0.967	0.1	-12.994	1.0
c	-0.186	0.03	0	0
RSN.Epp				
	before 45.60	Standard Error	After 45.60	Standard Error
a	86.105	0.5	1.75E+21	-
b	-1.271	0.1	-12.994	1.0
c	-0.225	0.03	0	0
RSN.Ohalele				
	before 45.60	Standard Error	After 45.60	Standard Error
a	5.660	0.2	1.75E+21	-
b	-0.593	0.1	-12.994	1.0
c	-0.103	0.02	0	0
RSN.Fulton				
	before 45.60	Standard Error	After 45.60	Standard Error
a	7.025	0.1	1.75E+21	3.8
b	-0.747	0.04	-12.994	1.0
c	0.000	0	0	0

4.2.1 Multi-Variable Nonlinear Regression Graphical Representation

After determining an appropriate split in the data at 45 kW/m², a multi-variable nonlinear regression was applied to both materials' datasets. Figure 4.5 shows a comparison between the predicted and measured tensile strength results. As a reminder, exposures above 40 kW/m² (45, 50, 60, and 70 kW/m²) are using the second regression. This data is presented as heat flux, temperature versions of this graph can be found in Appendix E.

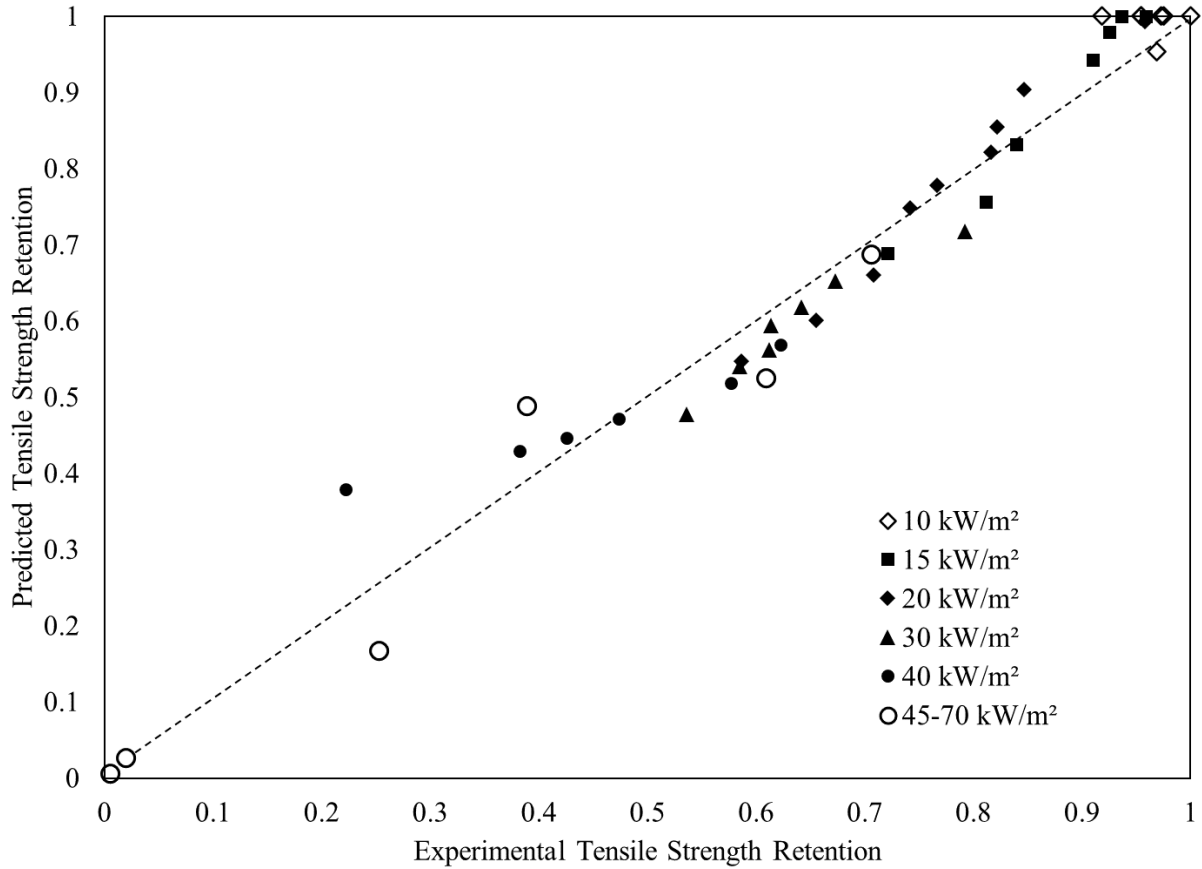


Figure 4.5 Ability Of A Split-Region Multi-Variable Nonlinear Regression Correlation To Predict Tensile Strength Of Kombat Flex Fabrics After Exposures To Various Heat Fluxes

In Figure 4.5, the weaker correlation at high heat fluxes is due to how many data points are supporting the correlation. The two weakest points of correlation occur at 40 kW/m² and 300 s and 50 kW/m² and 60 s with standard errors of 70% and 34% respectively. Exposures of 20 kW/m² through to 40 kW/m² are reasonably close to the 45 degree line, with standard errors as high as 10% at 30 kW/m² and 15 s. This is where this correlation is most effective in its predictions.

Another way of examining the effectiveness of this correlation is to look at how the correlation predicts points on a per-exposure basis. Figure 4.6 shows the experimental points at 20 kW/m² on top of the predicted tensile strength. The correlation is able to predict Kombat Flex's tensile strength for the first 120 s, after which the correlation underestimates the tensile strength.

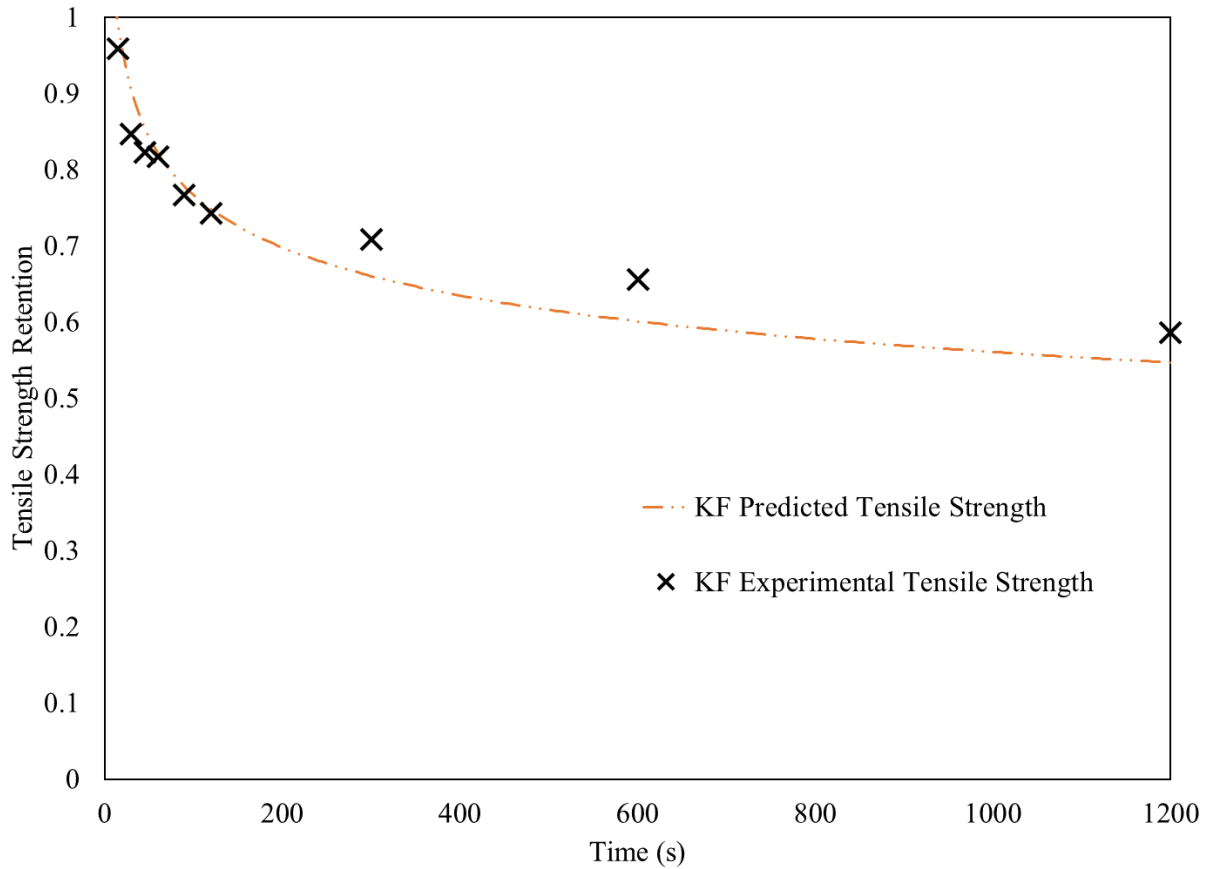


Figure 4.6 Comparison Of Kombat Flex Heat Flux Experimental Data To The Multivariable Nonlinear Regression Correlation At 20 kW/m²

Using the multi-variable nonlinear regression for Ripstop Natural results in a weaker correlation compared to Kombat Flex. Figure 4.7 shows the comparison between experimental and predicted tensile strength results. This Figure considers datasets developed by Epp, Ohalele (2020), and Fulton (2017). Figure 4.8 shows the 20 kW/m² datapoints alongside the predicted 20 kW/m² line.

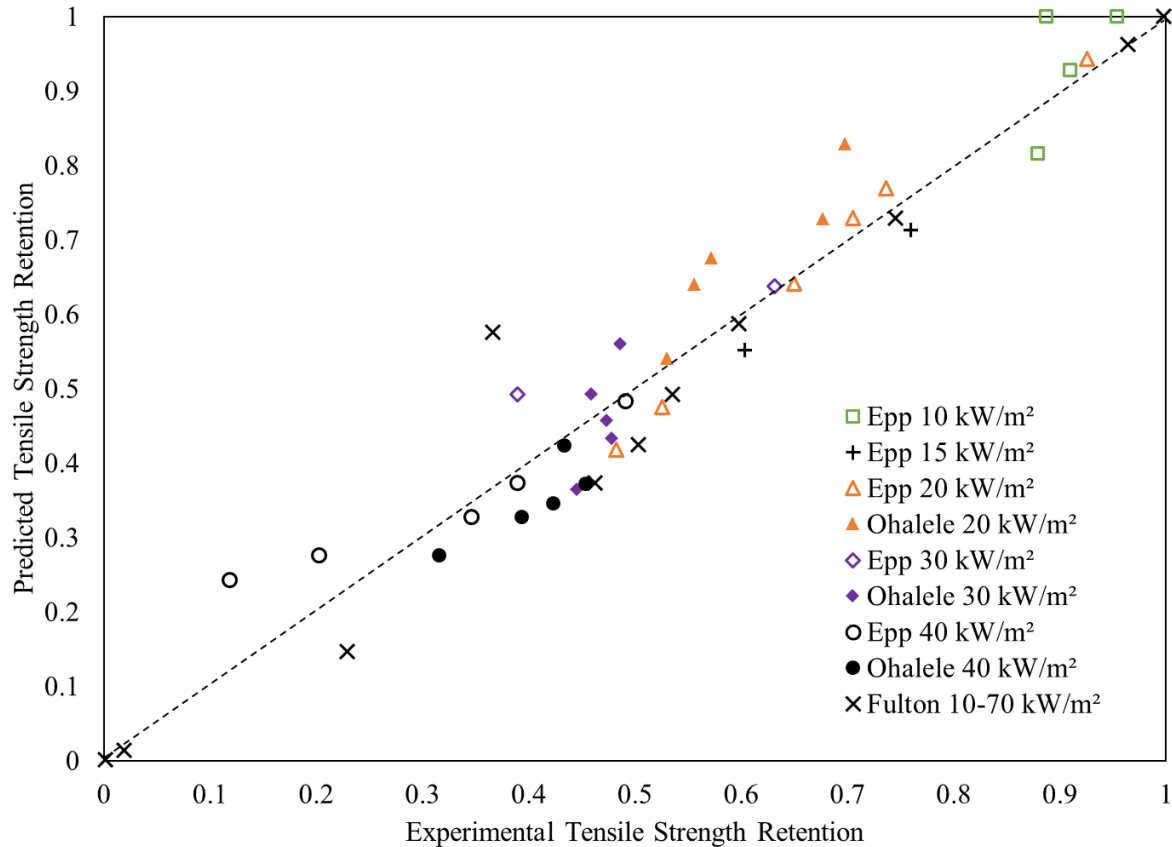


Figure 4.7 Ability Of A Split-Region Multi-Variable Nonlinear Regression Correlation To Predict Tensile Strength Of Ripstop Natural Fabrics After Exposures To Various Heat Fluxes Using Multiple Datasets (Fulton 2017; Ohalele 2020)

In general, Ripstop Natural results for the multi-variable nonlinear regression correlation are similar to Kombat Flex. The biggest difference comes from the amount of uncertainty that resulted from attempting to correlate between three sets of data that were obtained from different researchers. For this research’s experimental tests, there is reasonable agreement with the weakest correlation happening at high durations of 40 kW/m², which is expected due to the sparseness of datapoints. At this exposure, 300 s and 600 s had standard errors of 31% and 69% respectively. The next lowest error is at 30 kW/m² and 60 s at 23%. Outside of these points, the multi-variable nonlinear regression Ripstop Natural approach was around or below 10%.

The standard errors of previous research showed similar levels (Fulton 2017; Ohalele 2020). Ultimately this correlation does show that it is possible to relate across the three datasets. Further comparisons using the Ripstop Natural data, such as applying multi-variable nonlinear

regressions using only a single researcher's set of data and correlations made with different regions can be found in Appendix E.

As a representation of this correlation's effectiveness, Figure 4.8 shows the Ripstop Natural multi-variable nonlinear regression prediction compared against this research's experimental data. Further comparisons can be found in Section 4.4 with other correlation comparisons. At 20 kW/m², the multi-variable nonlinear regression correlates quite well to the predicted line using the multi-variable nonlinear regression. The highest error of 13% comes at the longest duration.

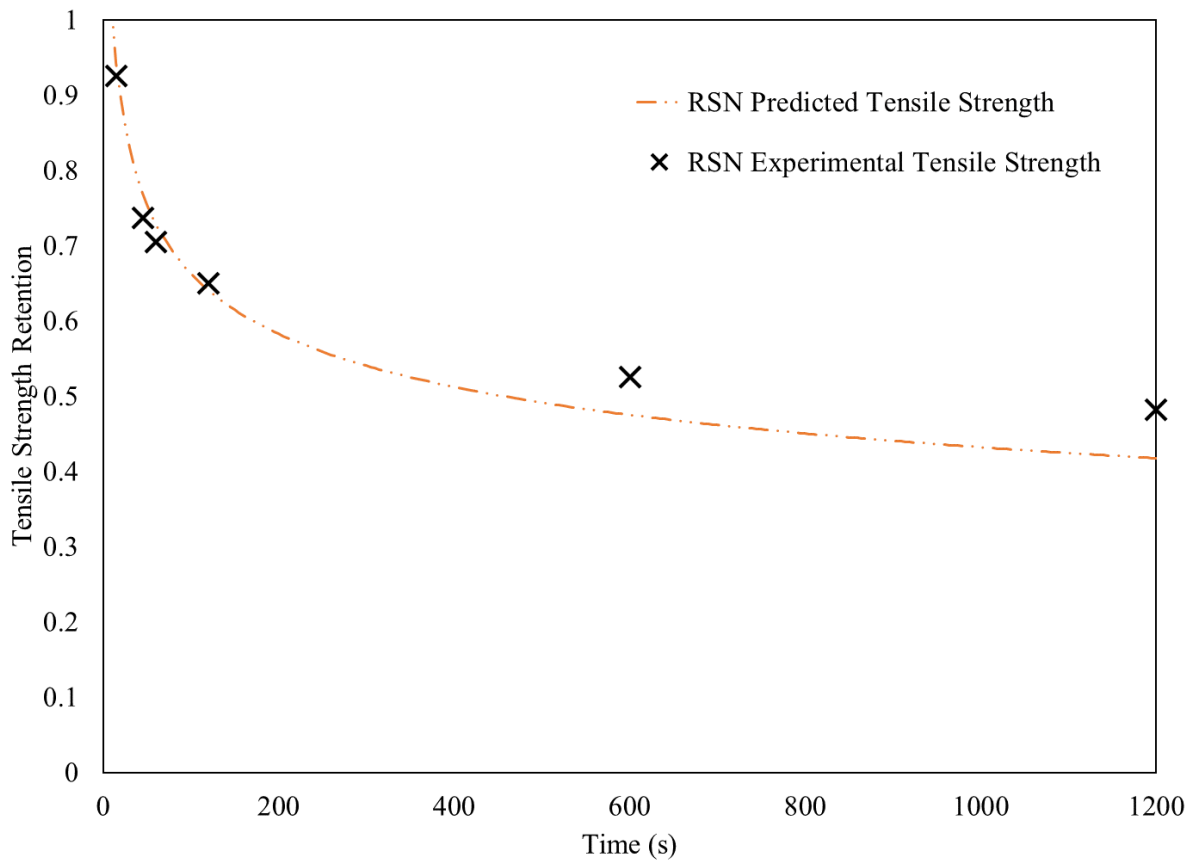


Figure 4.8 Comparison Of Ripstop Natural Heat Flux Experimental Data To The Multivariable Nonlinear Regression Correlation At 20 kW/m² (Fulton 2017; Ohalele 2020)

4.2.2 Multi-Variable Nonlinear Regression Accuracy And Limitations

This correlation established the strongest relationship when predicting tensile strength retention when varying heat flux. It also excels at predictions at lower exposures and durations.

This is particularly important when considering Veghte’s (1988) study mentioned in Chapter 1, which indicates that routine and ordinary exposures for Firefighters are below 20 kW/m². Table 4.4 outlines standard error statistics for Kombat Flex and Ripstop Natural, with the average error typically residing under 10%. When considering statistics at 45 kW/m² and below, Kombat Flex’s standard errors all improve, reinforcing the effectiveness of this correlation for typical exposures. As noted in Chapter 3, at high exposures these materials become damaged rapidly, and would be retired immediately for the safety of the user (see Figures 3.1 And 3.2).

Table 4.4 Kombat Flex And Ripstop Natural Standard Error Statistics For Multi-Variable Nonlinear Regression With Comparative Splits For All Durations And For Durations Under 60 s / Exposures Under 45 kW/m²

Kombat Flex		
	All Data	Under 60 s, Under 45 kW/m²
Average (%)	8.6	6.6
Median (%)	5.4	4.1
Standard Deviation	12.1	5.9

Ripstop Natural		
	All Data	Under 60 s, Under 45 kW/m²
Average (%)	11.3	10.4
Median (%)	8.3	7.5
Standard Deviation	11.6	11.7

4.3 Single-Variable Nonlinear Correlation

This third approach is also a nonlinear regression, but with a single-variable approach to the datasets. Instead of taking all the data at once into a regression based on an assumed equation, it will first split the data into regressions at single heat flux values. This approach was applied by Arrieta (2011) and by Dolez (2019) in similar research. Three correlations were tested, which were an exponential correlation, an Arrhenius correlation, and a power law correlation. Of these three, the power law correlation had the more consistent fit with an R² value of 0.82, and so it was selected for this correlation. This selection was also anticipated as it was supported by the literature (Vyazovkin and Wight 1999; Arrieta 2011; Dolez 2019). Appendix G outlines all three of these tested correlations and more justification behind the selection of the power law

correlation for this approach. The power law correlation equation in question is represented in equation 4.4. the coefficient values can be found in Table 4.5.

$$\frac{TS}{TS_i} = at^n \quad (4.4)$$

Where,

a and n are coefficients that can be found in the generalised Table 4.5.

For this development, the test exposures which have multiple durations have been selected. This includes exposures at 10, 15, 20, 30, and 40 kW/m² for Kombat Flex and 10, 20, and 40 kW/m² for Ripstop Natural. The same approach was used as for the multi-variable nonlinear regression correlation, namely first linearizing equation 4.4. Table 4.5 summarises the coefficients for Kombat Flex Ripstop Natural, Ripstop Black, and PBI Max for datasets from this research and Ohalele (2020).

Table 4.5 Power Law Correlation Coefficients For Equation 4.4 For Kombat Flex, Ripstop Natural, PBI Max, And Ripstop Black Using The Five Exposures With Multiple Durations (Ohalele 2020).

Heat Flux (kW/m ²)	Epp Kombat Flex		Epp Ripstop Natural		Ohalele Ripstop Natural		Ohalele Ripstop Black		Ohalele PBI Max	
	a	n	a	n	a	n	a	n	a	n
10	1.017	-0.009	0.976	0.046	1.017	-0.255	1.008	-0.153	1.013	-0.107
15	1.275	-0.075	-	-	-	-	-	-	-	-
20	1.224	-0.101	0.867	0.263	0.876	0.091	0.838	0.306	0.924	0.206
30	1.045	-0.121	-	-	0.971	-0.626	0.896	-0.398	0.960	-0.106
40	1.742	-0.334	0.687	0.487	0.863	-0.251	0.684	0.588	0.974	-0.246

4.3.1 Single-Variable Nonlinear Graphical Representation

In contrast to the multi-variable nonlinear regression approach, the single-variable nonlinear approach can only be applied at exposures where there are multiple duration points. Figures 4.9 and 4.10 show the capabilities of this approach for Kombat Flex and Ripstop Natural respectively. Further comparisons can be found in Appendix F and G.

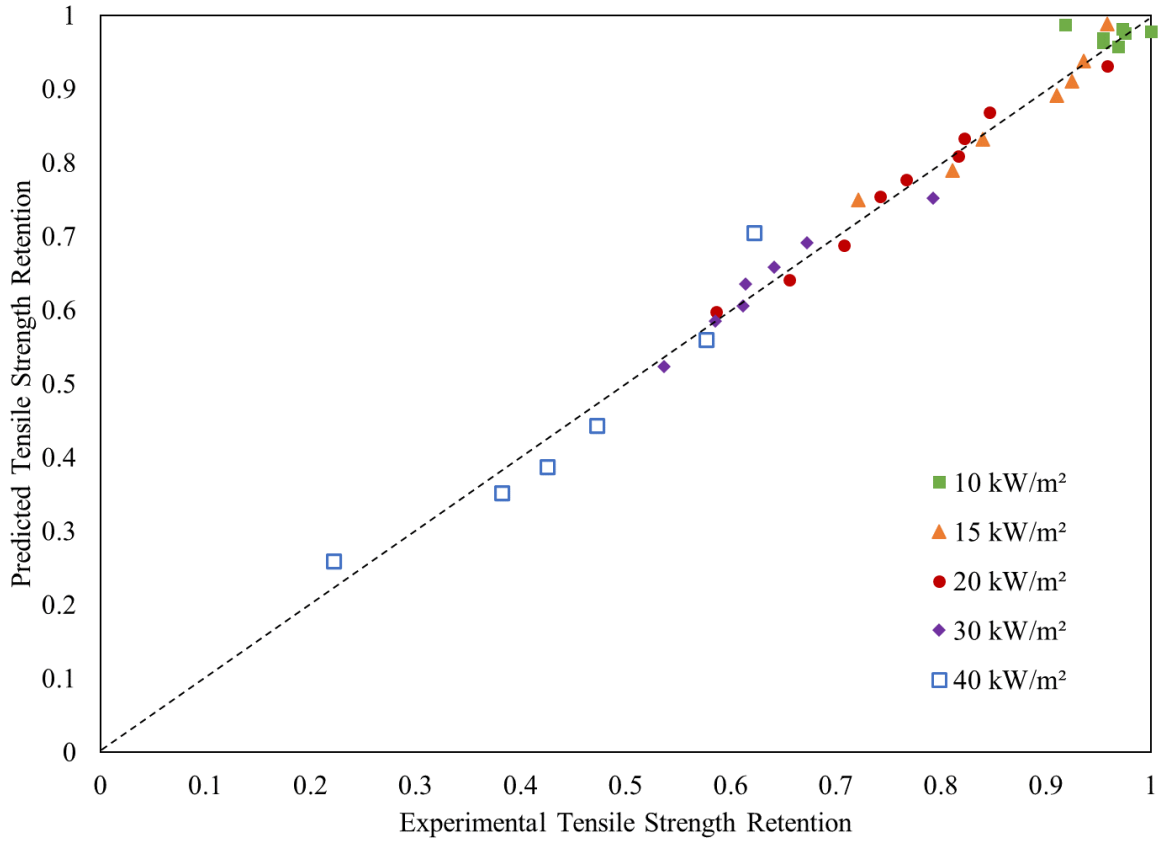


Figure 4.9 Ability Of A Single-Variable Nonlinear Correlation To Predict Tensile Strength Of Kombat Flex Fabrics After Exposures To Various Heat Fluxes

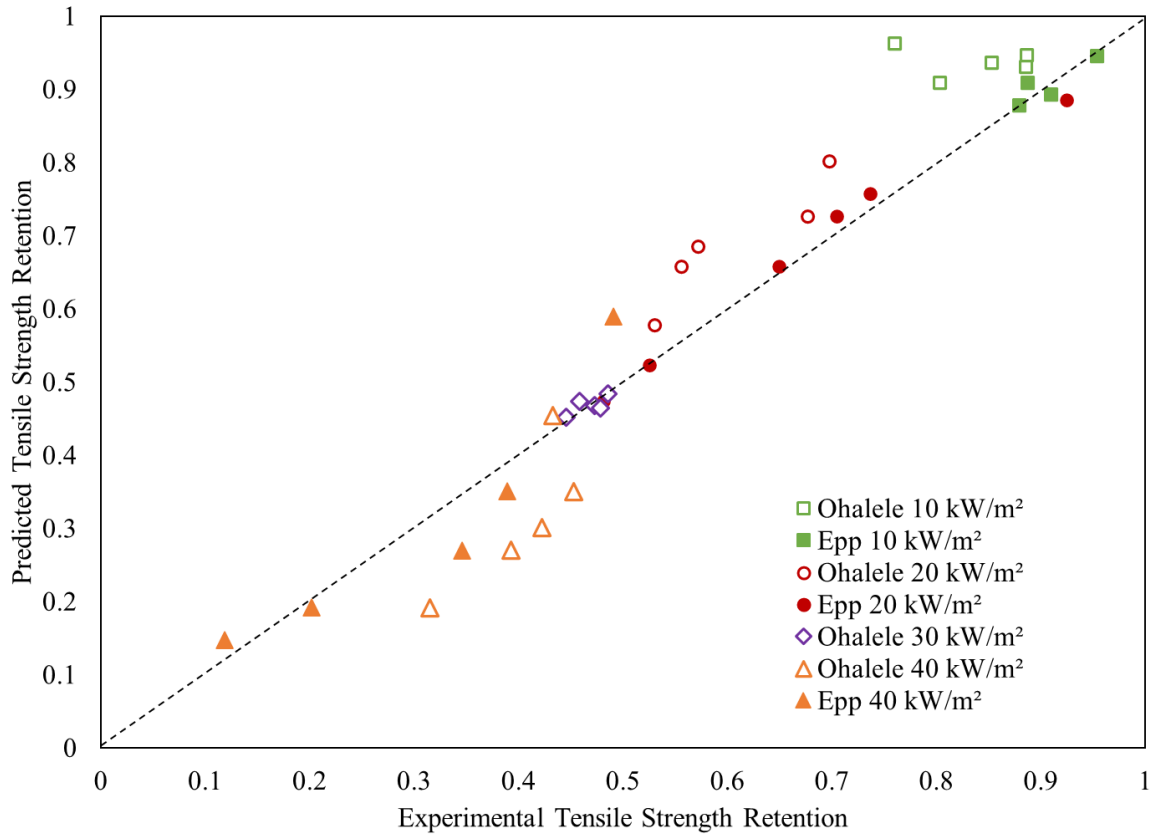


Figure 4.10 Ability Of A Single-Variable Nonlinear Correlation To Predict Tensile Strength Of Ripstop Natural Fabrics After Exposures To Various Heat Fluxes (Ohalele 2020)

The single-variable nonlinear method shows excellent correlation for Kombat Flex, but for Ripstop Natural suffers from more uncertainty. For Ripstop Natural at 10 and 20 kW/m², standard errors were less than 4% when compared to this research’s experimental data. This error was much worse at 40 kW/m² with the worst occurring at 600 s with an error of 25%. Figures 4.11 and 4.12 present a comparison between the predicted tensile strength to the experimental tests for Kombat Flex and Ripstop Natural respectively. Figure 4.12 shows Ripstop Natural for 20 and 40 kW/m² with correlations made from this research and Ohalele’s (2020) datasets separately.

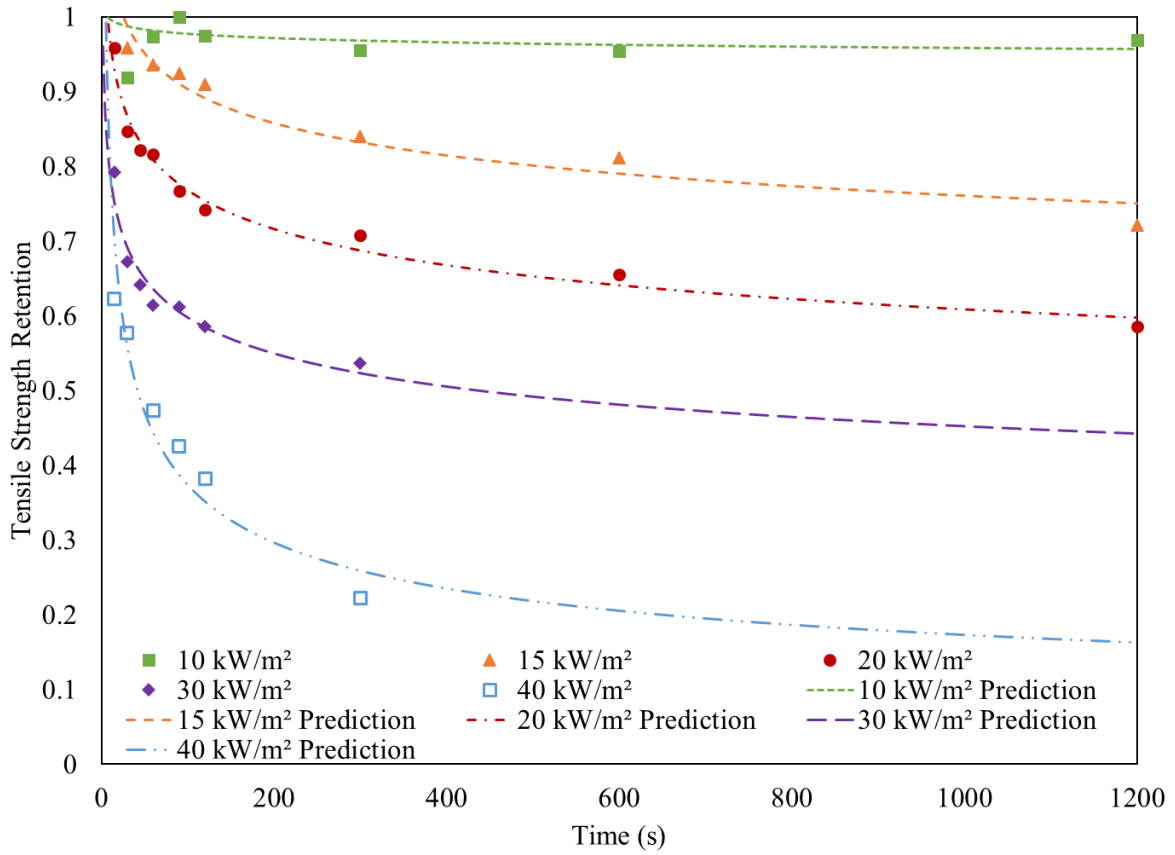


Figure 4.11 Kombat Flex Single-Variable Nonlinear Method Compared Over Time For 10, 15, 20, 30, and 40 kW/m²

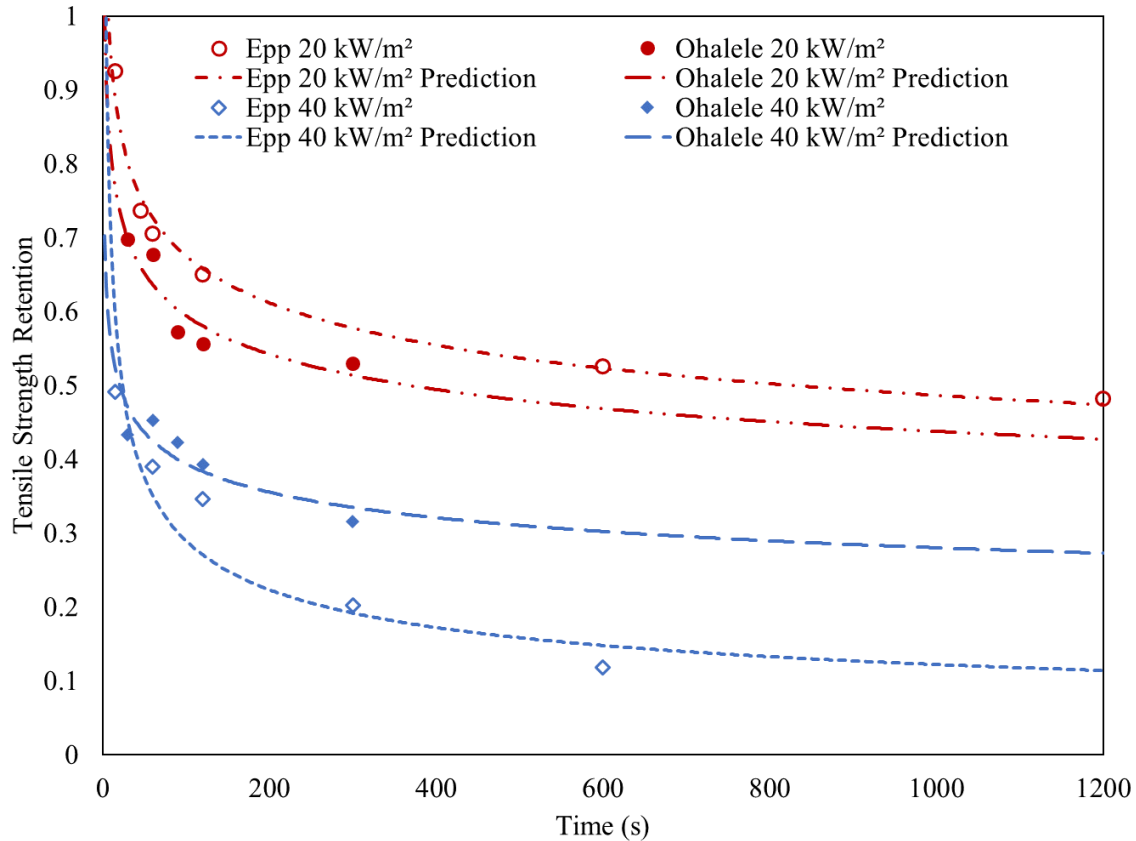


Figure 4.12 Ripstop Natural Single-Variable Nonlinear Method Compared Over Time for 20 and 40 kW/m²

4.3.2 Single-Variable Nonlinear Correlation Accuracy And Limitations

Of the three correlations, this correlation was the most accurate (see Table 4.7), though can only be applied to a single heat flux exposure. The correlations for Ripstop Natural do not have the same accuracy that Kombat Flex exhibits, but are still useful. Table 4.6 outlines the average, median, and standard deviation for the standard error of Kombat Flex and Ripstop Natural using the single-variable nonlinear correlation. This data has also been split by duration to showcase this correlation's ability to capture the early tensile strength loss that happens within the first 60 s.

Table 4.6 Average, Median, And Standard Deviation Of Standard Error For Kombat Flex And Ripstop Natural For Single-Variable Nonlinear Method (Ohalele 2020; Fulton 2017).

	Average (%)	Median (%)	Standard Deviation
Kombat Flex	3.3	2.3	3.6
Ripstop Natural (Epp, Ohalele, Fulton)	11.1	6.8	10.5

Similar to the multi-variable nonlinear regression correlation, improvements on this correlation could be made by increasing the number of test points that this correlation is relying on. In this case, this would include both having more timesteps within the already tested exposures as well as expanding number of exposures that have multiple timesteps. By expanding timesteps within an already tested exposure, this would help determine how long these trends hold up, particularly at lower exposures. By expanding exposures, this improves the cross-exposure correlation developed in Section 4.2.3, potentially making it a viable estimation tool for tensile strength.

4.4 Correlation Comparison

Thus far, several correlations have been created, but not all of them can be considered effective. The following section is a graphical comparison of the developed correlations. All experimental data herein is this research’s tests. Error bars represent the standard deviation from the tensile strength tests conducted at the University of Alberta and were rescaled for tensile strength retention. The main exposures of interest presented here are those with the most tests. Excluded in this section are any correlations using the multi-variable linear regression correlation as these correlations were developed as a visual aid rather than predicting data.

As this section focuses on showcasing the ability of these correlations at predicting tensile strength retention, 10 kW/m² was excluded. This was done as at this exposure, both Kombat Flex and Ripstop Natural did not exhibit consistent tensile strength loss. Throughout Chapter 4, statistics on the standard error of the effectiveness of these correlations have been shared. Table 4.7 shows a comparison of these statistics.

Table 4.7 Standard Error Comparison Across Correlations

Kombat Flex		
	Multi-Variable Nonlinear	Single-Variable Nonlinear
Average (%)	8.6	3.3
Median (%)	5.4	2.3
Standard Deviation	12.1	3.6
Ripstop Natural		
	Multi-Variable Nonlinear	Single-Variable Nonlinear
Average (%)	11.3	11.1
Median (%)	8.3	6.8
Standard Deviation	11.6	10.5

4.4.1 Kombat Flex Correlation Comparison

For Kombat Flex, the correlations for comparison include the multivariable nonlinear regression correlations for both heat flux and temperature, and the single-variable nonlinear correlations. All Kombat Flex experimental data was collected for this research. Exposures 15 kW/m² (Figure 4.13), 20 kW/m² (Figure 4.14), 30 kW/m² (Figure 4.15), and 40 kW/m² (Figure 4.16) are compared below. These five correlations have a reasonable number of exposure points and correlations that present a good representation of comparison.

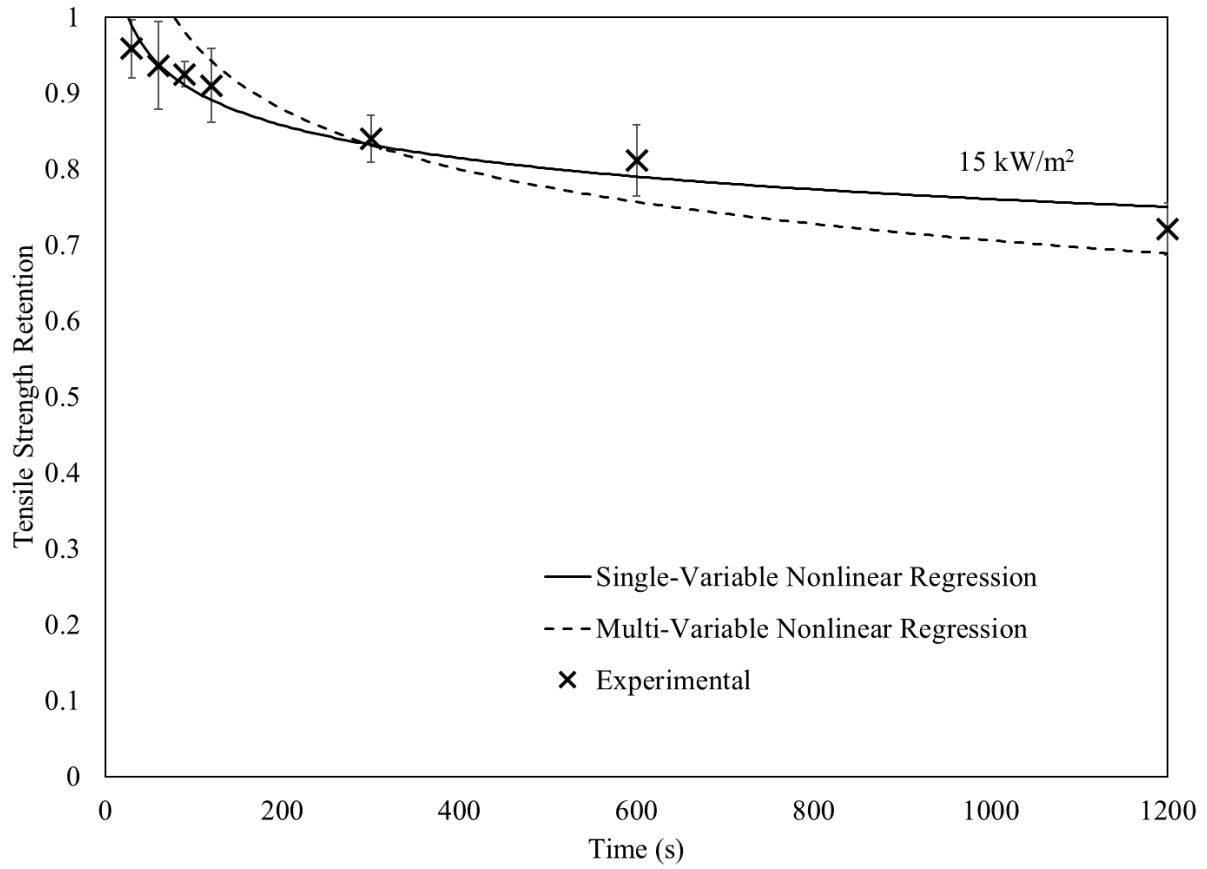


Figure 4.13 Kombat Flex Correlation Comparison For Exposure 15 kW/m². Error Bars Represent Standard Deviation.

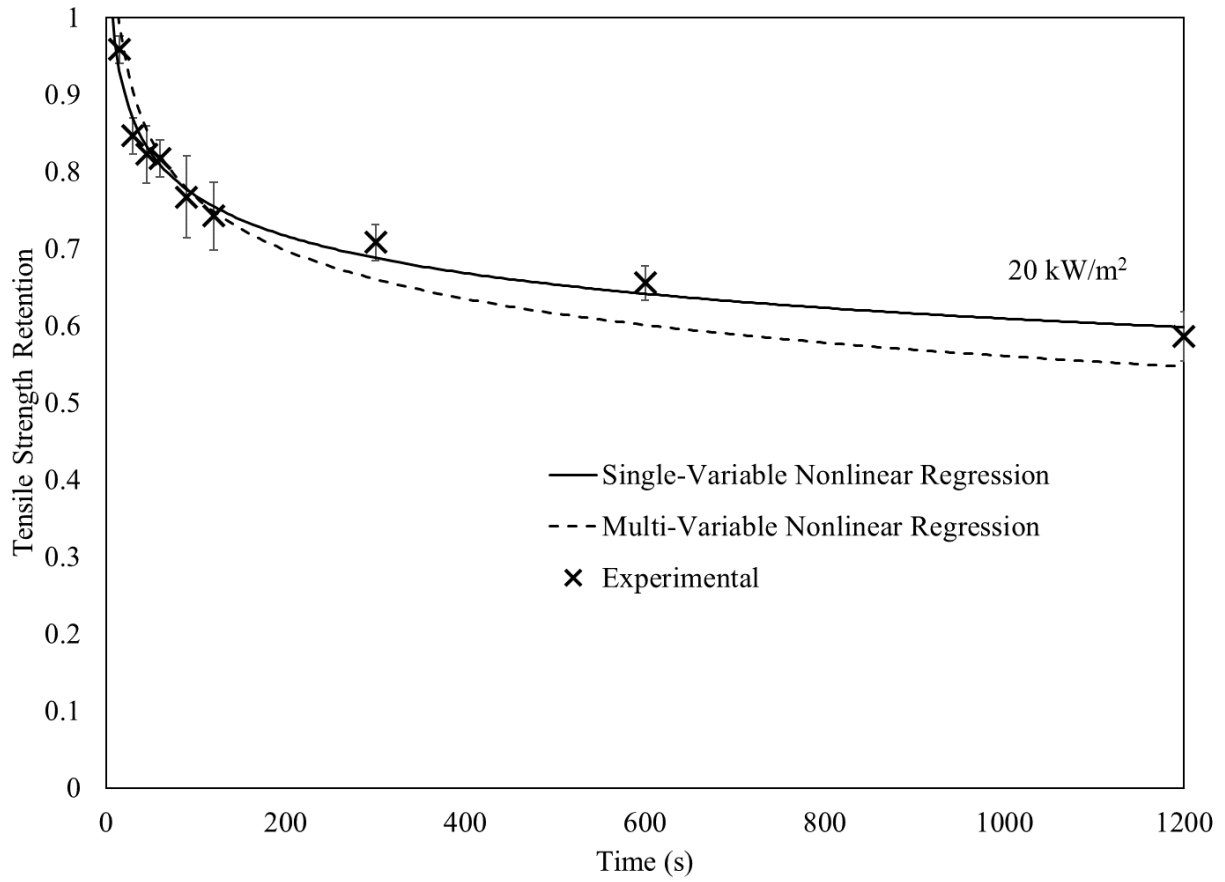


Figure 4.14 Kombat Flex Correlation Comparison For Exposure 20 kW/m². Error Bars Represent Standard Deviation.

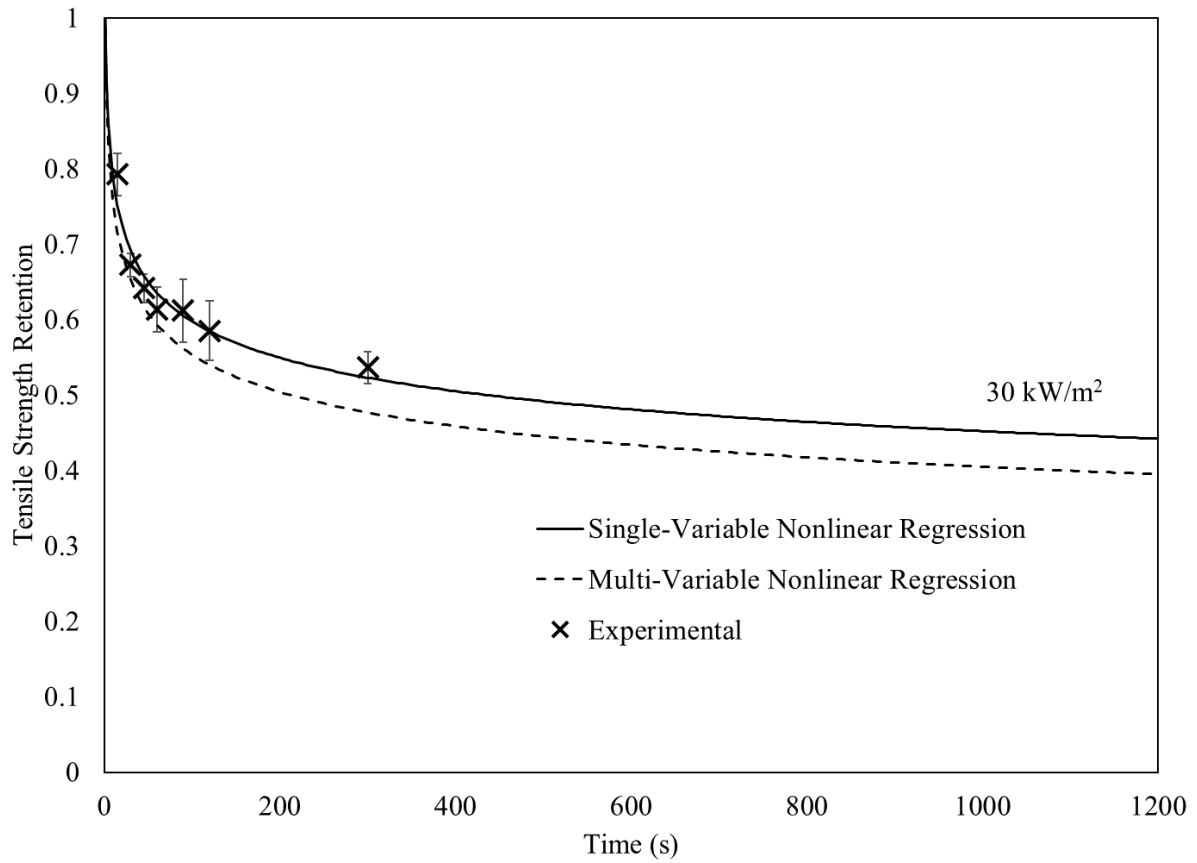


Figure 4.15 Kombat Flex Correlation Comparison For Exposure 30 kW/m². Error Bars Represent Standard Deviation.

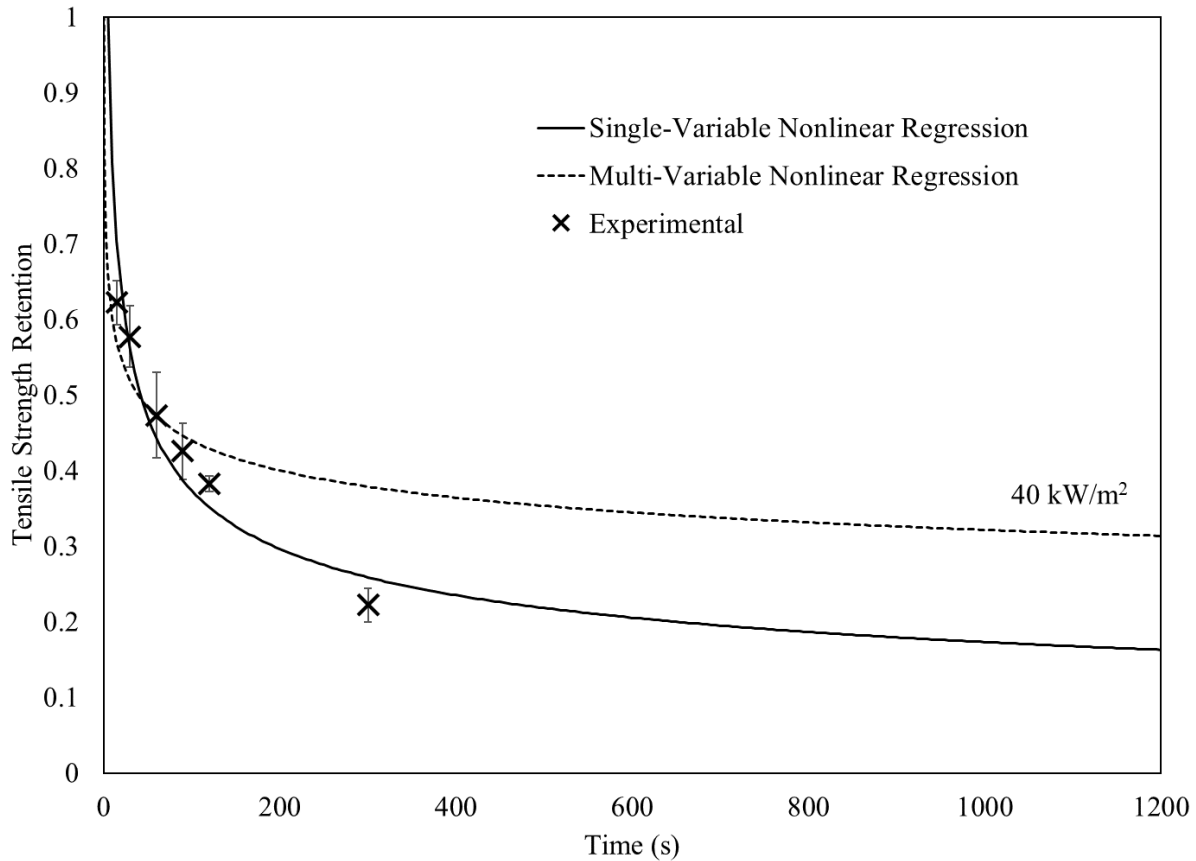


Figure 4.16 Kombat Flex Correlation Comparison For Exposure 40 kW/m². Error Bars Represent Standard Deviation.

Two things become noticeable when examining these four figures. First the single-variable nonlinear approach replicates the experimental data the closest. Second the multi-variable nonlinear regression approach overestimates at 15 kW/m² and underestimates at 40 kW/m², though at 15 kW/m² its predictions were just within the standard deviation of the tensile strength retention tests. The inability to predict at 1200 s for 40 kW/m² is likely related to the number of tests conducted at higher exposures, the increase in the number of material reactions at higher exposures (see TGA Figures 3.16 and 3.17 at temperatures above 400 °C), and the exclusion of a test at 1200 s from the test matrix.

4.4.2 Ripstop Natural Correlation Comparison

For Ripstop Natural, the correlations for comparison include the multi-variable nonlinear regression correlations for both heat flux and temperature, multi-variable nonlinear regression

correlations for heat flux constructed from Epp’s and Ohalele’s data exclusively, and the single-variable nonlinear correlations (for when an exposure has been explored). Experimental data present in this comparison was all from Epp’s research, thus correlations present were taken from exposures of 20 kW/m² (Figure 4.17), 30 kW/m² (Figure 4.18), and 40 kW/m² (Figure 4.19) to best showcase a comparison between these correlations and the experimental data.

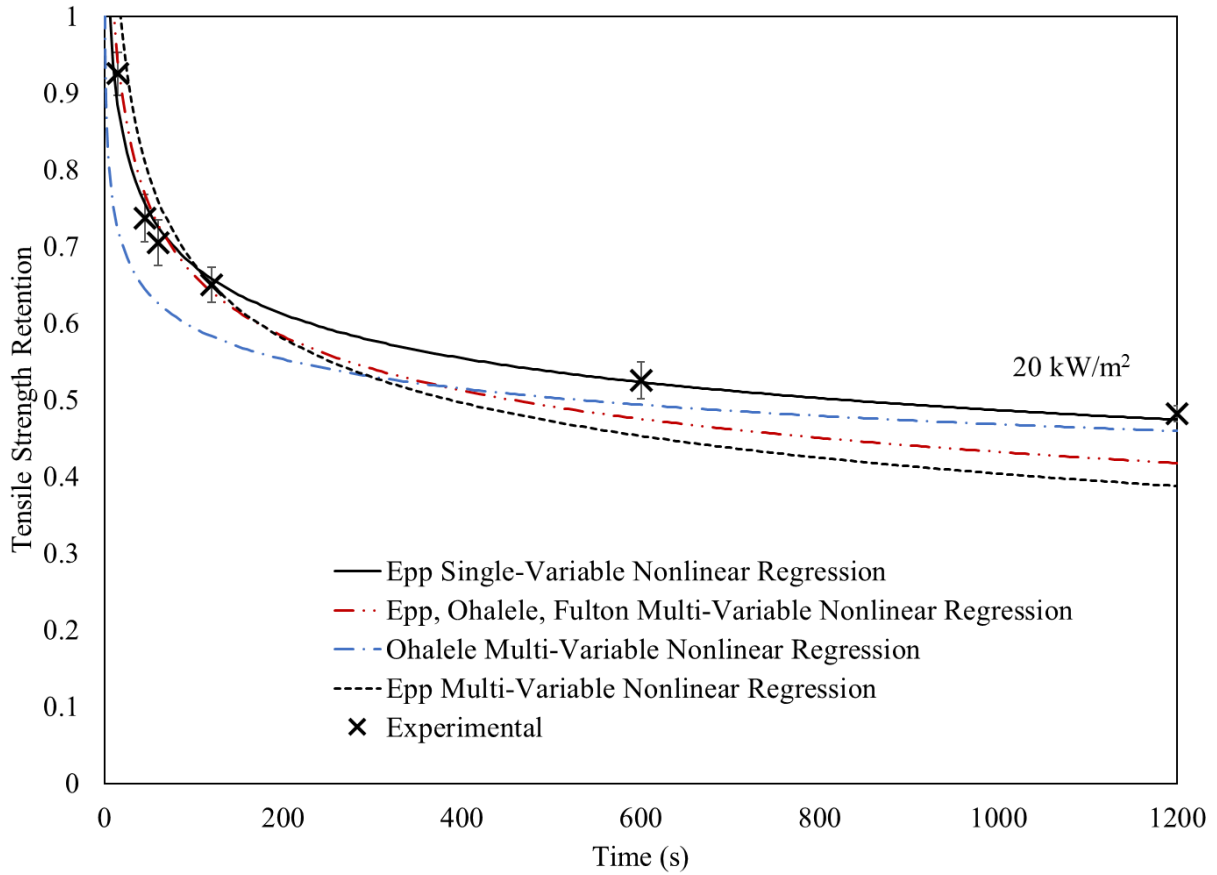


Figure 4.17 Ripstop Natural Correlation Comparison Of Exposure 20 kW/m² (Fulton 2017; Ohalele 2020)

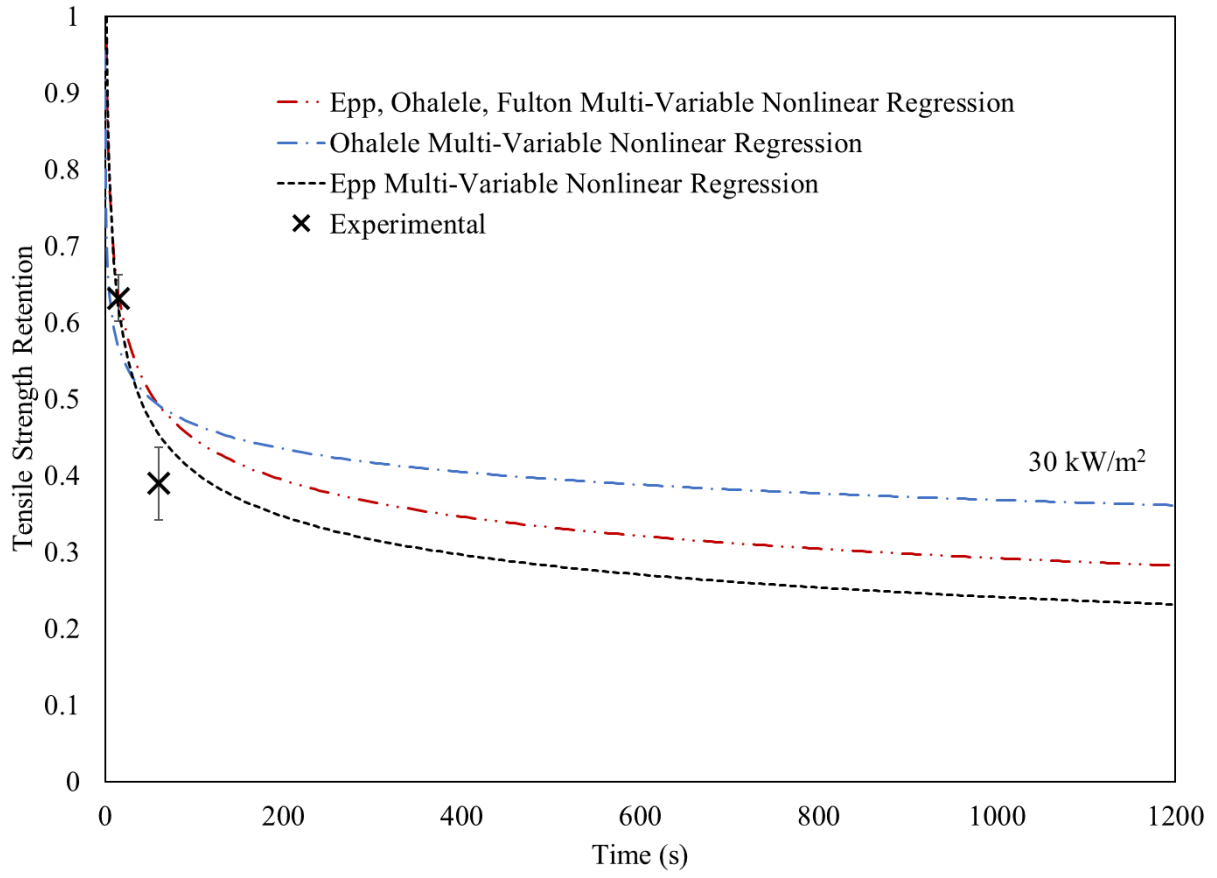


Figure 4.18 Ripstop Natural Correlation Comparison Of Exposure 30 kW/m² (Fulton 2017; Ohalele 2020)

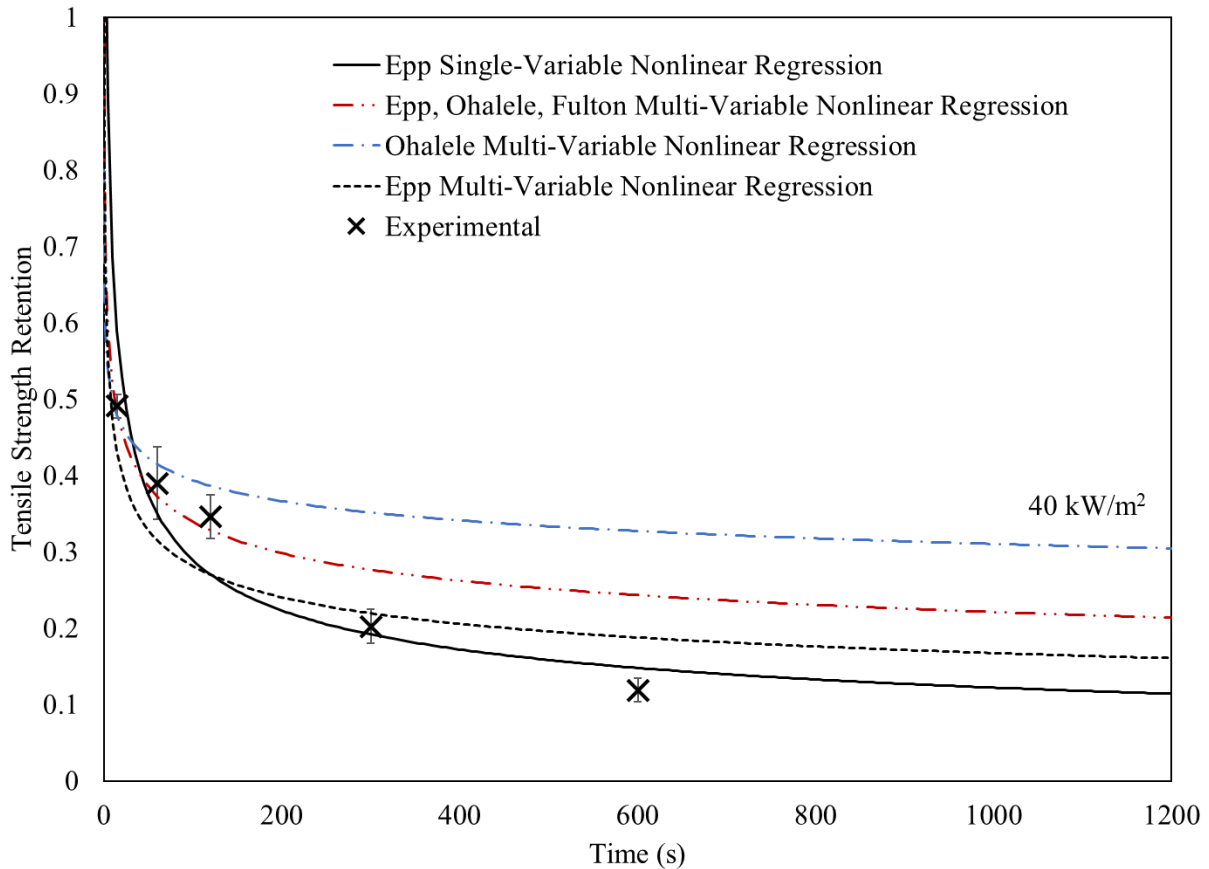


Figure 4.19 Ripstop Natural Correlation Comparison Of Exposure 40 kW/m², Showing Epp’s Correlations Only (Fulton 2017; Ohalele 2020)

Similar to the Kombat Flex comparisons, the single-variable nonlinear approach predicts the experimental data the closest. This is particularly noticeable at 40 kW/m² (Figure 4.19) where this is the only correlation that follows the experimental data. Most correlations at 20 kW/m² are able to effectively capture the early tensile strength loss (in the first two minutes of exposure). The exception to this is the multi-variable nonlinear regression constructed from Ohalele’s data (2020). Important to remember with Ohalele’s data is that this is constructed from five durations (30 s, 60 s, 90 s, 120 s, and 300 s). The longest duration correlations made with Ohalele’s data would be at five minutes. This correlation overestimates the damage at these points, which could be because Ohalele tested the Ripstop Natural in a different direction. Regardless, this highlights a fascinating comparison between correlations made from Ohalele’s data and when this research’s data is included, under which more tests could be done in the future for improvement.

At 30 kW/m², there is reduced consistency between the prediction of tensile strength retention at 20 min. This is anticipated due to how few datapoints are present at this exposure. Overall most of the correlations are able to capture the early tensile strength loss. This is the part of the exposure that is the most important to capture as this is when most of the tensile strength is lost in these fire protective garments. This is also when tensile strength will dip below the 623 N standard tensile strength requirement at these exposures (NFPA 1971, 2013).

4.5 Correlation Summary

Three approaches to correlating the experimental data were developed. These three approaches were a multi-variable linear regression correlation, a multi-variable nonlinear regression correlation, and a single-variable nonlinear correlation. The multi-variable linear regression correlation was useful for visualizing the tensile strength loss compared to heat flux and time, but was not effective at predicting tensile strength. When examining specific exposures, the single-variable nonlinear approach was able to effectively predict the tensile strength. This single exposure correlation is strongest when there is more experimental data, which is evident with Kombat Flex (Figures 4.13 to 4.16). The multi-variable nonlinear regression approach was able to predict tensile strength in between tested exposures, but its effectiveness at longer durations is limited.

Ultimately, the strength of all of these correlations is in predicting early tensile strength loss. This is the critical part of any exposure as this is when most of the tensile strength is lost in this type of protective garment. This is also when tensile strength drops below the standard 623 N (NFPA 1971, 2013) for higher exposures. Firefighters would retire these garments after high exposures as the material would visibly be damaged beyond safe use (see Figures 3.1 and 3.2).

Improvements in these correlations can be made. The simplest improvement would be to conduct more tests, which would strengthen the correlations overall. Conducting tests at a regular interval in both exposure and duration could improve understanding of what is occurring at the initial rapid drop in tensile strength at low durations. This could also improve understanding of what is happening at the high exposures above 50 kW/m² where few data points have been collected.

5.0 Conclusions and Future Work

5.1 Conclusions

One way of looking at this research is to split it into thermal aging, and correlating data. The following conclusions have been organised to follow these two components.

5.1.1 Thermal Aging

- A major contribution of this research project is the increased testing of previously studied materials and the inclusion of a new material (Kombat Flex). This expansion helped provide further insight into the thermochemical changes in these fabrics.
- Previous research noted that at 10 kW/m^2 , little to no thermochemical change occurs. In this research, an investigation of much longer durations was undertaken. It was found that over longer durations, these fabrics do decrease in tensile strength retention, but not by much. This establishes a similarity between this research and low exposure research found in the literature review (Arrieta 2011; Dolez 2019).

5.1.2 Correlations and Tensile Strength Testing

- Tensile strength results indicate materials failed the NFPA 1971 (2013) tensile strength test of 623 N at the lowest exposure of 20 kW/m^2 and a duration of 20 min for Kombat Flex, and before 20 kW/m^2 and 10 min for Ripstop Natural. This is in line with what Ohalele (2020) found in their research, where their tests passed this point for Ripstop Natural at exposures at and above 20 kW/m^2 .
- Three different correlations were constructed from the collected experimental data for both Kombat Flex and Ripstop Natural. The multi-variable nonlinear correlation and the single-variable nonlinear correlation are both effective correlations for predicting tensile strength, particularly at durations under five minutes.
- The multi-variable nonlinear correlation is an effective technique for predicting tensile strength when varying heat flux, particularly at heat fluxes below 40 kW/m^2 .
- The single-variable nonlinear correlation was the most effective correlation examined, with the drawback of being only usable within single heat flux exposures. Errors for this

approach averaged less than 4%, able to predict durations accurately and effectively over a large window of time.

5.2 Future Work

- It has been established in this and previous research that minimal thermochemical change occurs in the fabrics at 10 kW/m^2 , yet a rapid tensile strength loss is present at 15 and 20 kW/m^2 . There is potential for an expanded exploration of at what exposure these fabrics begin to have this rapid tensile strength loss. This would improve the accuracy of correlations at these low exposures for accurately capturing this change in reaction rate.
- Currently, these developed correlations are able to effectively predict early tensile strength loss, which is the more important portion to capture as this is when much of the tensile strength is lost. Further testing at lower heat flux exposures over extended durations reaching above one hour would help capture the tensile strength loss for when the tensile strength is not lost rapidly. This would help identify, for example, at what duration does the material drop below a tensile strength of 623 N at an exposure of 10 kW/m^2 . These increased duration tests would also improve the quality of the proposed correlations here, and help improve future developed correlations.
- Increased tests at low duration tests of exposures above when the fabric begins to rapidly decay would help to better establish the tensile strength degradation curve. This curve is when most of the tensile strength is lost, and having a detailed understanding of it would be a major contribution in predicting tensile strength.
- NIR reflectance data was collected for all specimens tested in this research. This data was examined in a limited capacity here. Similar analysis to what was done in Rezazadah (2014), Fulton (2017), and Ohalele (2020) could be conducted on these datasets.
- This research was conducted on outer layer specimens, but a similar regime of tests could be conducted on the moisture barrier, thermal lining, or a full ensemble. This was previously approached in Rezazadeh's dissertation (2014), but could be explored further. Ohalele (2020) posited that the use of transmittance NIR spectroscopy could be applied to ensembles for their degradation.

- This research was conducted with single thermal exposures, where multi-stage exposures could be employed to evaluate the thermal response of fabrics in a more accurate simulation of firefighting conditions.

This research represents the first attempt by the University of Saskatchewan to employ a universal fabric correlation from tensile strength based off of various exposures and durations. Much more work in this area could be explored, such as employing Arrhenius Kinetic models to characterize exposure tensile strength losses.

References

- Alexander, B. M., and C. S. Baxter. 2016. "Flame-retardant contamination of firefighter personal protective clothing - A potential health risk for firefighters." *Journal of Occupational and Environmental Hygiene* 13 (9): D148-55.
- Arrieta, C. 2011. "Étude de L'Effet du Vieillissement sur les Propriétés d'un Tissu en Mélange Kevlar(R)-PBI Utilisé dans le Revêtement Extérieur des Habits de Protection Contre le Feu" Ph.D. Thesis, École de Technologie Supérieure, Université du Québec.
- Arrieta, C., E. David, P. Dolez, and T. Vu-Khanh. 2010. "Thermal aging of a blend of high-performance fibres." *Journal of Applied Polymer Science* 93: 3031-3039.
- ASTM. 2022. *ASTM E1354: Standard Test Method for Heat and Visible Smoke Release Rates for Materials and Products Using an Oxygen Consumption Calorimeter*. West Conshohocken, PA: ASTM International.
- . 2020. *ASTM D1776: Standard practice for conditioning and testing textiles*. West Conshohocken, PA: ASTM International.
- . 2020. *ASTM E104: Standard practice for maintaining constant relative humidity by means of aqueous solutions*. West Conshohocken, PA: ASTM International.
- . 2020 *ASTM F2700-08: Standard test method for unsteady-state heat transfer evaluation of flame resistant materials for clothing with continuous heating*. West Conshohocken, PA: ASTM International.
- . 2020. *ASTM F1939-15: Standard test method for radiant heat resistance of flame resistant clothing materials with continuous heating*. West Conshohocken, PA: ASTM International.
- . 2019. *ASTM D5035: Standard test method for breaking force and elongation of textil fabrics (strip method)*. West Conshohocken, PA: ASTM International.
- . 2018. *ASTM D3766: Standard Terminology Relating to Catalysts and Catalysis*. West Conshohocken, PA: ASTM International.

- Bespflug, Christopher J., D. A. Torvi, S. D. Noble, M. Fulton, C. J. Vanderschaaf, and J. C. Batcheller. 2020. "The Impact of Soiling, Moisture Content, Abrasion and Ultraviolet Exposure on Near-Infrared Evaluation of In-Use Firefighter Protective Clothing." In *Performance of Protective Clothing and Equipment: 11th Volume, Innovative Solutions to Evolving Challenges*, ed. K. Lehtonen, B. P. Shiels, and R. B. Ormond. West Conshohocken, PA: ASTM International, 2020. 40-63.
- Bruns, M. C., and I. T. Leventon. 2020. "Automated fitting of thermogravimetric analysis data." *Fire and Materials* 45 (3): 406-414.
- Campbell, R., and S. Hall. 2022. *Firefighter Injuries in the United States*. Quincy, MA: National Fire Protection Association Research.
- Clark, R. N., and T. L. Roush. 1984. "Reflectance spectroscopy: Quantitative analysis techniques for remote sensing applications." *Journal of Geophysical Research: Solid Earth* 89 (B7): 6329-6340.
- Collier, B. J., M. Bide, and P. G. Tortora. 2009. *Understanding Textiles*. 7th ed. Upper Saddle River, New Jersey, USA: Pearson Prentice Hall.
- Collin, A., A. Marchand, A. Kadi, Z. Acem, P. Boulet, J. Pageaux, S. Pinson, M. Lepelletier, Y. Van Waelfelghem, F. Magnolini, and H. Charette. 2015. "Study on visible-IR radiative properties of personal protective clothings for firefighting." *Fire Safety Journal* 71: 9-19.
- Cui, Z., C. Ma, and N. Lv. 2015. "Effects of heat treatment on the mechanical and thermal performance of fabric used in firefighter protective clothing." *Fibres and Textiles in Eastern Europe* 23 (2): 74-78.
- Dewaghe, C., C. Lew, M. Claes, S. Belgium, and P. Dubois. 2011. *Fire-retardant applications of polymer-carbon nanotubes composites: improved barrier effect and synergism*. Ed by T.; Potschke McNally, P. *Polymer-Carbon Nanotube Composites*. Cambridge, MA: Woodhead Publishing Limited.
- Dolez, P. I., N. S. Tomer, and Y. Malajati. 2019. "A quantitative method to compare the effect of thermal aging on the mechanical performance of fire protective fabrics." *Journal of Applied Polymer Science* 136 (6).

- Fahy, R. F., and J. T. Petrillo. 2022. *NFPA's Firefighter Fatalities in the US in 2021*. Quincy, MA: National Fire Protection Association Research.
- Fahy, R., and J. Molis. 2019. *Firefighter Fatalities in the US - 2018*. Quincy, MA: National Fire Protection Association.
- Federal Trade Commission. 2009. "Generic Names and Definitions for Manufactured Fibres." Code of Federal Regulations, Title 16, Chapter I, Subchapter C, Part 303.7. Washington, DC: Federal Trade Commission.
- Feng, Q., F. L. Zhu, and J Hu. 2019. "Estimation of the radiant performance of flame-retardant fabrics considering thermal degradation effect." *Journal of Engineered Fibers and Fabrics* 14: 1-10.
- Fulton, M., M. Rezazadeh, and D. Torvi. 2018. "Tests for Evaluating Textile Aging." In *Advanced Characterization and Testing of Textiles*, edited by Patricia Dolez, Olivier Vermeersch; and Valerio Izquierdo, 93-126. Duxford, United Kingdom: Elsevier.
- Fulton, M. 2017. "Evaluating the Performance of Thermally and UV Aged Firefighters' Protective Clothing Using both Destructive and Non-Destructive Methods." M.Sc. Thesis, Department of Mechanical Engineering, University of Saskatchewan.
- Han, L., X. Zhao, and Y. Shen. 2019. "An investigation into the ease of ice removal properties of fabrics used for the outer layer of firefighter clothing." *Textile Research Journal* 89 (23-24): 5108-5118.
- Horn, G. P., S. Kerber, J. Andrews, R. M. Kesler, H. Newman, J. W. Stewart, K. W. Fent, and D. L. Smith. 2020. "Impact of Repeated Exposure and Cleaning on Protective Properties of Structural Firefighting Turnout Gear." *Fire Technology* 57 (2): 791-813.
- Huang, J., and C. Yu. 2019. "Determination of cellulose, hemicellulose and lignin content using near-infrared spectroscopy in flax fiber." *Textile Research Journal* 89: 4875-4883.
- Kiran, D. R. 2017. *Total Quality Management: Key Concepts and Case Studies*. edited by D.R. Kiran. Oxford, United Kingdom: Butterworth-Heinemann.

- Li, M., G. Han, W. Jiang, C. Zhou, Y. Zhang, S. Wang, J. Su, and X. Li. 2020. "Rapid identification of plant- and chemical-dyed cotton fabrics using the near-infrared technique." *Textile Research Journal* 90 (19-20): 2275-2283.
- Liu, X., M. Tian, Y. Wang, Y. Su, and J. Li. 2021. "Modeling to predict thermal aging for flame-retardant fabrics considering thermal stability under fire exposure." *Textile Research Journal* 91 (21-22): 2656-2668.
- Mayer, A. C., G. P. Horn, K. W. Fent, S. J. Bertke, S. Kerber, R. M. Kesler, H. Newman, and D. L. Smith. 2020. "Impact of select PPE design elements and repeated laundering in firefighter protection from smoke exposure." *J Occup Environ Hyg* 17 (11-12): 505-514.
- McQuerry, M., S. Klausing, D. Cotterill, and E. Easter. 2014. "A Post-use Evaluation of Turnout Gear Using NFPA 1971 Standard on Protective Ensembles for Structural Fire Fighting and NFPA 1851 on Selection, Care and Maintenance." *Fire Technology* 51 (5): 1149-1166.
- NASA. 2008. "Polymer Fabric Protects Firefighters, Military, and Civilians." National Aeronautics and Space Administration. Accessed March 3rd. https://spinoff.nasa.gov/Spinoff2008/ps_3.html.
- NFPA. 2020 *NFPA 1851: Selection, Care, and Maintenance of Protective Ensembles for Structural Fire Fighting and Proximity Fire Fighting*. Quincy, MA: National Fire Protection Association.
- . 2013. *NFPA 1971: Standard on Protective Ensemble for Structural Firefighting and Proximity Fire Fighting*. Quincy, MA: National Fire Protection Association.
- Ohalele, H. 2020. "Evaluating Effects of Heat Fluxes and Duration on Performance of Firefighters' Protective Clothing Using Destructive and Non Destructive Methods." M.Sc. Thesis, Department of Mechanical Engineering, University of Saskatchewan.
- Ohalele, H., M. Fulton, D. A. Torvi, S. D. Noble, and J. C. Batcheller. 2022. "Comparison of Techniques for Prediction of Mechanical Strength of Firefighters' Protective Clothing Using Near-Infrared Spectral Data." *Fire Technology* 58 (1): 591-613.

- Ormond, B. R., and W.J. Gabler. 2017. "Non Destructive Assessment of Outer Shell Degradation for Firefighter Turnouts." *Fire Protection Research Foundation*. Quincy, MA: National Fire Protection Association.
- Pellatt, M. G., Marian M. M., and R. W Mathewes. 2015. "Paleoecology and Fire History of Garry Oak Ecosystems in Canada: Implications for Conservation and Environmental Management." *Biodiversity and Conservation*. 24 (7): 1621-639.
- Rezazadeh, M. 2014. "Evaluation of Performance of In-use Firefighter's Protective Clothing using Non-destructive Tests." Ph.D. Thesis, Department of Mechanical Engineering, University of Saskatchewan.
- Rezazadeh, M., C. J. Bessflug, D. A. Torvi, S. D. Noble, and M. Fulton. 2018. "Predicting Mechanical Strength of In-Use Firefighter Protective Clothing Using Near-Infrared Spectroscopy." *Fire Technology* 54 (6): 1759-1781.
- Rezazadeh, M., and D. A. Torvi. 2010. "Assessment of Factors Affecting the Continuing Performance of Firefighters' Protective Clothing: A Literature Review." *Fire Technology* 47 (3): 565-599.
- . 2012. "Non-destructive Test Methods to Assess the Level of Damage to Firefighters' Protective Clothing." In *Performance of Protective Clothing and Equipment: Emerging Issues and Technologies*. 202-226. STP 1544. West Conshohocken, PA: ASTM International.
- Rippe, C. M., and B. Y. Lattimer. 2021. "Post-fire modeling of aluminum structures using a kinetic driven approach." *Fire Safety Journal* 120: 1-8
- Rossi, R. M., W. Bolli, and R. Stampfli. 2008. "Performance of firefighter's protective clothing after heat exposure." *International Journal of Occupational Safety and Ergonomics* 14 (1): 55-60.
- Settle, F.A. 1997. *Handbook of Instrumental Techniques for Analytical Chemistry*. University of Michigan: Prentice Hall PTR.
- Slater, K. 1986. "The Progressive Deterioration of Textile Materials, Part I: Characteristics of Degradation." *Journal of the Textile Institute* 77 (2): 76-87.

- Smith, B, 1995. *The Emergence of Agriculture*. Scientific American Library, New York.
- Tencate. 2014. *Tencate Kombat Flex*. edited by Tencate Protective Fabrics. Union City, Georgia.
- Thorpe, P. 2004. "Assessment of In-Use Firefighter's Protective Clothing." M.Sc. Thesis, Department of Mechanical Engineering, University of Saskatchewan.
- Tian, M., Q. Wang, Y. Xiao, Y. Su, X. Zhang, and J. Li. 2020. "Investigating the Thermal-Protective Performance of Fire-Retardant Fabrics Considering Garment Aperture Structures Exposed to Flames." *Materials (Basel)* 13: 1-17.
- Timiras, P.L., W.B. Quay, and A. Vernadakis. 1995. *Hormones and Aging*. Boca Raton, Florida: CRC Press.
- Torvi, D.A. 1997. "Heat transfer in thin fibrous materials under high heat flux conditions." Ph.D. Thesis, University of Alberta.
- Torvi, D., M. Rezazadeh, and C. Bessflug. 2016. "Effects of Convective and Radiative Heat Sources on Thermal Response of Single- and Multiple-Layer Protective Fabrics in Benchtop Tests." In *Performance of Protective Clothing and Equipment: 10th Volume, Risk Reduction Through Research and Testing*, 131-158. STP 1593. West Conshohocken, PA: ASTM International.
- Ugo-Okeke, O. 2019. "Experimental and Numerical Investigation of Fire Behaviour in Polyurethane Foams." M.Sc. Thesis, Department of Mechanical Engineering, University of Saskatchewan.
- Veghte, J.H. 1988. *Firefighters' Protective Clothing: Design Criteria*. Second Edition. Dayton, OH: Lion Apparel.
- Vyazovkin, S., and C. A. Wight. 1999. "Model-free and model-fitting approaches to kinetic analysis of isothermal and nonisothermal data." *Thermochemica Acta*. 53-68.

Appendices

Appendix A. Mass Measurements

Tables A.1 and A.2 present the mass measurements gathered for this research. Some of these measurements include the mass of the thermocouples, and have a larger mass difference due to operator error.

Table A.1 Kombat Flex Mass Measurements With IR Temperatures

Sample Name	Average Initial Mass (g)	Average Final Mass (g)	Mass Difference (g)	Average IR Temp (K)
KF.Unexposed	-	-	-	-
KF.10.30	5.250	5.100	0.149	492.5
KF.10.60	24.119	23.604	0.516	511.8
KF.10.90	5.183	5.041	0.142	510.6
KF.10.120	5.282	5.124	0.159	513.2
KF.10.300	5.284	5.078	0.206	512.9
KF.10.600	5.273	5.016	0.257	515.5
KF.10.1200	5.289	4.990	0.299	516.1
KF.15.30	5.300	5.187	0.112	562.0
KF.15.60	5.162	5.033	0.129	554.5
KF.15.90	5.310	5.165	0.145	561.9
KF.15.120	5.233	5.068	0.165	564.5
KF.15.300	5.271	5.018	0.252	564.1
KF.15.600	5.232	4.906	0.326	564.7
KF.15.1200	5.249	4.899	0.351	567.1
KF.20.15	5.309	5.180	0.129	581.4
KF.20.30	5.252	5.106	0.146	602.7
KF.20.45	5.264	5.101	0.163	604.5
KF.20.60	5.250	5.096	0.154	605.8
KF.20.90	5.294	5.090	0.204	605.6
KF.20.120	5.343	5.124	0.219	605.5
KF.20.300	5.268	4.983	0.285	601.9
KF.20.600	5.275	4.920	0.355	597.2
KF.20.1200	5.261	4.842	0.419	598.9
KF.25.60	5.275	5.095	0.180	635.9
KF.30.15	5.239	5.100	0.139	651.9
KF.30.30	5.260	5.079	0.181	665.3
KF.30.45	5.295	5.082	0.213	666.8
KF.30.60	5.296	5.064	0.232	667.4
KF.30.90	5.272	4.987	0.285	666.9
KF.30.120	5.280	4.993	0.287	665.0
KF.30.300	5.292	4.907	0.386	664.4
KF.35.60	5.210	4.948	0.262	684.0
KF.40.15	5.257	5.058	0.199	707.5
KF.40.30	5.276	5.033	0.243	715.0
KF.40.60	22.918	22.268	0.651	725.6
KF.40.90	5.296	4.934	0.361	717.3
KF.40.120	5.286	4.906	0.380	717.5
KF.40.300	5.311	4.843	0.468	721.3
KF.45.60	5.277	4.973	0.304	735.3
KF.50.60	5.282	4.975	0.307	756.2
KF.60.60	5.239	4.765	0.474	838.1
KF.70.60	5.274	4.288	0.985	1029.7

Table A.2 Ripstop Natural Mass Measurements With IR Temperatures

Sample Name	Average Initial Weight (g)	Average Final Weight (g)	Mass Difference (g)	Average IR Temp (K)
RSN.Unexposed	-	-	-	-
RSN.10.60	24.143	23.539	0.605	506.8
RSN.10.300	5.586	5.379	0.207	513.2
RSN.10.600	5.663	5.399	0.264	515.3
RSN.10.1200	5.609	5.288	0.320	515.2
RSN.15.300	5.601	5.363	0.238	559.8
RSN.15.1200	5.581	5.206	0.375	563.7
RSN.20.15	5.554	5.411	0.143	563.5
RSN.20.45	5.613	5.435	0.178	596.2
RSN.20.60	5.584	5.348	0.236	601.8
RSN.20.120	5.601	5.371	0.230	598.8
RSN.20.600	5.640	5.253	0.386	594.1
RSN.20.1200	5.575	5.177	0.398	596.1
RSN.30.15	5.609	5.444	0.165	641.0
RSN.30.60	5.605	5.361	0.244	664.9
RSN.40.15	5.568	5.398	0.170	698.6
RSN.40.60	25.994	25.378	0.616	727.7
RSN.40.120	5.588	5.235	0.354	717.9
RSN.40.300	5.616	5.153	0.462	719.3
RSN.40.600	5.596	5.043	0.552	724.2

Appendix B. Near Infrared Reflectance Results With Comparable Exposure And Durations

The following series of graphs are presented with the purpose of outlining the degradation of Kombat Flex. To improve clarity, this has been broken into parts to help illustrate the change in NIR (Figures B.1, B.2, and B.3). The final Figure (B.4) presents a few selected exposures which have similar NIR reflectance results. Finally, Table B.1 presents the exposures from Figure B.4, looking at the tensile strength results. In this table, tensile strength has been compared using percent difference. These paired exposures indicate intersections between high exposures and low durations with low exposures and high durations where a similar level of tensile strength damage occurs.

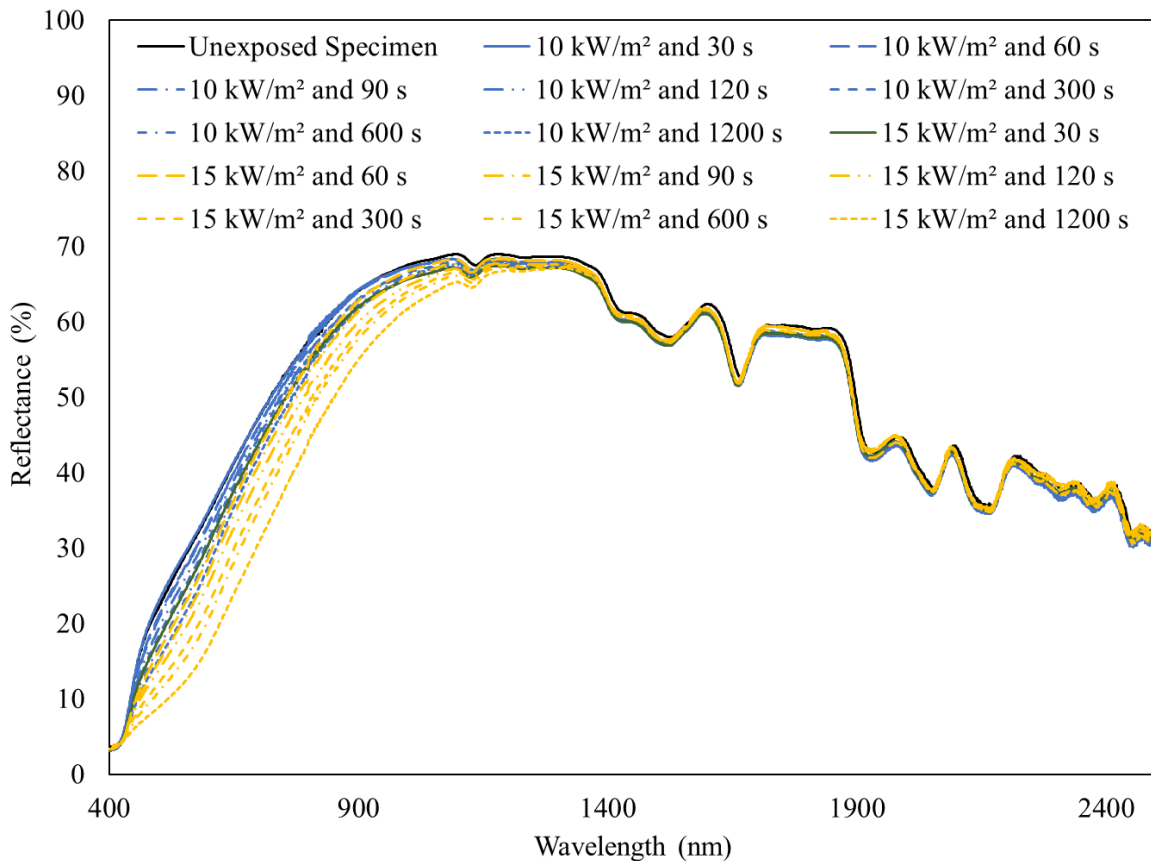


Figure B.1 Kombat Flex NIR Test Results For Exposures At 10 And 15 kW/m²

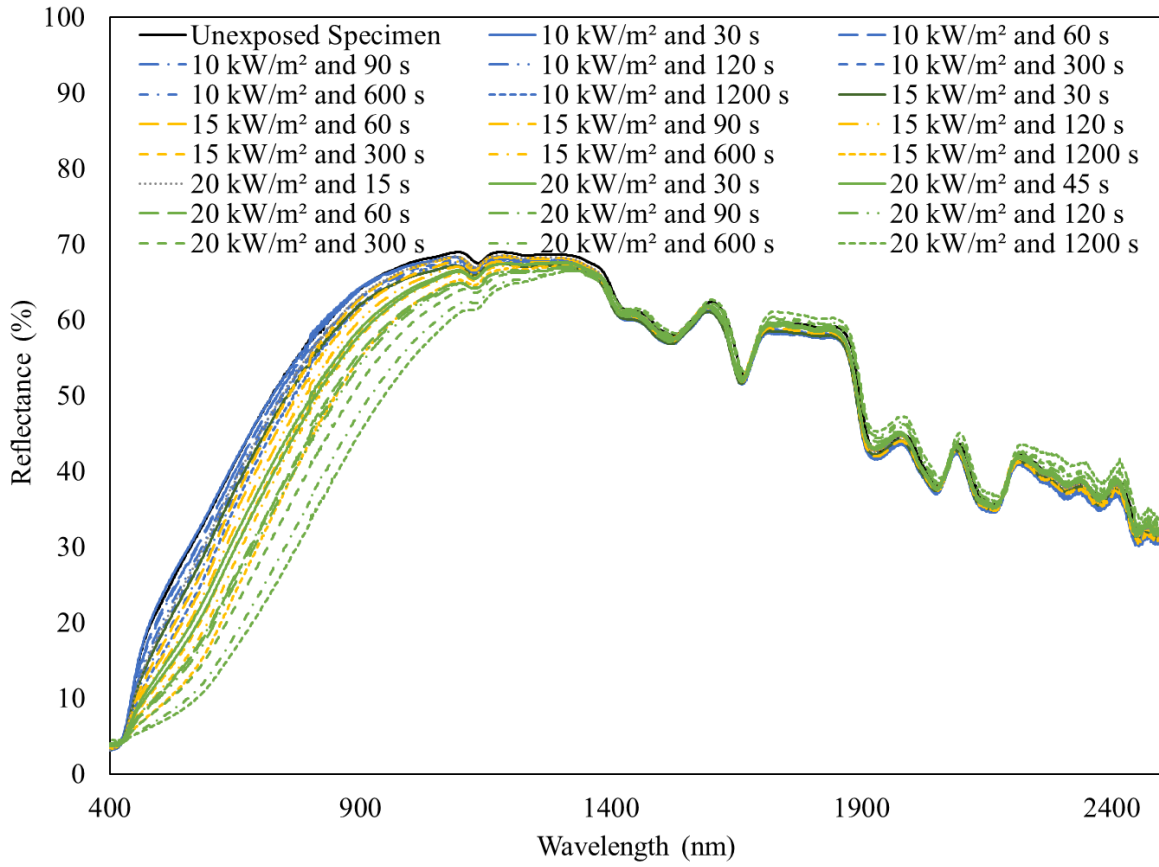


Figure B.2 Kombat Flex NIR Test Results For Exposures At 10, 15, And 20 kW/m²

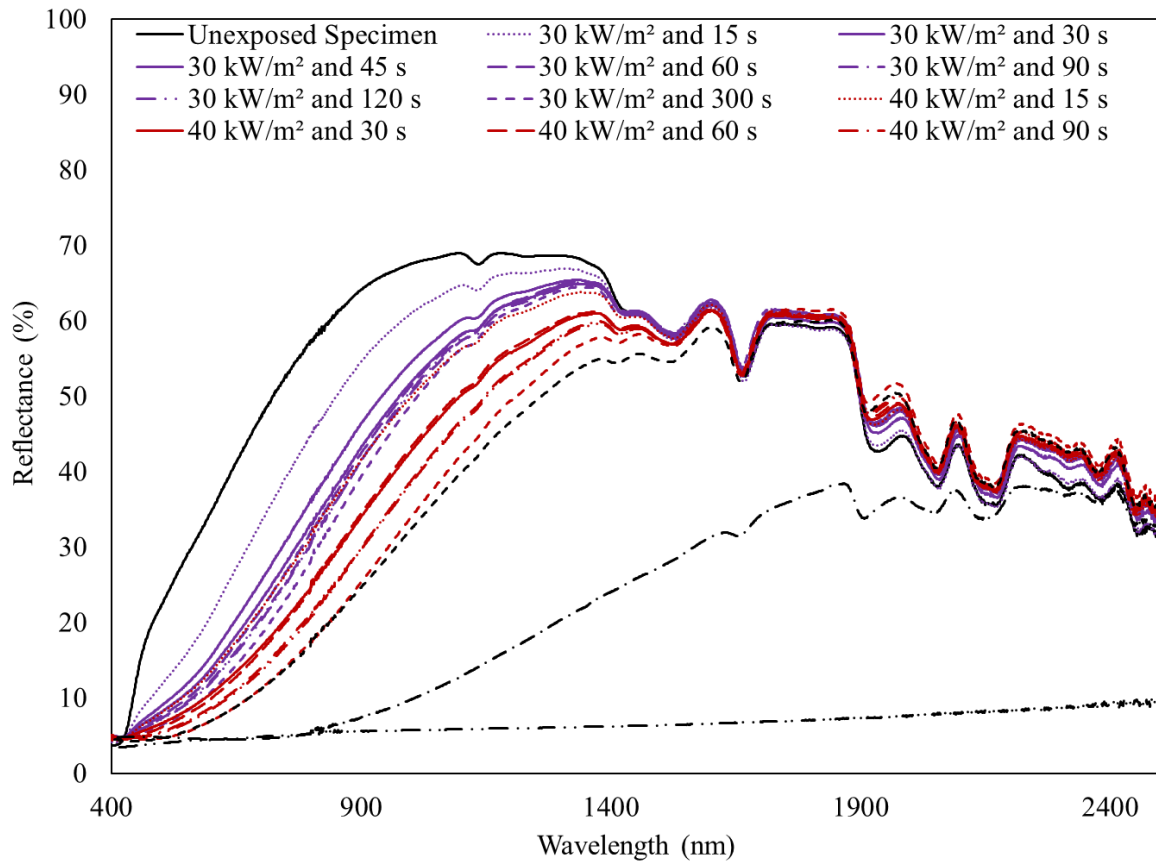


Figure B.3 Kombat Flex NIR Test Results For Exposures From 30 To 70 kW/m²

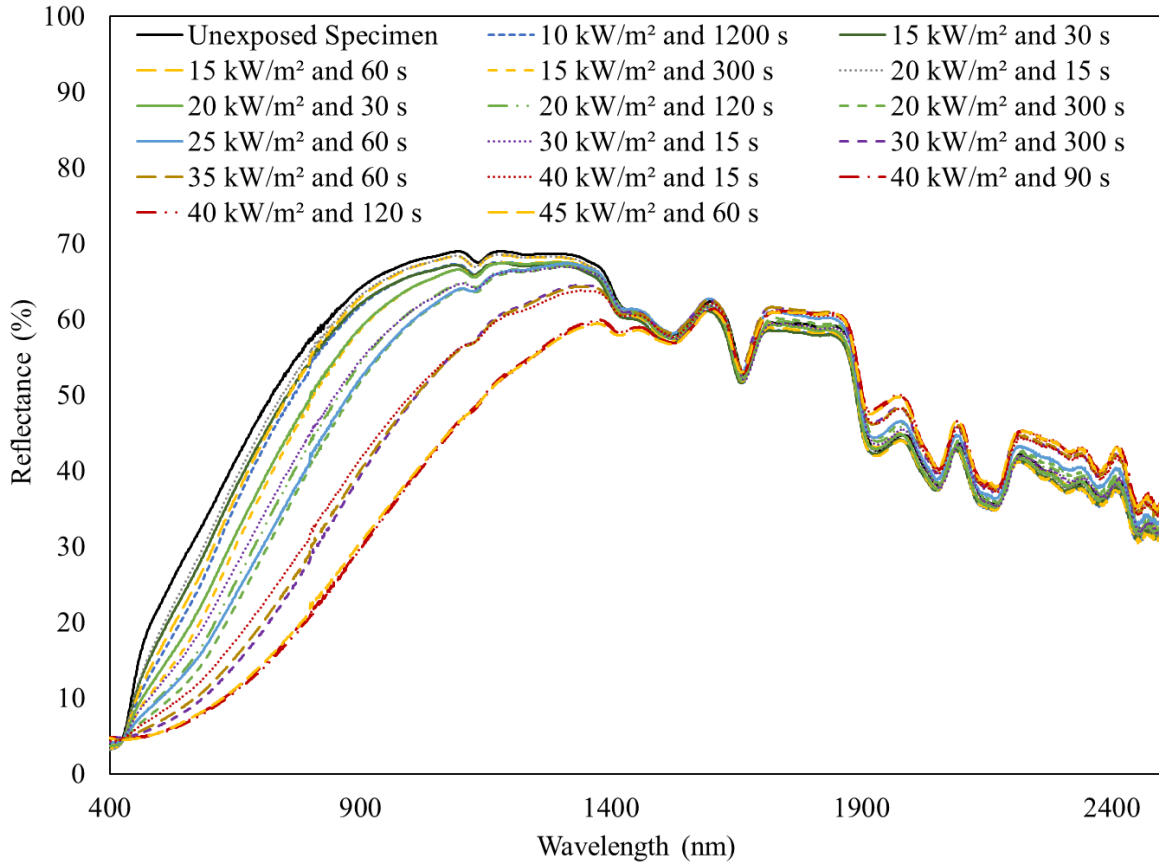


Figure B.4 Kombat Flex NIR Test Results That Have Comparatively Close Results

Table B.1 Kombat Flex NIR Test Results Which Are Visually Similar Compared Using Tensile Strength

Sample Name	Tensile Strength (N)	Standard Deviation	Tensile Strength Retention	Retention Standard Deviation	% Diff
KF.20.15	929	16.9	0.96	0.0002	2.3%
KF.15.60	908	56.3	0.94	0.0006	
KF.15.30	929	37.1	0.96	0.0004	1.0%
KF.10.1200	939	22.3	0.97	0.0002	
KF.20.30	821	22.6	0.85	0.0002	0.8%
KF.15.300	814	29.6	0.84	0.0003	
KF.30.15	768	27.0	0.79	0.0003	6.6%
KF.20.120	719	42.4	0.74	0.0004	
KF.25.60	685	48.6	0.71	0.0005	0.2%
KF.20.300	686	22.6	0.71	0.0002	
KF.30.300	520	20.7	0.54	0.0002	-
KF.40.15	603	28.3	0.62	0.0003	
KF.35.60	590	36.7	0.61	0.0004	
KF.45.60	377	43.2	0.39	0.0004	1.6%
KF.40.120	371	9.6	0.38	0.0001	

Appendix C: Temperature Measurements

The following temperature measurements have been directly compared to the experimental tensile strength tests in the following figures. Presented here are heat flux exposures for 10, 20, 30, and 40 kW/m² for both Kombat Flex (Figures C.1 to C.4) and Ripstop Natural (Figures C.5 to C.8). Ripstop Natural's results also include the tensile strength tests conducted by Ohalele (2020).

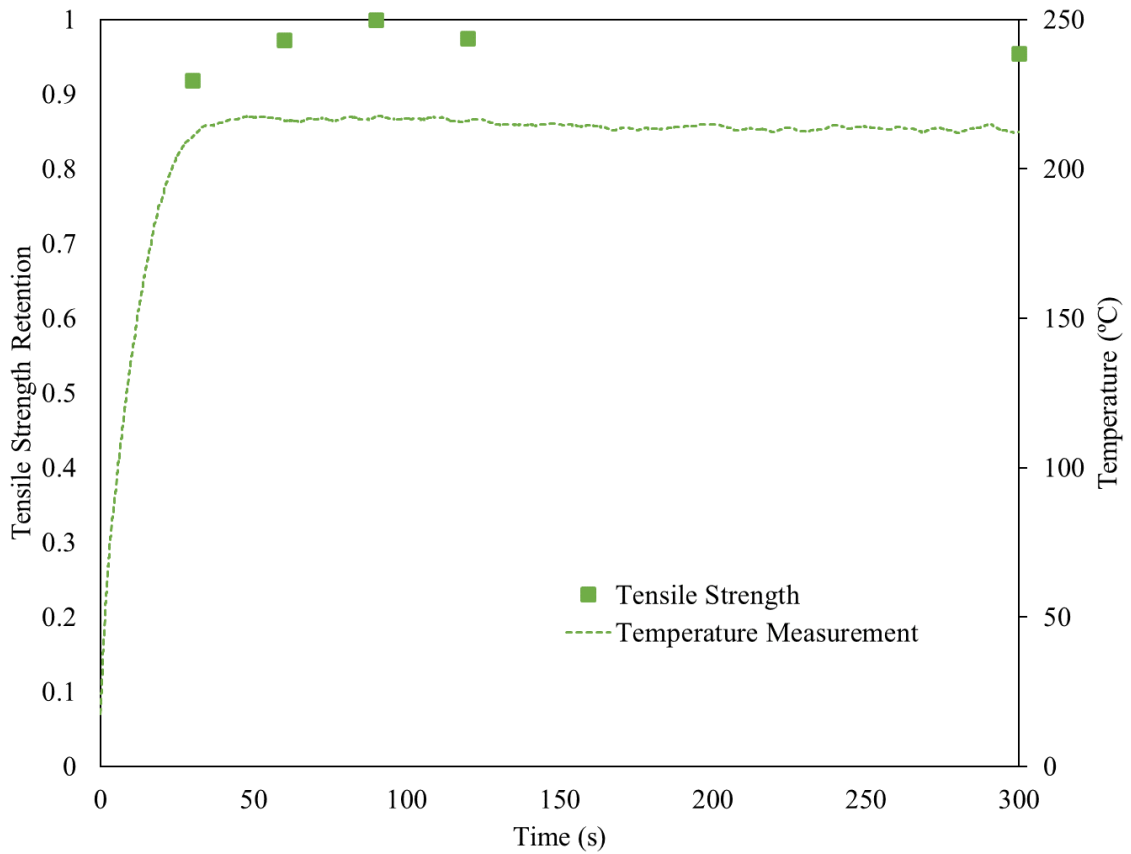


Figure C.1 Kombat Flex Temperature Measurements For 10 kW/m² With Tensile Strength Data.

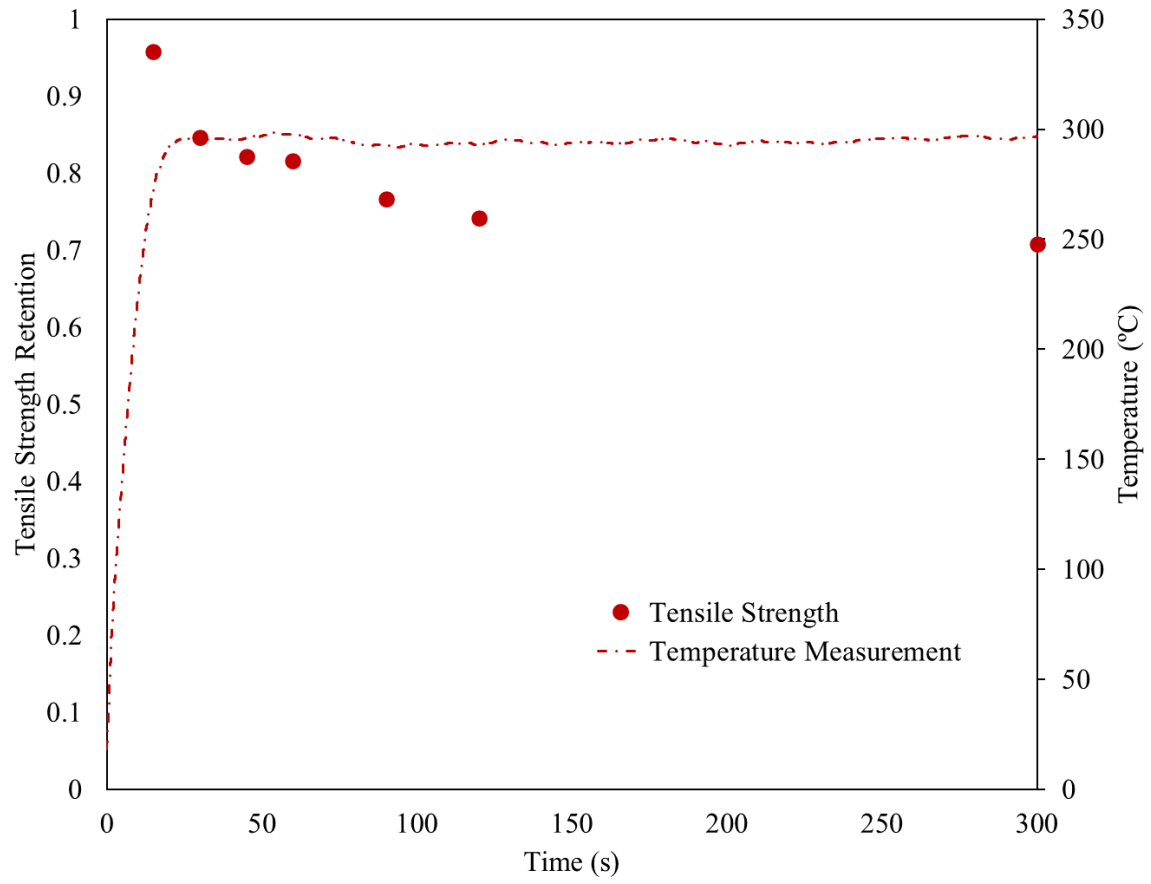


Figure C.2 Kombat Flex Temperature Measurements For 20 kW/m² With Tensile Strength Data.

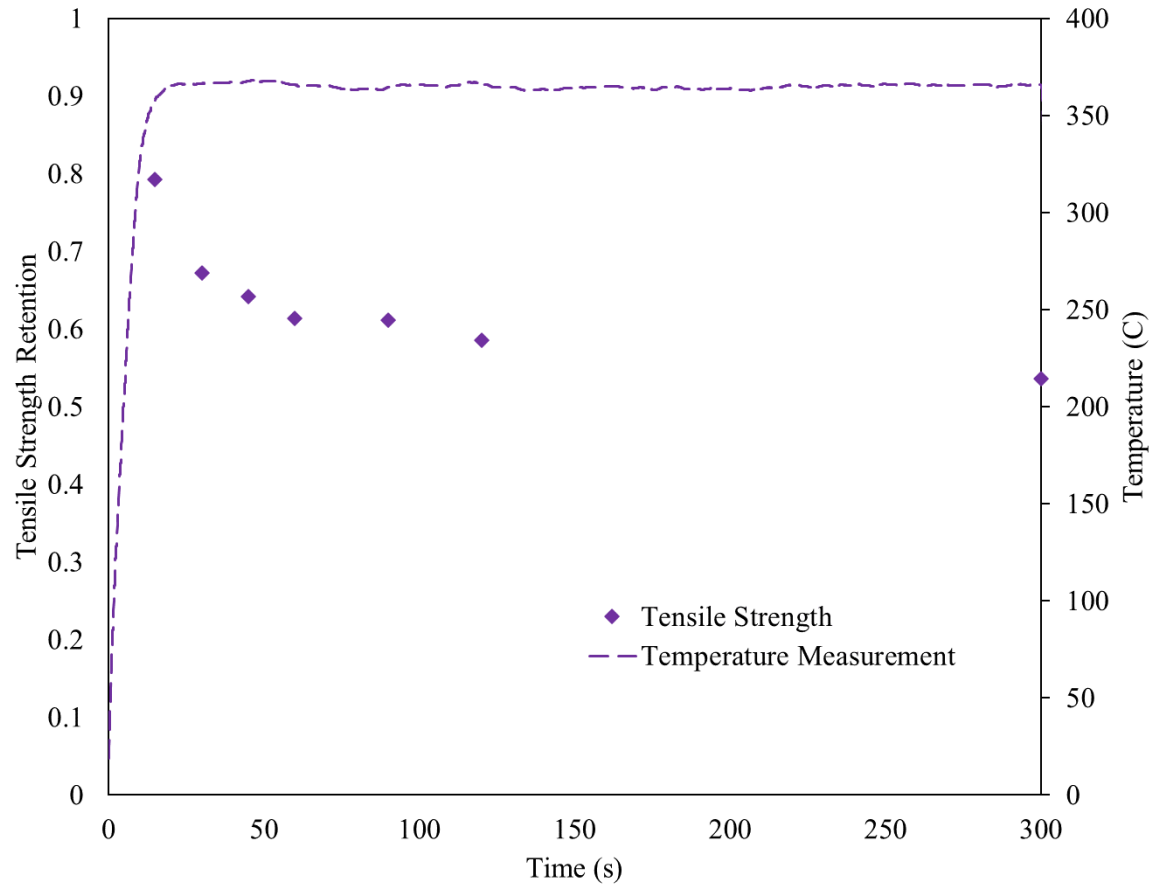


Figure C.3 Kombat Flex Temperature Measurements For 30 kW/m2 With Tensile Strength Data.

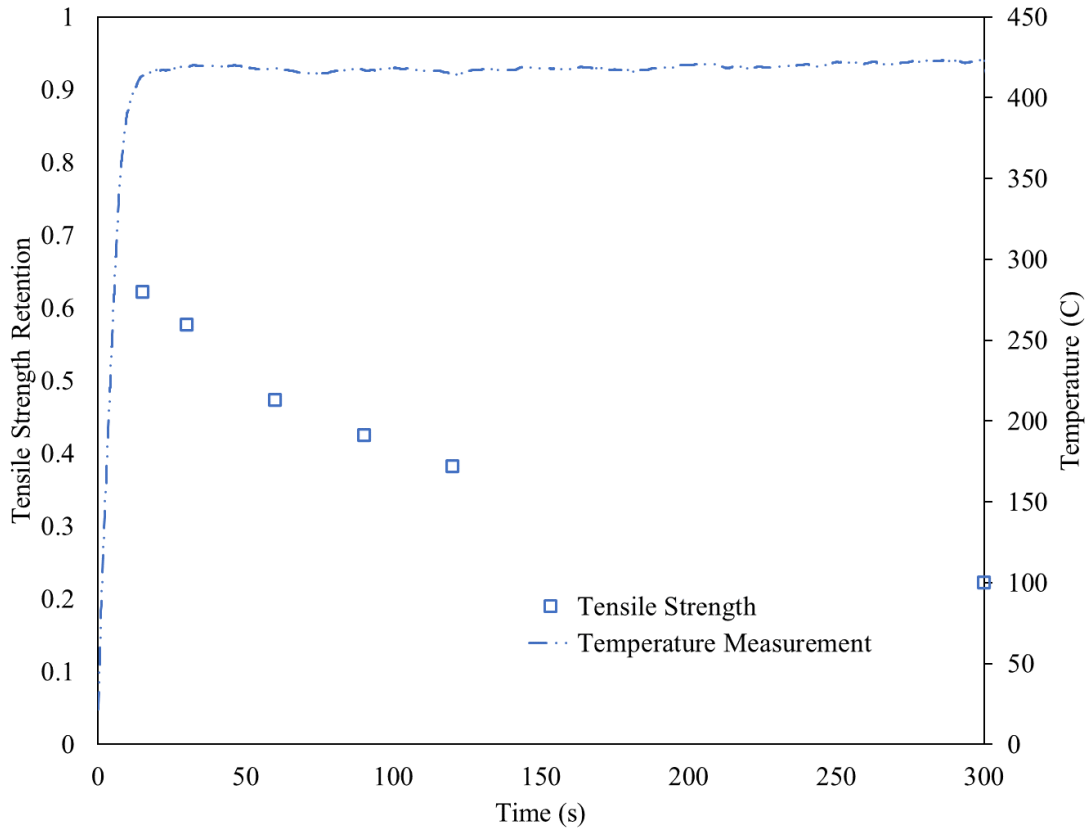


Figure C.4 Kombat Flex Temperature Measurements For 40 kW/m² With Tensile Strength Data.

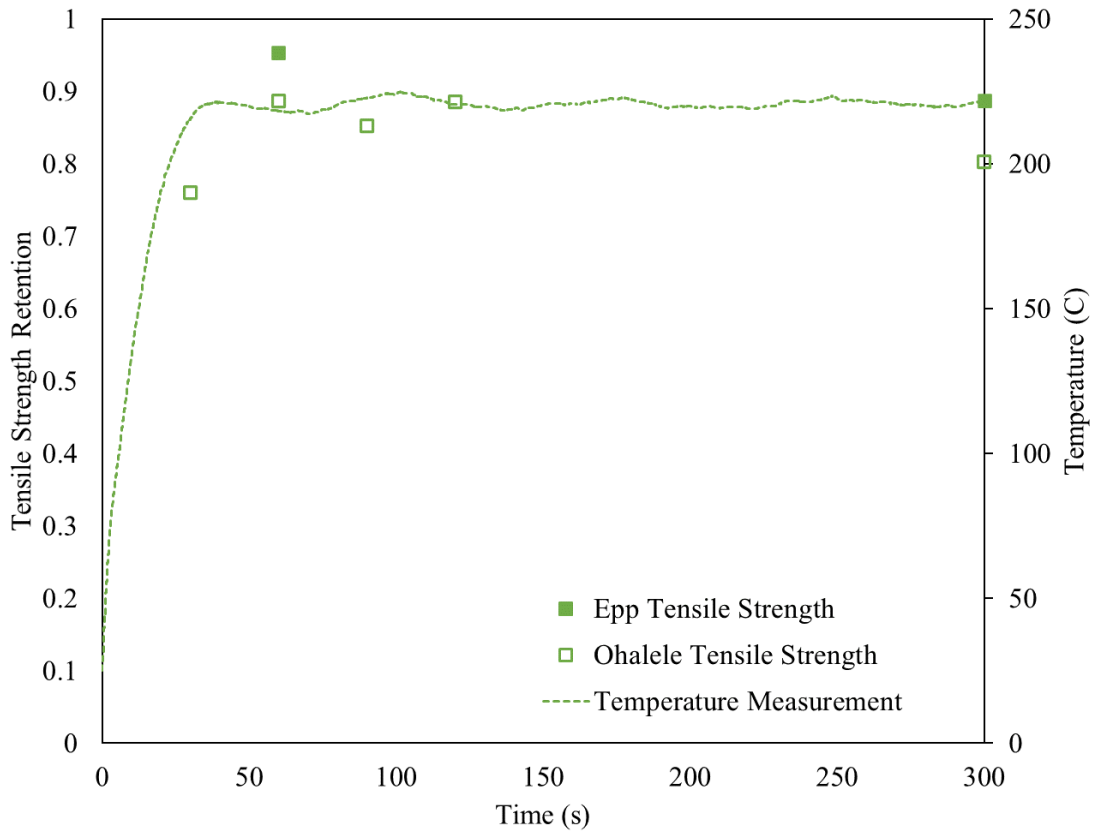


Figure C.5 Ripstop Natural Temperature Measurements For 10 kW/m² With Tensile Strength Data For Both This Research And Ohalele's (2020) Research.

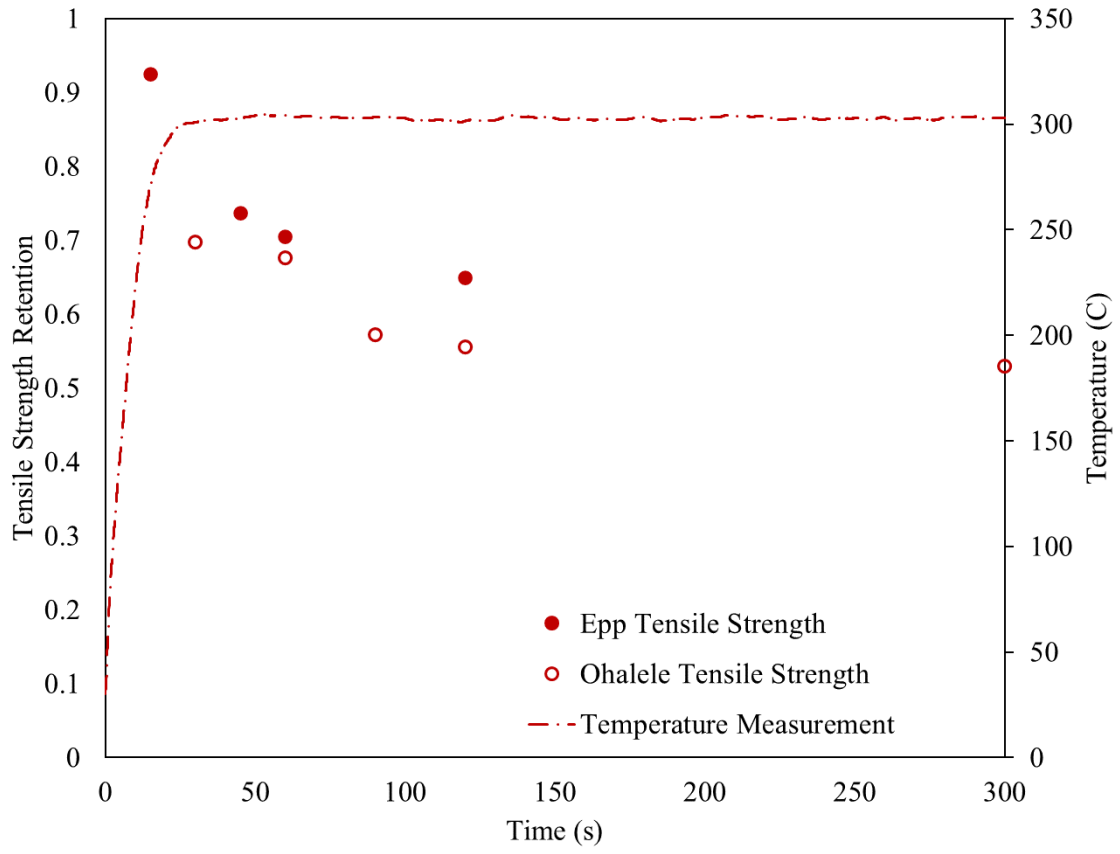


Figure C.6 Ripstop Natural Temperature Measurements For 20 kW/m² With Tensile Strength Data For Both This Research And Ohalele's (2020) Research.

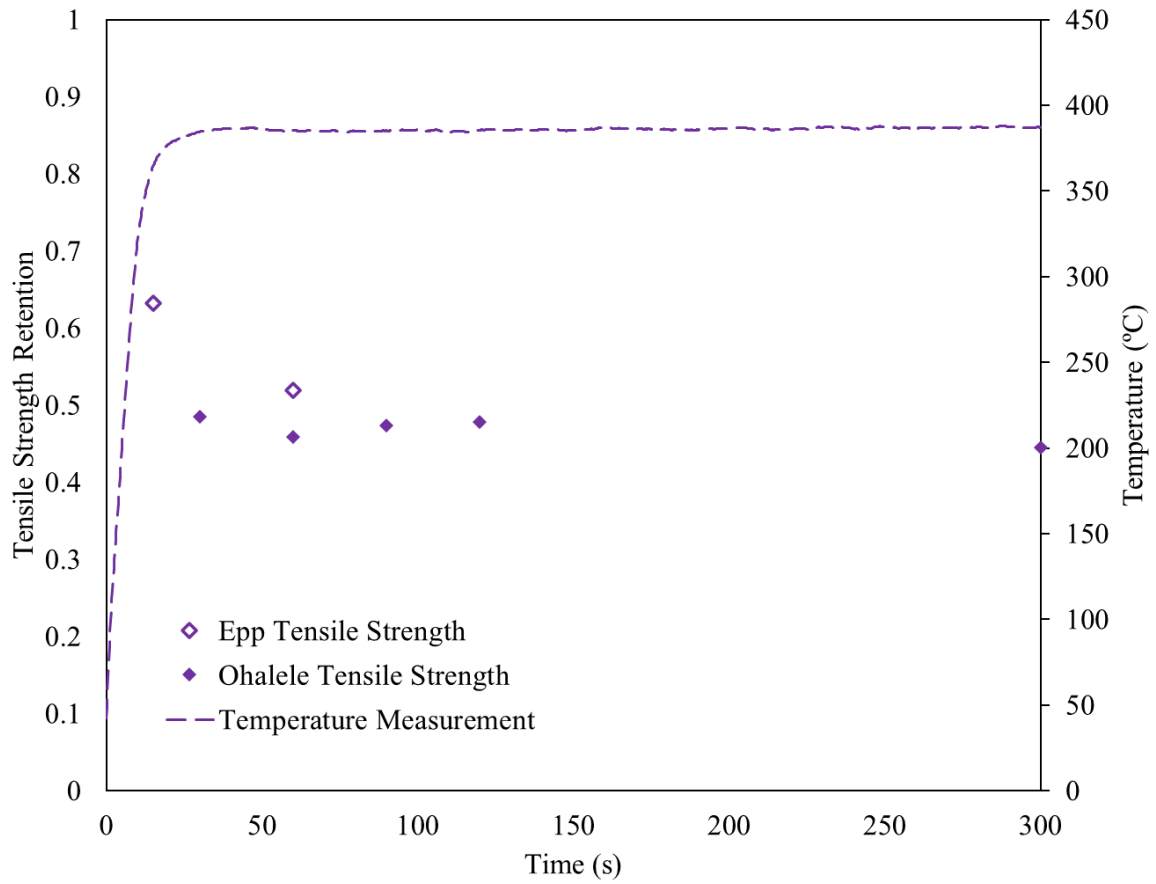


Figure C.7 Ripstop Natural Temperature Measurements For 30 kW/m² With Tensile Strength Data For Both This Research And Ohalele's (2020) Research.

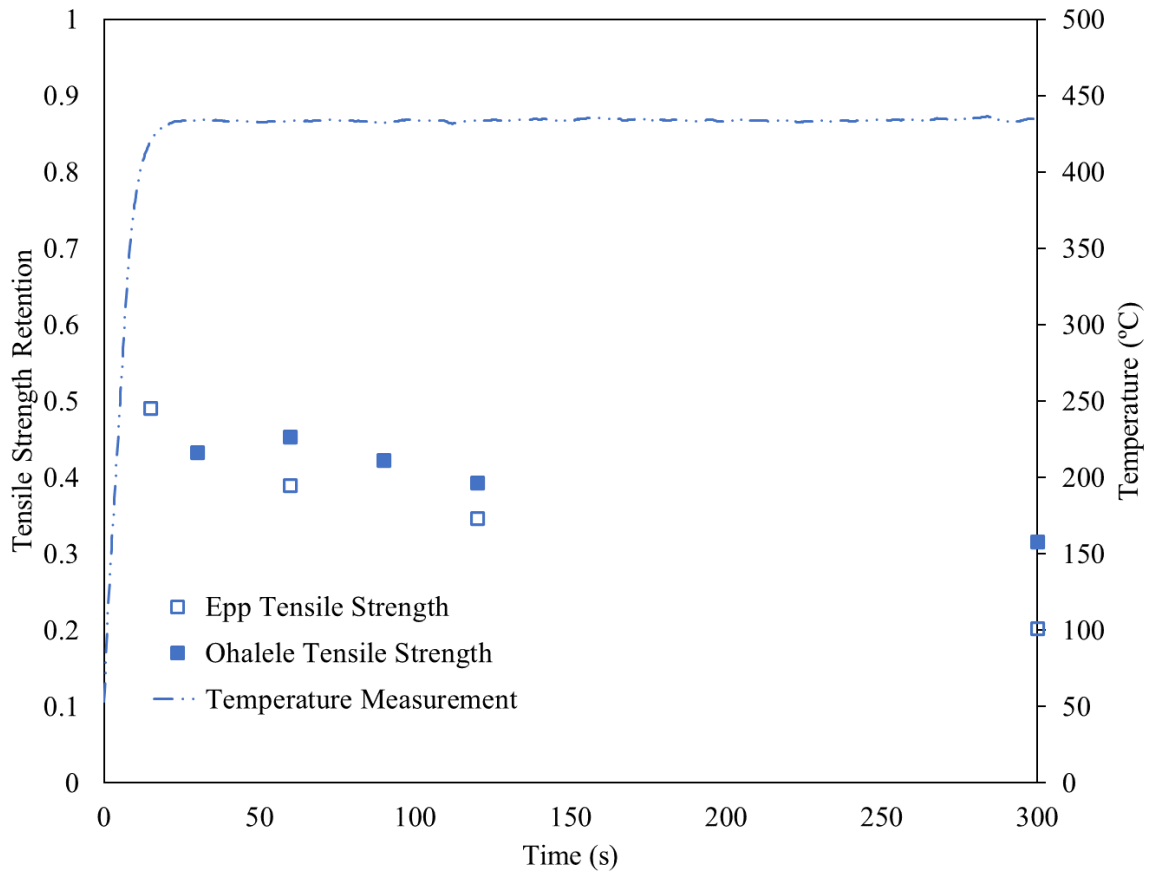


Figure C.8 Ripstop Natural Temperature Measurements For 40 kW/m² With Tensile Strength Data For Both This Research And Ohalele's Research (2020).

Appendix D. List Of Multi-Variable Linear Regression Correlation Equations

The multi-variable linear regression correlations developed in Chapter 4 is best portrayed as a generalized 1st order equation with a coefficient table. Outlined in Chapter 4 was this 1st order equation for heat flux. The following is a look at the generalized case for both heat flux and temperature. More statistics have been added to the following tables, unique to this section versus what is presented in Chapter 4. Additionally, two more three-dimensional representations of the experimental data are presented in Figure D.1 and D.2.

The generalized equation can be represented by the 1st order expression:

$$\frac{TS}{TS_i} = aQ + bt + c \quad (\text{B.1})$$

where,

$\frac{TS}{TS_i}$ is the tensile strength retention,

Q represents either the absolute temperature in K, or the heat flux in kW/m²,

t is time in seconds,

a , b , and c , are coefficients that can be found in the generalized Tables D.1 and D.2, where Table D.1 shows values for absolute temperature, and Table D.2 shows values for heat flux.

Table D.1 and D.2 express the coefficients that fit this generalized equation for heat flux and temperature respectively.

Table D.1 Coefficients For Kombat Flex, Ripstop Natural With Just Epp's Data, And Ripstop Natural With All Data For Coefficients With Absolute Temperature.

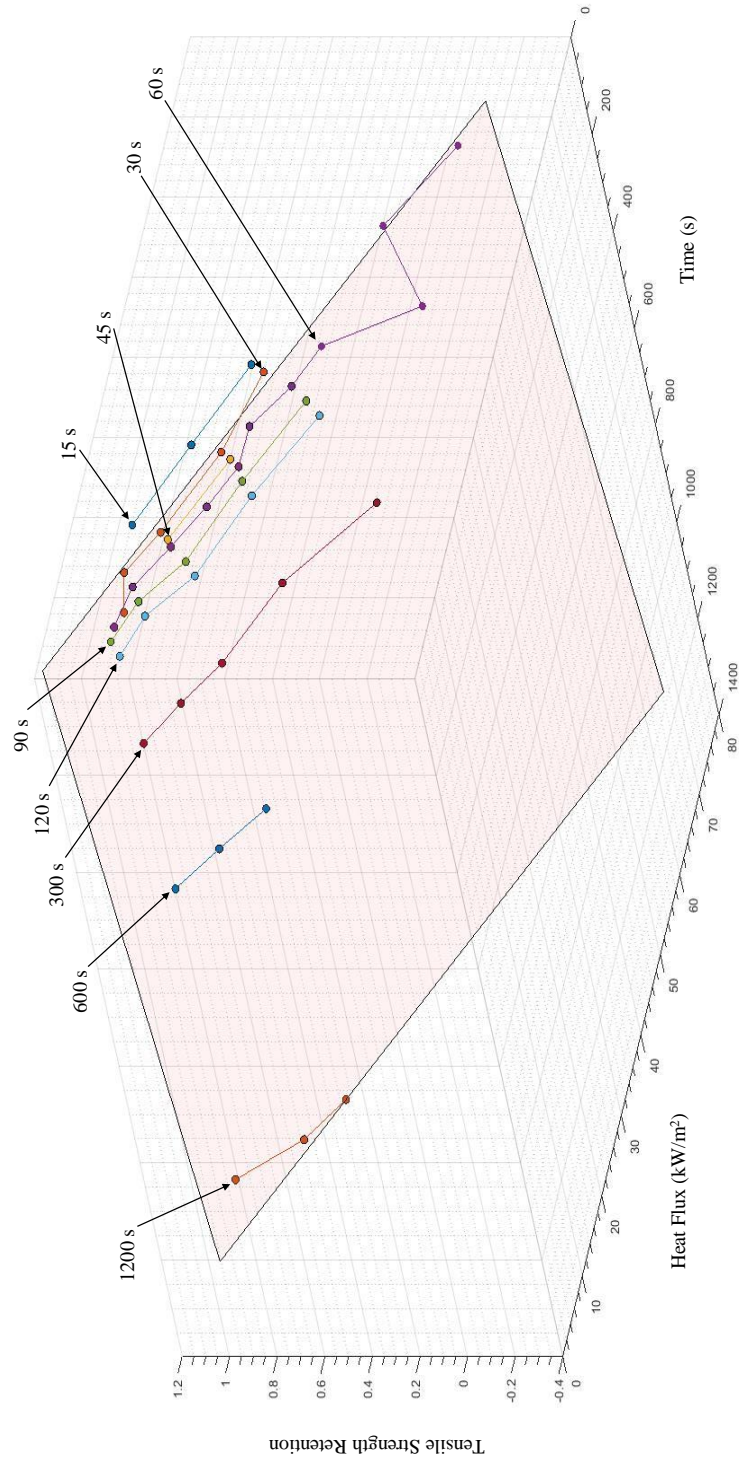
Kombat Flex		All Data	R²	0.878	
		Units	Coefficient Values	Lower 95%	Upper 95%
	Average				
<i>a</i>	Temperature	1/K	-2.43E-01	-2.73E-01	-2.14E-01
<i>b</i>	Exposure Time	1/s	-1.39E-02	-2.34E-02	-4.39E-03
<i>c</i>	Intercept	-	2.25E+02	2.06E+02	2.45E+02
Ripstop Natural		Epp Data Only	R²	0.904	
		Units	Coefficient Values	Lower 95%	Upper 95%
	Average				
<i>a</i>	Temperature	1/K	-3.26E-01	-3.77E-01	-2.76E-01
<i>b</i>	Exposure Time	1/s	-1.96E-02	-2.88E-02	-1.04E-02
<i>c</i>	Intercept	-	2.68E+02	2.35E+02	3.00E+02
Ripstop Natural		All Data	R²	0.829	
		Units	Coefficient Values	Lower 95%	Upper 95%
	Average				
<i>a</i>	Temperature	1/K	-2.26E-01	-2.56E-01	-1.96E-01
<i>b</i>	Exposure Time	1/s	-1.18E-02	-2.21E-02	-1.53E-03
<i>c</i>	Intercept	-	2.01E+02	1.81E+02	2.21E+02

Table D.2 Coefficients For Kombat Flex, Ripstop Natural With Just Epp's Data, And Ripstop Natural With All Data For Coefficients With Heat Flux.

Kombat Flex		All Data	R²	0.923	
		Units	Coefficient Values	Lower 95%	Upper 95%
<i>a</i>	Heat Flux	m ² /kW	-1.80E-02	-1.97E-02	-1.63E-02
<i>b</i>	Exposure Time	1/s	-1.70E-04	-2.47E-04	-9.38E-05
<i>c</i>	Intercept	-	1.19E+00	1.13E+00	1.25E+00

Ripstop Natural		Epp Data Only	R²	0.862	
		Units	Coefficient Values	Lower 95%	Upper 95%
<i>a</i>	Heat Flux	m ² /kW	-2.15E-02	-2.61E-02	-1.70E-02
<i>b</i>	Exposure Time	1/s	-2.16E-04	-3.40E-04	-9.22E-05
<i>c</i>	Intercept	-	1.20E+00	1.06E+00	1.34E+00

Ripstop Natural		All Data	R²	0.866	
		Units	Coefficient Values	Lower 95%	Upper 95%
<i>a</i>	Heat Flux	m ² /kW	-1.67E-02	-1.87E-02	-1.48E-02
<i>b</i>	Exposure Time	1/s	-1.72E-04	-2.65E-04	-7.98E-05
<i>c</i>	Intercept	-	1.06E+00	9.92E-01	1.12E+00



*Figure D.1 Three-Dimensional Representation Of Komбат Flex Data With The Multi-Variable Linear Regression Correlation
Showing Experimental Data By Time*

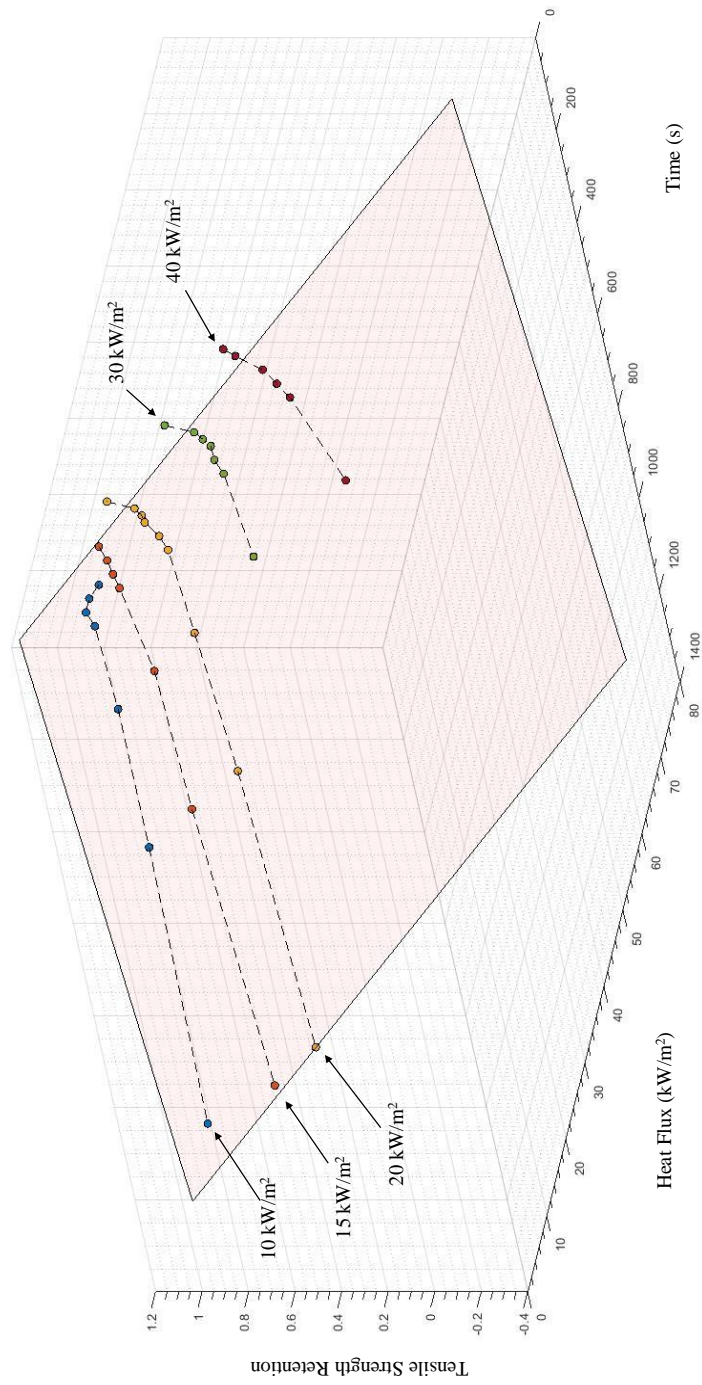


Figure D.1 Three-Dimensional Representation Of Kombar Flex Data With The Multi-Variable Linear Regression Correlation Showing Experimental Data By Heat Flux

Appendix E. Development Of Multi-Variable Nonlinear Regression

Correlation

To start this development, the following correlations were assumed:

$$\frac{TS}{TS_i} = aq''^b t^c \quad (\text{E.1})$$

$$\frac{TS}{TS_i} = dT^f t^g \quad (\text{E.2})$$

where,

$\frac{TS}{TS_i}$ is the tensile strength retention,

q'' is heat flux in kW/m²,

T is temperature in Kelvin, and

t is time in seconds.

Selection of this form of equation was based off of fit, and consistency with typical reaction models in solid thermal decomposition (Vyazovkin and Wight 1999).

These equations were linearized so that a linear regression could be conducted. The linearized equations become:

$$\ln\left(\frac{TS}{TS_i}\right) = \ln(a) + b\ln(q'') + c\ln(t) \quad (\text{E.3})$$

$$\ln\left(\frac{TS}{TS_i}\right) = \ln(d) + f\ln(T) + g\ln(t) \quad (\text{E.4})$$

Variables a, b, c, d, f, and g were then calculated through Microsoft Excel's linear regression software, and can be found in Table E.1. In the initial approach, linear regressions were conducted using all the data in a single regression. These resulted in curves that did not effectively predict the experimental data, which is likely due to rate of reaction change at higher exposures. To address this issue, the data was split into regions. The interchange point was selected based off the TGA data, as outlined in Chapter 4 (Figure E.1 and E.2).

Table E.1 Generalized Coefficients Table For Kombat Flex And Ripstop Natural For Heat Flux And Temperature

Kombat Flex	Heat Flux		After 45.60	Standard Error
	before 45.60	Standard Error		
<i>a</i>	15.864	-	3.40E+16	-
<i>b</i>	-0.802	0.064	-10.188	1.594
<i>c</i>	-0.136	0.020	0	0
Kombat Flex	Temperature (K)		After 45.60	Standard Error
	before 45.60	Standard Error		
<i>d</i>	1.26E+09	-	2.11E+35	-
<i>f</i>	-3.227	0.248	-12.519	1.359
<i>g</i>	-0.123	0.019	0	0
Kombat Flex	Temperature (°C)		After 45.60	Standard Error
	before 45.60	Standard Error		
<i>d</i>	4.79E+04	-	2.75E+22	-
<i>f</i>	-1.808	0.143	-8.625	0.960
<i>g</i>	-0.125	0.019	0	0
Ripstop Natural	Heat Flux		After 45.60	Standard Error
	before 45.60	Standard Error		
<i>a</i>	28.276	-	1.75E+21	-
<i>b</i>	-0.967	0.085	-12.994	0.951
<i>c</i>	-0.186	0.027	0	0
Ripstop Natural	Temperature (K)		After 45.60	Standard Error
	before 45.60	Standard Error		
<i>d</i>	3.36E+10	-	4.05E+40	-
<i>f</i>	-3.75	0.312	-14.454	1.177
<i>g</i>	-1.49E-01	0.025	0	0
Ripstop Natural	Temperature (°C)		After 45.60	Standard Error
	before 45.60	Standard Error		
<i>d</i>	2.67E+05	-	3.321E+25	-
<i>f</i>	-2.119	0.175	-9.886	0.858
<i>g</i>	-0.152	0.025	0	0

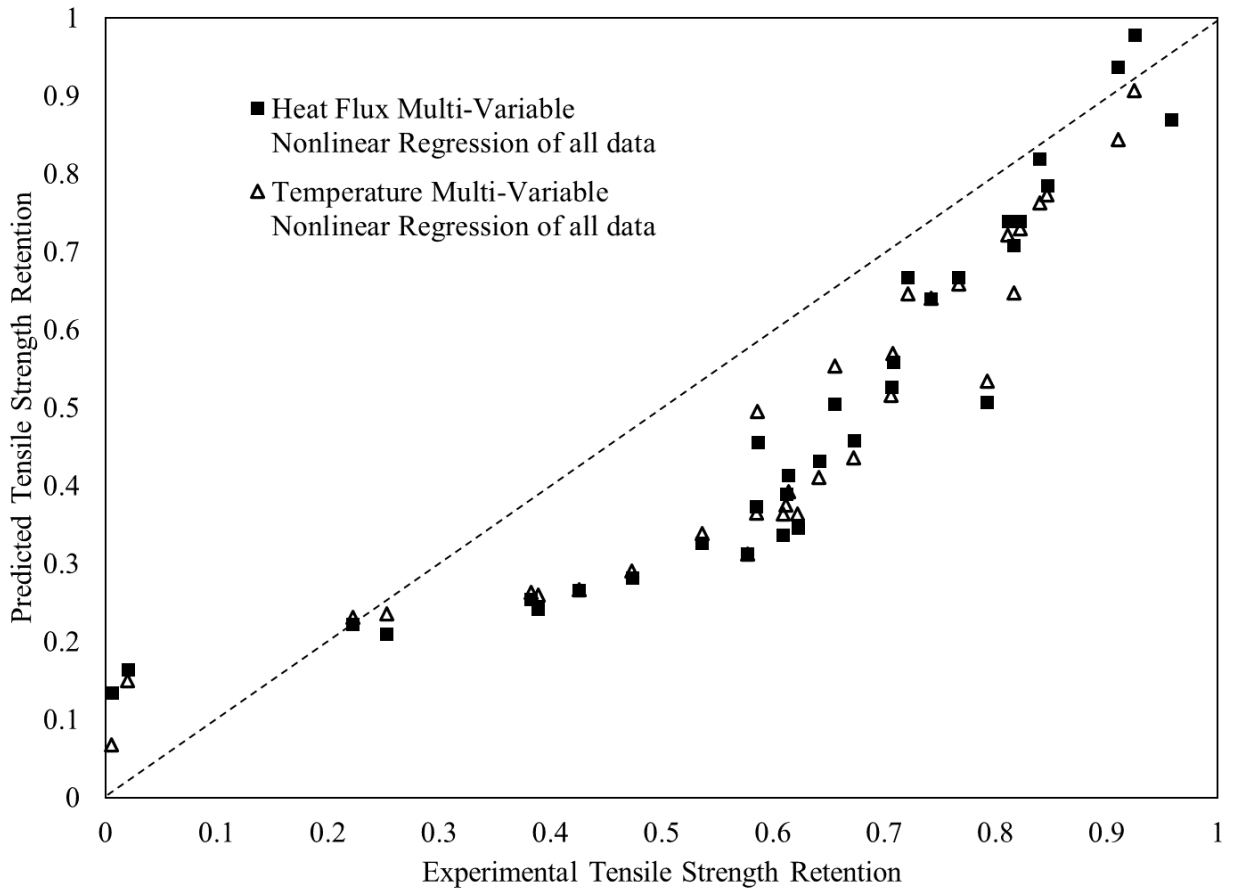


Figure E.1 Ability of a Multi-Variable Nonlinear Regression Correlation To Predict Tensile Strength Of Kombat Flex Fabrics After Exposures To Various Heat Fluxes With No Region Split

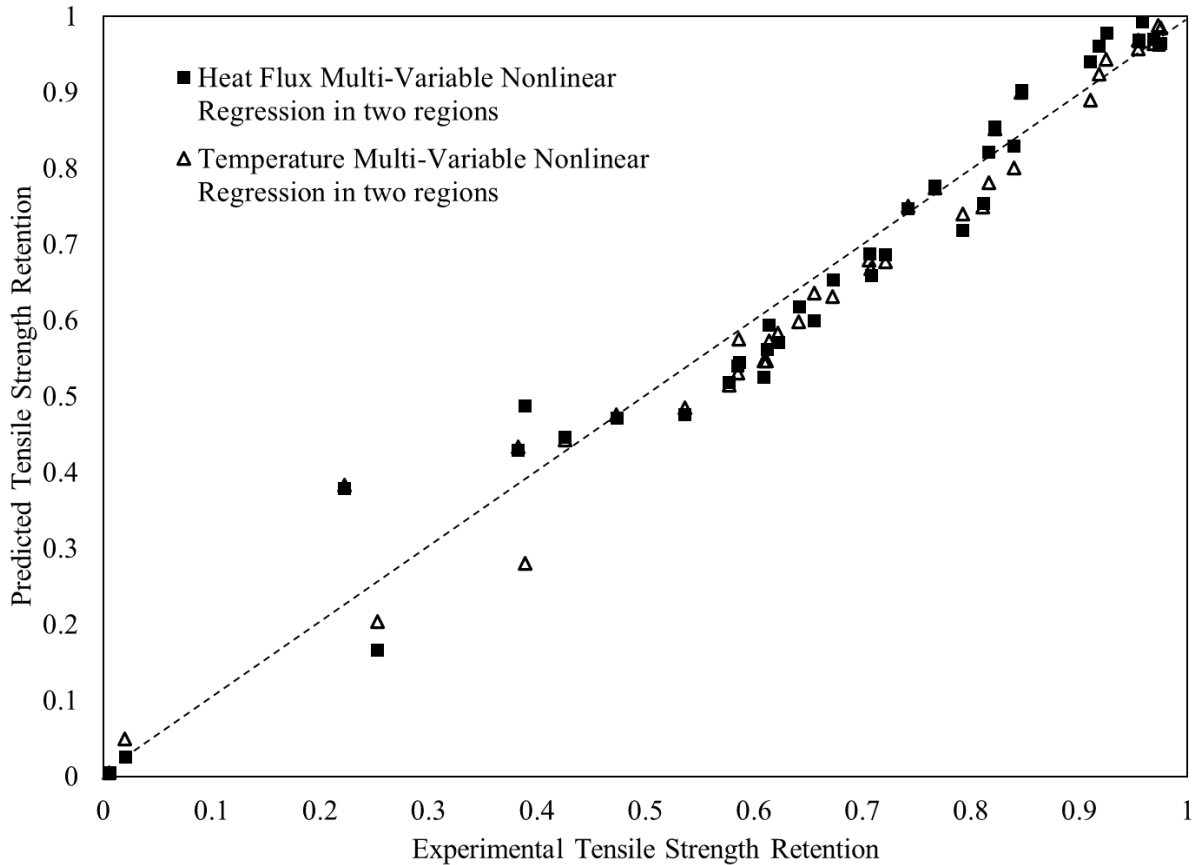


Figure E.2 Ability Of A Split-Region Multi-Variable Nonlinear Regression Correlation To Predict Tensile Strength Of Kombat Flex Fabrics After Exposures To Various Heat Fluxes Presenting Both Heat Flux And Temperature

Finally, to check the validity of this approach, a random point algorithm was developed and run which selects eight random exposure points (roughly 20% of the data for Kombat Flex) and removed these from the regression. This random point algorithm was done in excel using RAND functions to select points from the experimental data. These selected points were removed from the set that was used to create the multi-variable nonlinear regression. Using this new multi-variable nonlinear regression, predictions were made at the points that were removed. This check was iterated 10 times, and graphically compared for validity (Figure E.3).

Figure E.1 presents the Kombat Flex multi-variable nonlinear regression when all the data is taken into consideration with no regions applied to the data based on the TGA. Figure E.2 presents the temperature and heat flux Kombat Flex multi-variable nonlinear regression with the

data split into the regions as was presented in Chapter 4. Figure E.3 presents one of the iterated validity checks conducted on the Kombat Flex data.

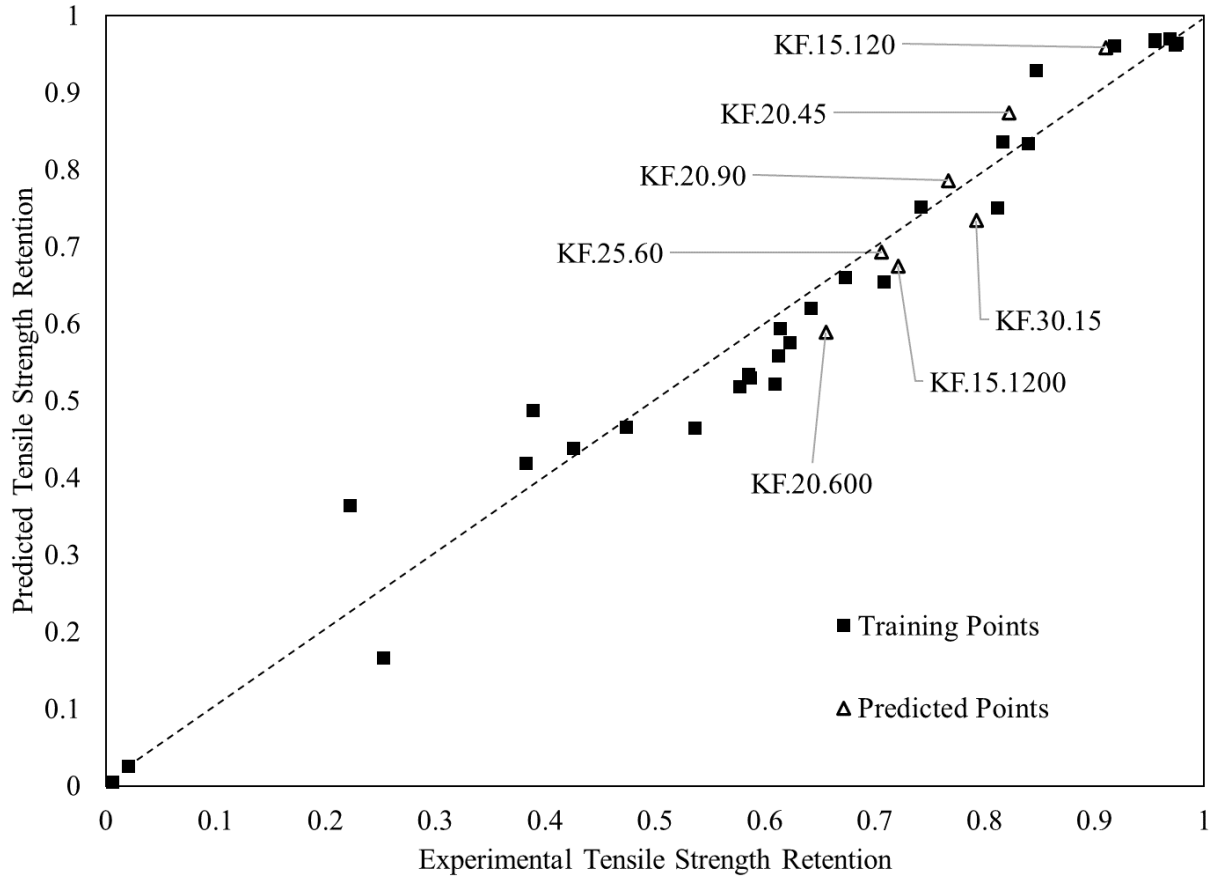


Figure E.3 Ability Of A Split-Region Multi-Variable Nonlinear Regression Correlation To Predict Tensile Strength Of Kombat Flex Fabrics After Exposures To Various Heat Fluxes Example Of When 1/5th Of The Data Is Predicted From A Regression Constructed From 4/5th Of The Data

Appendix F. Ripstop Black And PBI Max Analysis

In previous research at the University of Saskatchewan, thermal aging, NIR, and tensile strength data has been collected on two other Kevlar-PBI blended materials known as Ripstop Black and PBI Max. The following appendix explores collected data from Ohalele (2020) and Fulton (2017) examining and applying both the multi-variable nonlinear regression correlation and the single-variable nonlinear correlation. This analysis is limited due to the number of available datapoints in these sets. Fulton's tests ranged from 10 to 70 kW/m² at durations of 60 seconds, while Ohalele's tests ranged from 10 to 40 kW/m² with durations ranging from 30 seconds up to five minutes. Tables F.1 and F.2, and Figures F.1 and F.2 outline the multi-variable nonlinear regression approach for both Ripstop Black and PBI Max. Tables F.3 and F.4, and Figures F.3 and F.4 outline the single-variable nonlinear approach for both Ripstop Black and PBI Max. As was the case in Chapter 4, both approaches work reasonably well, and would be improved if there were more datapoints.

Table F.1: Multi-Variable Nonlinear Regression Data For Ripstop Black

Sample Name	q'' kW/m ²	t s	Tensile Strength Retention	q'' Multi- Variable Nonlinear	% Error	T Multi- Variable Nonlinear	% Error
O.RSB.10.30	10	30	0.859	1.518	77%	1.763	105%
O.RSB.10.60	10	60	0.911	1.311	44%	1.522	67%
F.RSB.10.60	10	60	0.959	1.311	37%	1.522	59%
O.RSB.10.90	10	90	0.898	1.203	34%	1.397	56%
O.RSB.10.120	10	120	0.902	1.132	25%	1.314	46%
O.RSB.10.300	10	300	0.883	0.932	6%	1.082	23%
F.RSB.15.60	15	60	0.977	0.882	-10%	0.874	-11%
O.RSB.20.30	20	30	0.752	0.771	3%	0.775	3%
O.RSB.20.60	20	60	0.653	0.666	2%	0.670	3%
F.RSB.20.60	20	60	0.675	0.666	-1%	0.670	-1%
O.RSB.20.90	20	90	0.618	0.611	-1%	0.614	-1%
O.RSB.20.120	20	120	0.563	0.575	2%	0.578	3%
O.RSB.20.300	20	300	0.502	0.474	-6%	0.476	-5%
F.RSB.25.60	25	60	0.467	0.535	15%	0.537	15%
O.RSB.30.30	30	30	0.458	0.519	13%	0.514	12%
O.RSB.30.60	30	60	0.440	0.448	2%	0.444	1%
F.RSB.30.60	30	60	0.408	0.448	10%	0.444	9%
O.RSB.30.90	30	90	0.394	0.411	4%	0.407	4%
O.RSB.30.120	30	120	0.403	0.387	-4%	0.383	-5%
O.RSB.30.300	30	300	0.358	0.319	-11%	0.316	-12%
F.RSB.35.60	35	60	0.350	0.385	10%	0.387	11%
O.RSB.40.30	40	30	0.443	0.392	-12%	0.393	-11%
O.RSB.40.60	40	60	0.402	0.338	-16%	0.340	-16%
F.RSB.40.60	40	60	0.333	0.338	2%	0.340	2%
O.RSB.40.90	40	90	0.347	0.310	-11%	0.312	-10%
O.RSB.40.120	40	120	0.325	0.292	-10%	0.293	-10%
O.RSB.40.300	40	300	0.185	0.241	30%	0.242	30%
F.RSB.45.60	45	60	0.229	0.312	37%	0.195	-15%
F.RSB.50.60	50	60	0.130	0.094	-28%	0.100	-23%
F.RSB.60.60	60	60	0.014	0.012	-16%	0.026	90%
F.RSB.70.60	70	60	0.002	0.002	22%	0.001	-20%

Table F.2: Multi-Variable nonlinear Regression Data For PBI Max

Sample Name	q'' kW/m ²	t s	Tensile Strength Retention	q'' Multi-Variable Nonlinear	% Error	T Multi-Variable Nonlinear	% Error
O.PBI.10.30	10	30	0.923	1.167	26%	1.287	39%
O.PBI.10.60	10	60	0.965	1.126	17%	1.243	29%
F.PBI.10.60	10	60	0.993	1.126	13%	1.243	25%
O.PBI.10.90	10	90	0.957	1.103	15%	1.218	27%
O.PBI.10.120	10	120	0.957	1.087	14%	1.200	25%
O.PBI.10.300	10	300	0.958	1.038	8%	1.146	20%
F.PBI.15.60	15	60	1.014	0.980	-3%	1.001	-1%
O.PBI.20.30	20	30	0.926	0.920	-1%	0.924	0%
O.PBI.20.60	20	60	0.898	0.888	-1%	0.892	-1%
F.PBI.20.60	20	60	0.914	0.888	-3%	0.892	-2%
O.PBI.20.90	20	90	0.877	0.870	-1%	0.874	0%
O.PBI.20.120	20	120	0.839	0.857	2%	0.862	3%
O.PBI.20.300	20	300	0.776	0.819	5%	0.823	6%
F.PBI.25.60	25	60	0.834	0.823	-1%	0.816	-2%
O.PBI.30.30	30	30	0.790	0.801	1%	0.778	-1%
O.PBI.30.60	30	60	0.774	0.773	0%	0.751	-3%
F.PBI.30.60	30	60	0.786	0.773	-2%	0.751	-4%
O.PBI.30.90	30	90	0.721	0.757	5%	0.736	2%
O.PBI.30.120	30	120	0.734	0.746	2%	0.726	-1%
O.PBI.30.300	30	300	0.723	0.712	-2%	0.693	-4%
F.PBI.35.60	35	60	0.675	0.733	9%	0.733	9%
O.PBI.40.30	40	30	0.707	0.725	3%	0.741	5%
O.PBI.40.60	40	60	0.729	0.700	-4%	0.715	-2%
F.PBI.40.60	40	60	0.724	0.700	-3%	0.715	-1%
O.PBI.40.90	40	90	0.670	0.686	2%	0.701	5%
O.PBI.40.120	40	120	0.703	0.676	-4%	0.691	-2%
O.PBI.40.300	40	300	0.672	0.645	-4%	0.660	-2%
F.PBI.45.60	45	60	0.628	1.338	113%	1.376	119%
F.PBI.50.60	50	60	0.526	0.309	-41%	0.291	-45%
F.PBI.60.60	60	60	0.068	0.025	-64%	0.027	-61%
F.PBI.70.60	70	60	0.001	0.003	120%	0.003	110%

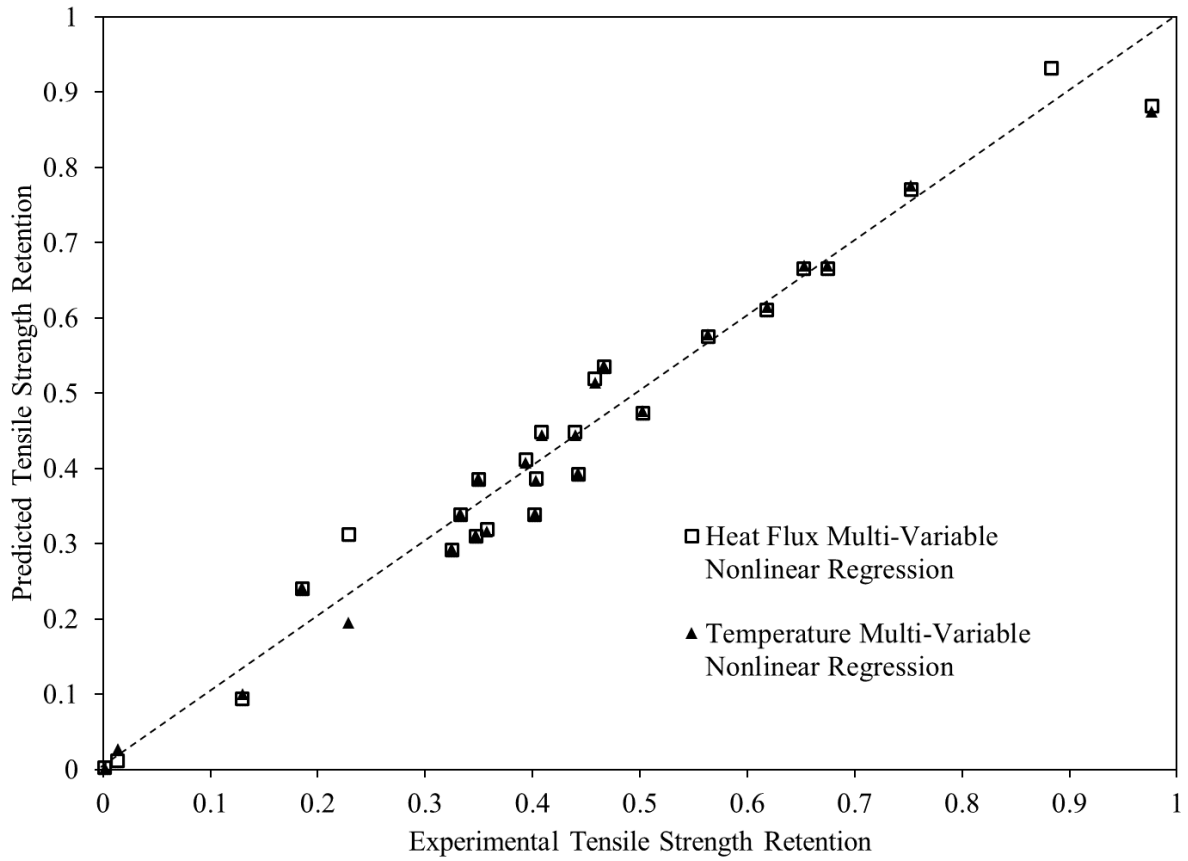


Figure F.1 Ability of a Multi-Variable Nonlinear Regression Correlation To Predict Tensile Strength Of Ripstop Black Fabrics After Exposures To Various Heat Fluxes

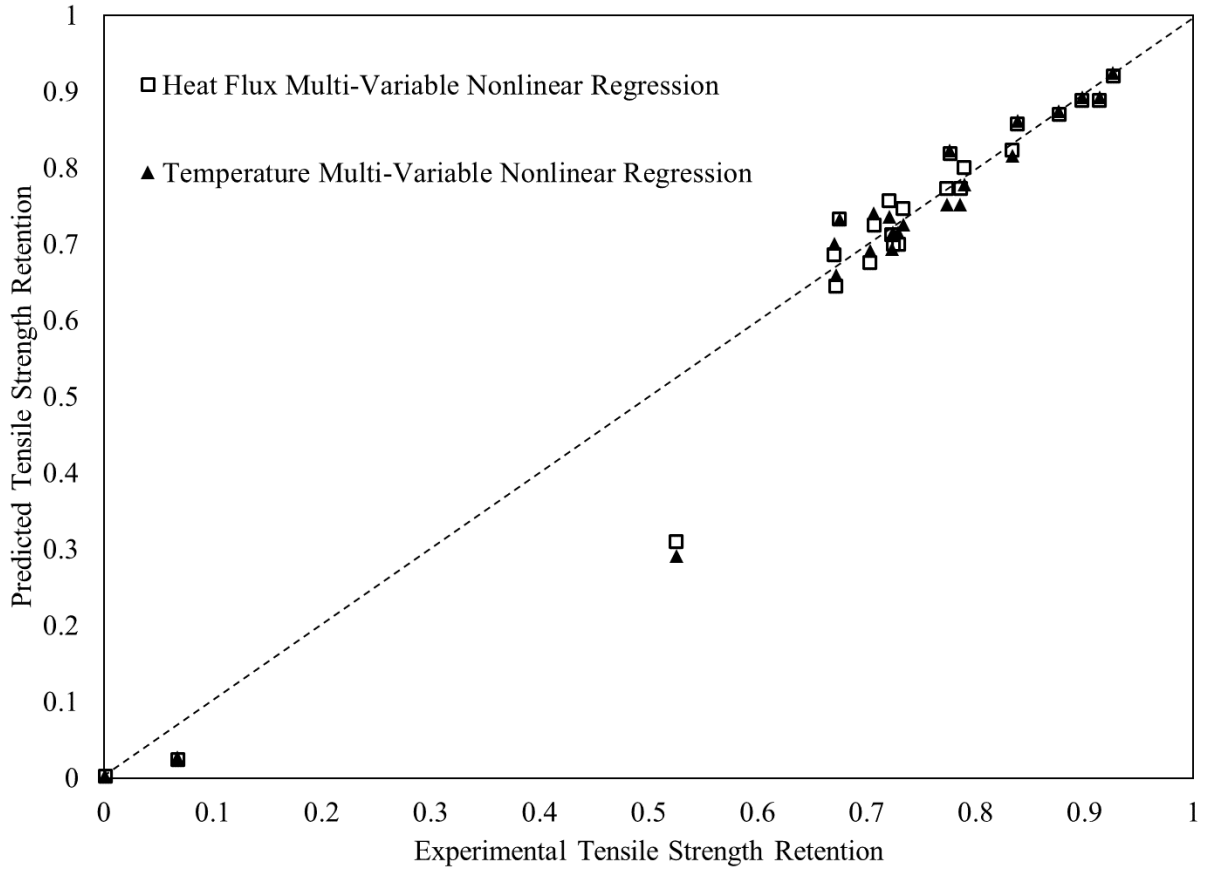


Figure F.2 Ability of a Multi-Variable Nonlinear Regression Correlation To Predict Tensile Strength Of PBI Max Fabrics After Exposures To Various Heat Fluxes

Table F.3 Single-Variable Nonlinear Correlation Per-Exposure Approach For Ripstop Black

Sample Name	Experimental Tensile Strength Retention	Per-Exposure Correlation	Percent Error
O.RSB.10.30	0.859	0.882	3%
O.RSB.10.60	0.911	0.888	-3%
O.RSB.10.90	0.898	0.890	-1%
O.RSB.10.120	0.902	0.893	-1%
O.RSB.10.300	0.883	0.899	2%
O.RSB.20.30	0.752	0.743	-1%
O.RSB.20.60	0.653	0.658	1%
O.RSB.20.90	0.618	0.612	-1%
O.RSB.20.120	0.563	0.582	3%
O.RSB.20.300	0.502	0.494	-2%
O.RSB.30.30	0.458	0.461	1%
O.RSB.30.60	0.440	0.427	-3%
O.RSB.30.90	0.394	0.409	4%
O.RSB.30.120	0.403	0.396	-2%
O.RSB.30.300	0.358	0.358	0%
O.RSB.40.30	0.443	0.495	12%
O.RSB.40.60	0.402	0.381	-5%
O.RSB.40.90	0.347	0.326	-6%
O.RSB.40.120	0.325	0.293	-10%
O.RSB.40.300	0.185	0.207	11%

Table F.4 Single-Variable Nonlinear Correlation Per-Exposure Approach For PBI Max

Sample Name	Experimental Tensile Strength Retention	Per-Exposure Correlation	Percent Error
O.PBI.10.30	0.923	0.939	2%
O.PBI.10.60	0.965	0.947	-2%
O.PBI.10.90	0.957	0.952	0%
O.PBI.10.120	0.957	0.956	0%
O.PBI.10.300	0.958	0.967	1%
O.PBI.20.30	0.926	0.939	1%
O.PBI.20.60	0.898	0.889	-1%
O.PBI.20.90	0.877	0.861	-2%
O.PBI.20.120	0.839	0.842	0%
O.PBI.20.300	0.776	0.783	1%
O.PBI.30.30	0.790	0.782	-1%
O.PBI.30.60	0.774	0.760	-2%
O.PBI.30.90	0.721	0.748	4%
O.PBI.30.120	0.734	0.739	1%
O.PBI.30.300	0.723	0.712	-2%
O.PBI.40.30	0.707	0.716	1%
O.PBI.40.60	0.729	0.703	-4%
O.PBI.40.90	0.670	0.696	4%
O.PBI.40.120	0.703	0.691	-2%
O.PBI.40.300	0.672	0.674	0%

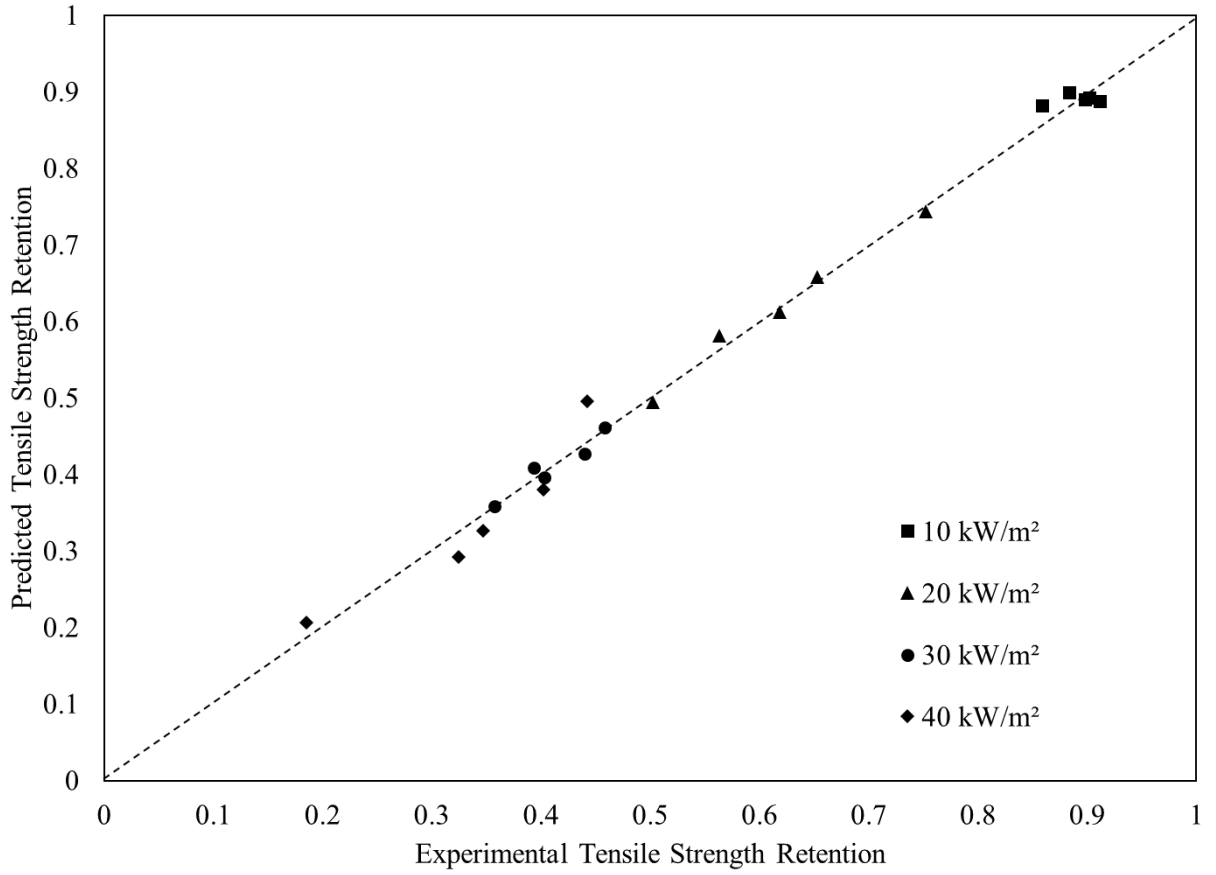


Figure F.3 Ability Of A Single-Variable Nonlinear Correlation To Predict Tensile Strength Of Ripstop Black Fabrics After Exposures To Various Heat Fluxes (Ohalele 2020)

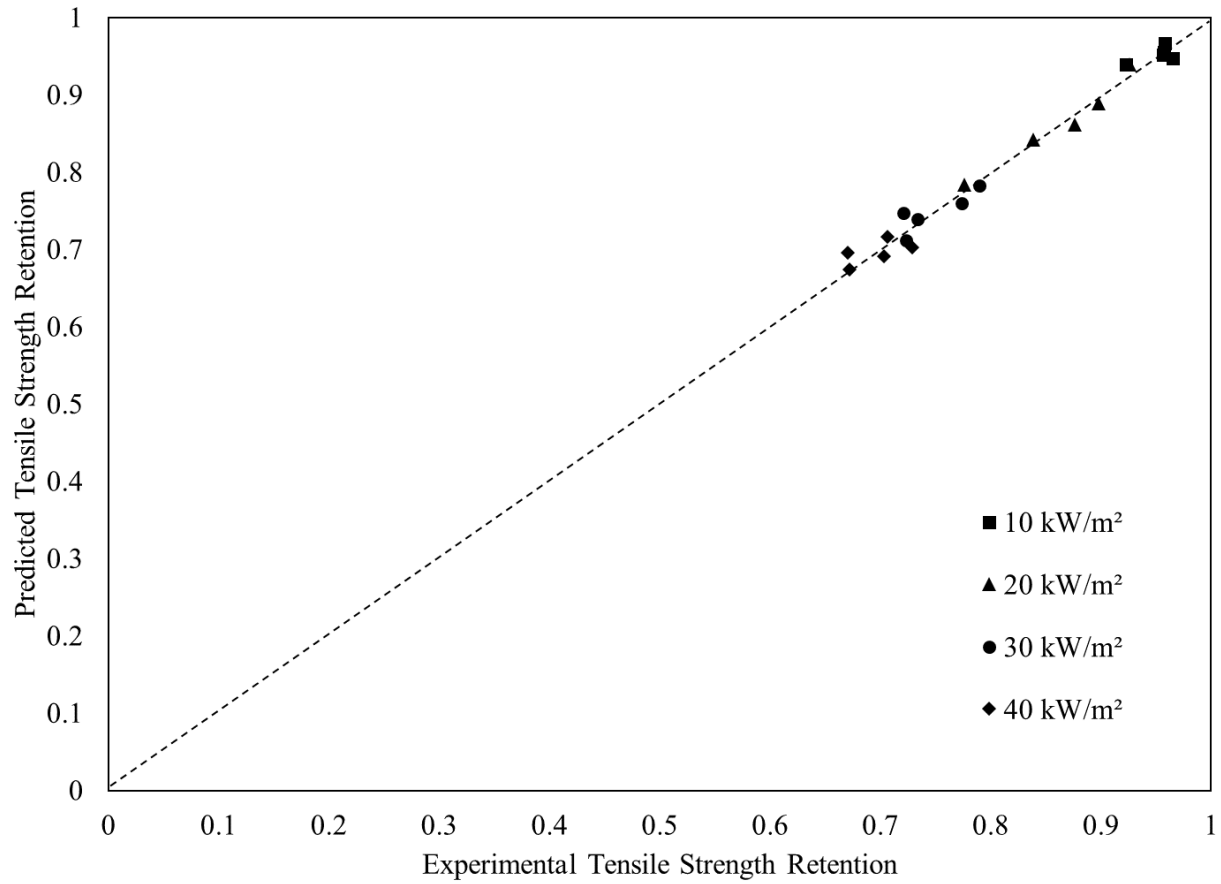


Figure F.4 Ability Of A Single-Variable Nonlinear Correlation To Predict Tensile Strength Of PBI Max Fabrics After Exposures To Various Heat Fluxes (Ohalele 2020)

Appendix G. Development Of The Single-Variable Nonlinear Correlation

Outlined here is an explanation of how the power law method was developed and applied. It follows the selection of the power law as well as how the equations were developed.

First, the datasets for both Kombat Flex and Ripstop Natural were split into the exposures that have the most duration points. In this case, these exposures include 10, 15, 20, 30, and 40 kW/m². Once these exposures were selected, they were applied to three regression models: the power law, the exponential law, and the Arrhenius law. These three approaches can be represented by Equations G.1 through G.3, with Equations G.4 through G.6 representing the linear forms of the power law, exponential law, and Arrhenius law respectively.

$$\frac{TS}{TS_i} = At^n \quad (G.1)$$

$$\frac{TS}{TS_i} = Ae^{nt} \quad (G.2)$$

$$\frac{TS}{TS_i} = Ae^{\frac{n}{t}} \quad (G.3)$$

$$\ln\left(\frac{TS}{TS_i}\right) = n \ln(t) + \ln(A) \quad (G.4)$$

$$\ln\left(\frac{TS}{TS_i}\right) = nt + \ln(A) \quad (G.5)$$

$$\ln\left(\frac{TS}{TS_i}\right) = n\left(\frac{1}{t}\right) + \ln(A) \quad (G.6)$$

where,

A is a coefficient representing intercept,

n is a coefficient representing slope,

t is time in seconds, and

$\frac{TS}{TS_i}$ is tensile strength retention.

Expressed in the body of this thesis is the correlation in regard to power which presented the most accurate linearity. These three correlations can be found in Figures G.1, G.2, and G.3.

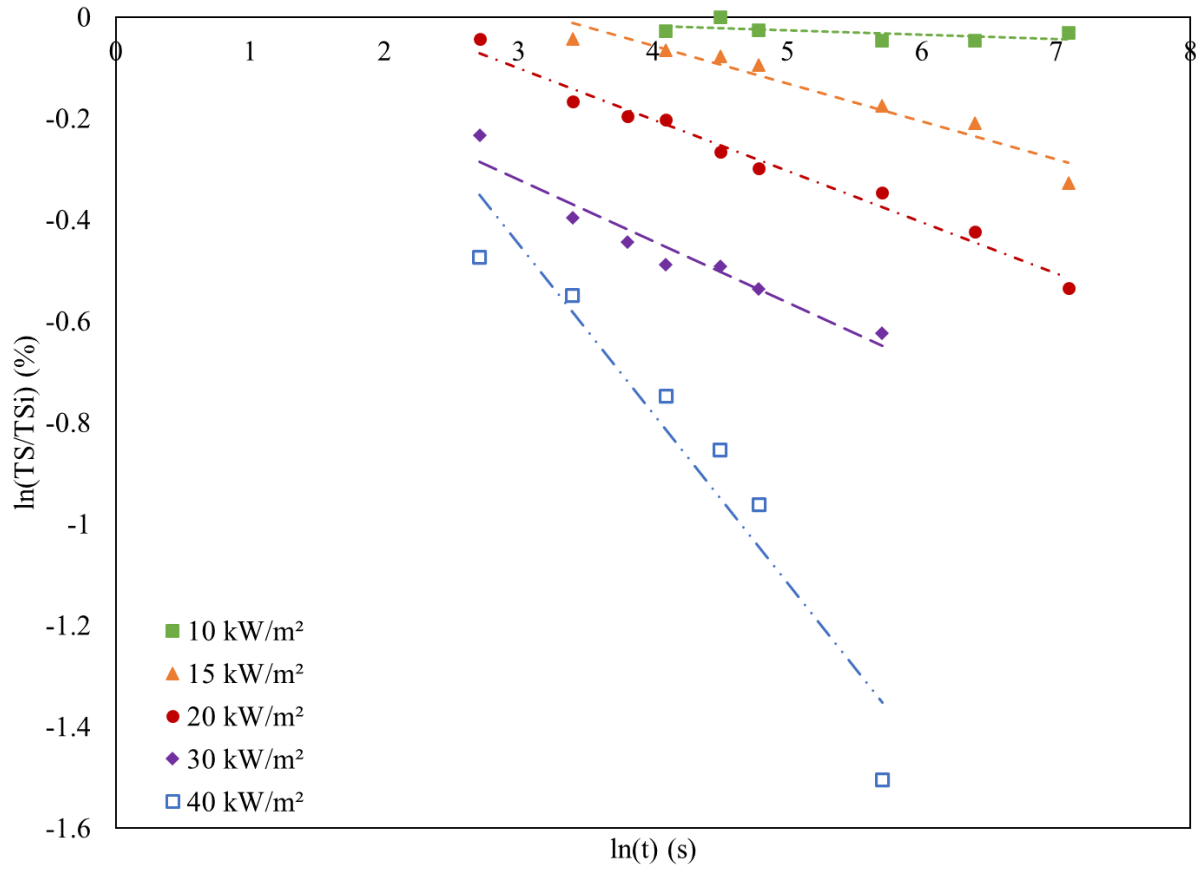


Figure G.1 Kombat Flex Nonlinear Regression Using A Power Correlation

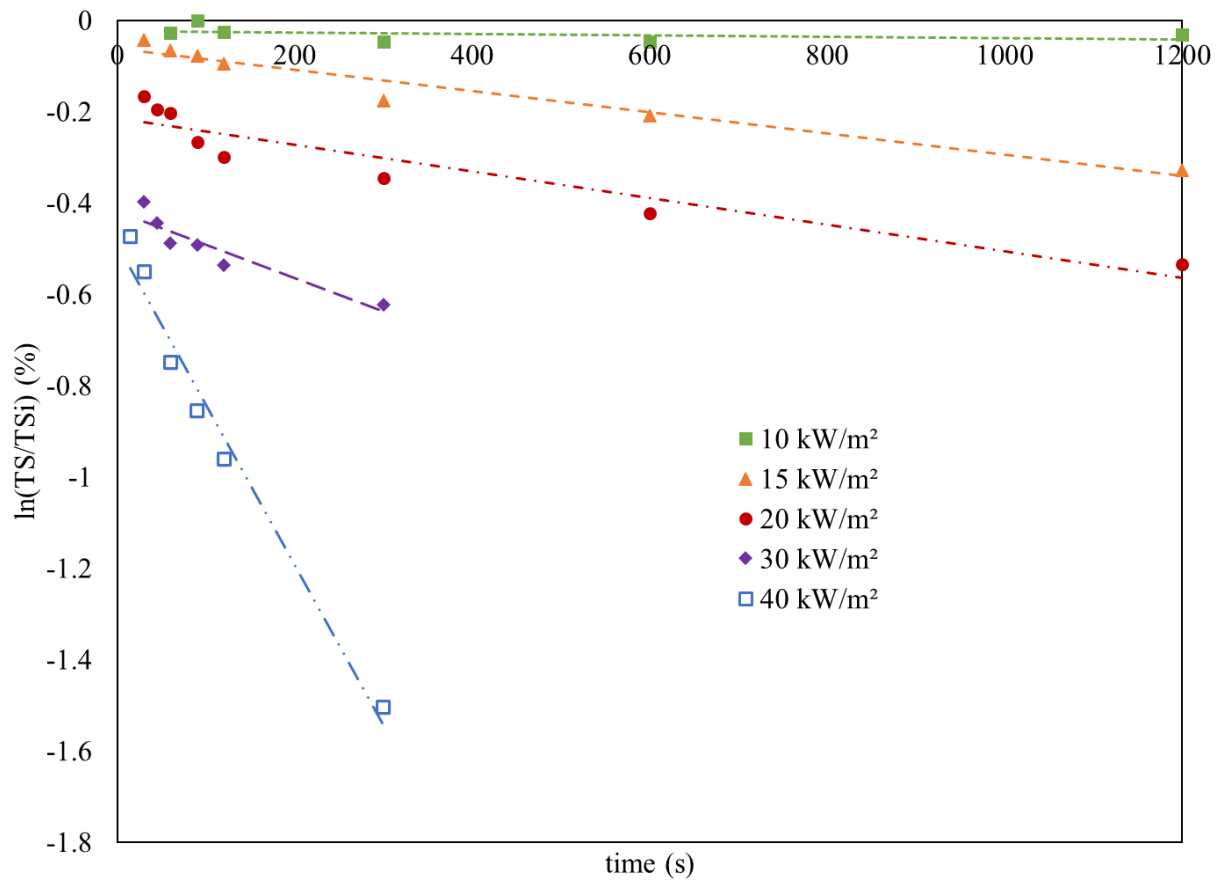


Figure G.2 Kombat Flex Nonlinear Regression Using An Exponential Correlation

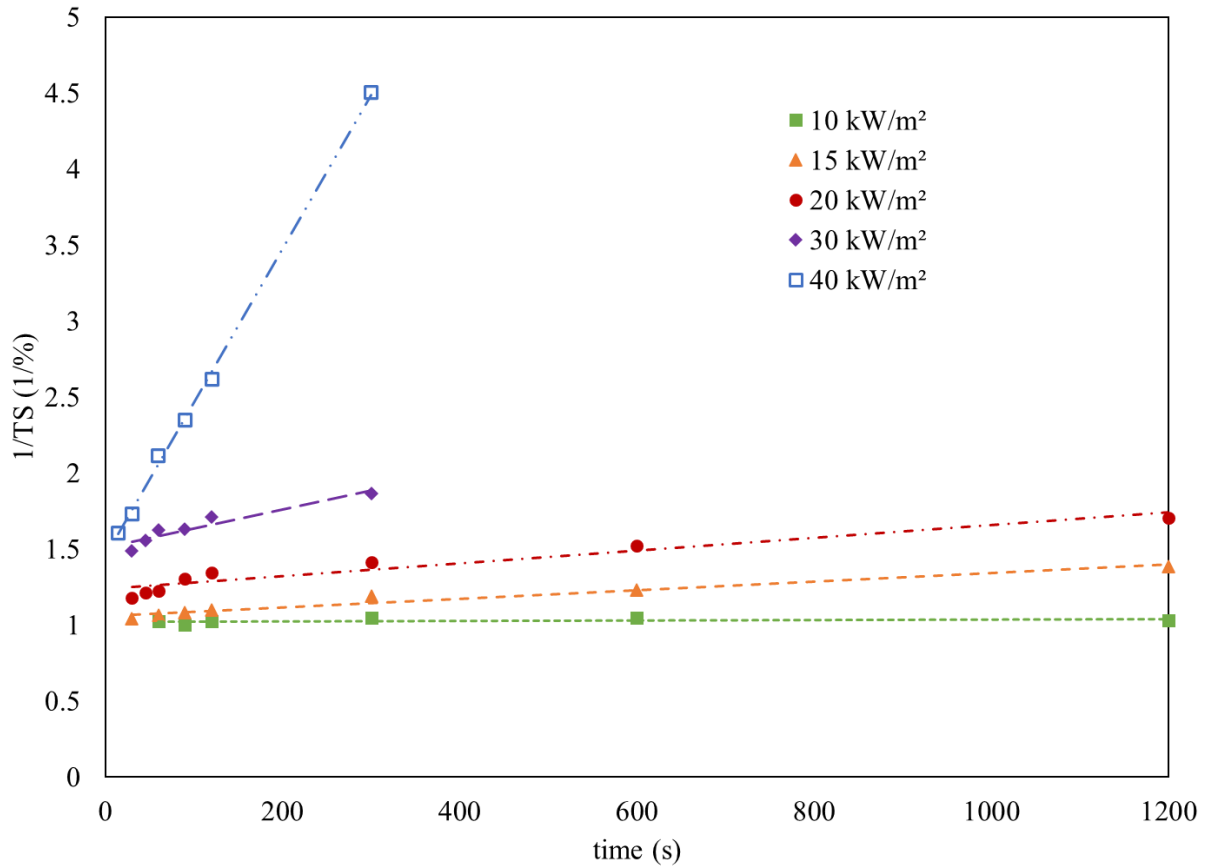


Figure G.3 Kombat Flex Nonlinear Regression Using An Arrhenius Correlation

When examining Figures G.1, G.2, and G.3, the key feature sought is how closely do the datapoints stick to a linear relationship. Under statistical comparisons, there is a higher level of linearity in the power relationship than the others at an average R^2 value of 0.82, which is 4% higher than the exponential relationship (Figure F.2). This value increases to 0.94 when excluding the data from 10 kW/m². As the goal of this correlation is to develop a cross exposure correlation, the relationship desired is one that performs well on all exposures versus relationships that work well under only some exposures. The exponential relationship is a great example of this as it provides an excellent linearity at 40 kW/m² but is weaker at both 20 and 30 kW/m² (both of which are arguably more valuable exposures for this research).

The lines found in Figure G.1 produce the equations in Table G.1. When reverted to their power form, these equations take the form of Equation G.7 whose coefficients can be found in Table G.2 for Kombat Flex, Ripstop Natural, Ripstop Black, and PBI Max.

Table G.1 Linearized Single-Variable Correlation Equations For Kombat Flex

Heat Flux (kW/m ²)	Linearised Equation
10	$\ln\left(\frac{TS}{TS_i}\right) = (-0.0085) \ln(t) + 0.0165$
20	$\ln\left(\frac{TS}{TS_i}\right) = (-0.0748) \ln(t) + 0.2427$
30	$\ln\left(\frac{TS}{TS_i}\right) = (-0.0955) \ln(t) + 0.1709$
40	$\ln\left(\frac{TS}{TS_i}\right) = (-0.0949) \ln(t) - 0.0803$
50	$\ln\left(\frac{TS}{TS_i}\right) = (-0.4106) \ln(t) + 0.9231$

$$\frac{TS}{TS_i} = at^b \quad (G.7)$$

Table G.2 Power Correlation Coefficients For Kombat Flex, Ripstop Natural, PBI Max, And Ripstop Black Using The Five Exposures With Multiple Durations (Ohalele 2020).

Heat Flux (kW/m ²)	Epp Kombat Flex		Epp Ripstop Natural		Ohalele Ripstop Natural		Ohalele Ripstop Black		Ohalele PBI Max	
	<i>a</i>	<i>n</i>	<i>a</i>	<i>n</i>	<i>a</i>	<i>n</i>	<i>a</i>	<i>n</i>	<i>a</i>	<i>n</i>
	10	1.017	-0.009	0.976	0.046	1.017	-0.255	1.008	-0.153	1.013
15	1.275	-0.075	-	-	-	-	-	-	-	-
20	1.224	-0.101	0.867	0.263	0.876	0.091	0.838	0.306	0.924	0.206
30	1.045	-0.121	-	-	0.971	-0.626	0.896	-0.398	0.960	-0.106
40	1.742	-0.334	0.687	0.487	0.863	-0.251	0.684	0.588	0.974	-0.246

This method was applied to single heat flux exposures with multiple duration points. In this research, a second regression was attempted using the slope and intercept values from the developed power equations (Equation G.7 and Table G.1). This approach did not result in accurate results and so was not included in this thesis. With more heat flux exposures, this second regression could be conducted.